

2

AD-A269 872



PL-TR-93-2122

**AN INVESTIGATION OF METHODS FOR UPDATING
IONOSPHERIC SCINTILLATION MODELS USING
TOPSIDE *IN-SITU* PLASMA DENSITY
MEASUREMENTS**

James A. Secan

**Northwest Research Associates, Inc.
P.O. Box 3027
Bellevue, Washington 98009**

1 May 1993

**DTIC
ELECTE
SEP 28 1993
S E D**

**Final Report
Period Covered 1 May 1990 through 30 April 1993**

Approved for public release; distribution unlimited




**PHILLIPS LABORATORY
Directorate of Geophysics
AIR FORCE MATERIEL COMMAND
HANSCOM AIR FORCE BASE, MA 01731-3010**

93 9 27 03 9

93-22351

11500

"This technical report has been reviewed and is approved for publication"



EDWARD J. WEBER
Contract Manager



EDWARD J. BERGHORN
Branch Chief



WILLIAM K. VICKERY
Division Director

This document has been reviewed by the ESD Public Affairs Office (PA) and is releasable to the National Technical Information Service (NTIS).

Qualified requestors may obtain additional copies from the Defense Technical Information Center. All others should apply to the National Technical Information Service.

If your address has changed, or if you wish to be removed from the mailing list, or if the addressee is no longer employed by your organization, please notify PL/TSI, Hanscom AFB, MA 01731-5000. This will assist us in maintaining a current mailing list.

Do not return copies of this report unless contractual obligations or notices on a specific document requires that it be returned.

REPORT DOCUMENTATION PAGE			Form Approved OMB No. 0704-0188	
<small>Public reporting burden for this collection of information is estimated to average 1 hour per response, including the time for reviewing instructions, searching existing data sources, gathering and maintaining the data needed, and completing and reviewing the collection of information. Send comments regarding this burden estimate or any other aspect of this collection of information, including suggestions for reducing this burden, to Washington Headquarters Services, Directorate for Information Operations and Reports, 1215 Jefferson Davis Highway, Suite 1204, Arlington, VA 22202-4302, and to the Office of Management and Budget, Paperwork Reduction Project (0704-0188), Washington, DC 20503.</small>				
1. AGENCY USE ONLY (Leave blank)	2. REPORT DATE 1 May 1993	3. REPORT TYPE AND DATES COVERED Final Report (1 May 90 - 30 Apr 93)		
4. TITLE AND SUBTITLE An Investigation of Methods for Updating Ionospheric Scintillation Models Using Topside <u>In-Situ</u> Plasma Density Measurements		5. FUNDING NUMBERS F19628-90-C-0072 PE 35160F PR DMSS TA01 WUAB		
6. AUTHOR(S) James A. Secan				
7. PERFORMING ORGANIZATION NAME(S) AND ADDRESS(ES) Northwest Research Associates, Inc. PO Box 3027 Bellevue, WA 98009		8. PERFORMING ORGANIZATION REPORT NUMBER NWRA-CR-93-R096		
9. SPONSORING / MONITORING AGENCY NAME(S) AND ADDRESS(ES) Phillips Laboratory 29 Randolph Road Hanscom AFB, MA 01731-3010 Contract Manager: Edward Weber/GPIA		10. SPONSORING / MONITORING AGENCY REPORT NUMBER PL-TR-93-2122		
11. SUPPLEMENTARY NOTES				
12a. DISTRIBUTION / AVAILABILITY STATEMENT approved for public release; distribution unlimited		12b. DISTRIBUTION CODE		
13. ABSTRACT (Maximum 200 words) Modern military communication, navigation, and surveillance systems depend on reliable, noise-free transionospheric radio-frequency channels and can be severely impacted by small-scale electron-density irregularities in the ionosphere. This report summarizes the results of a three-year investigation into the methods for updating ionospheric scintillation models using observations of ionospheric plasma-density irregularities measured by the DMSP Scintillation Meter (SM) sensor. Results are reported from the analysis of data from a campaign conducted in January 1990 near Tromso, Norway, in which near coincident <i>in-situ</i> plasma-density and transionospheric scintillation measurements were made. Estimates for the level of intensity and phase scintillation on a transionospheric UHF radio link in the early-evening auroral zone were calculated from DMSP SM data and compared to the levels actually observed. Results are also presented from a comparison with scintillation observations made with a coincident DNA Polar BEAR satellite pass.				
14. SUBJECT TERMS Ionosphere, Ionospheric Scintillation, Radiowave Scintillation Defense Meteorology Satellite Program (DMSP)		15. NUMBER OF PAGES 112		
		16. PRICE CODE		
17. SECURITY CLASSIFICATION OF REPORT Unclassified	18. SECURITY CLASSIFICATION OF THIS PAGE Unclassified	19. SECURITY CLASSIFICATION OF ABSTRACT Unclassified	20. LIMITATION OF ABSTRACT SAR	

CONTENTS	Page
Figures	iv
Tables	xv
Preface	xvi
1. Introduction	1
2. Summary of the 1990 Campaign	2
2.1 17 January 1990 — DMSP F8 — AIO RR#1	3
2.2 23 January 1990 — DMSP F9 — AIO RR#3	9
2.3 24 January 1990 — DMSP F8 — AIO RR#4	15
2.4 25 January 1990 — DMSP F8 — AIO RR#5	21
2.5 28 January 1990 — DMSP F9 — AIO RR#7	27
3. Detailed Analysis — 17 January 1990	33
3.1 Drift Velocity Effects	33
3.2 Background Electron Density Profile	40
3.3 Height Variation of ΔN	45
4. Detailed Analysis — 24 January 1990	48
5. Drift Velocity Effects	63
6. Discussion	71
7. Conclusion	72
References	72
Appendix A. Data Analysis Procedures (AIO and DMSP)	74
Appendix B. Phase Spectrum Plots — Polar BEAR and AIO-AFSATCOM	79

FIGURES

Figure	Caption	Page
1	Locations of the DMSP F8 satellite traced down to 350 km altitude and the 350 km ionospheric penetration point (IPP) for the AIO-AFSATCOM link for the 17 January 1990 data set. The location marked by a cross-bar on both traces indicates the point where the two experiments were collecting data on the same geomagnetic latitude. The symbols are plotted at center-points for data samples used to generate various irregularity/scintillation parameters. The circled numbers on the AIO-AFSATCOM trace are used to identify individual data samples.	4
2	Plots from the DMSP SSIES/SM (total ion density) and SSIES/DM (horizontal cross-track ion drift velocity) sensors over the geomagnetic (apex) latitude range of 55° to 75° for 17 January 1990. The latitude range covered by the AIO-AFSATCOM data set (IPP) is indicated in both plots. These data are plotted in time-reverse order so that latitude increases from left to right, and the locations printed along the x-axis are for the DMSP 350 km footprint locations.	5
3	Data from the AIO-AFSATCOM link and the DMSP SSIES/SM sensor for the intervals shown in Figure 1. The top plot is the detrended intensity and the middle plot is the detrended phase from the AIO-AFSATCOM link. The times along the bottom of the phase plot are the time difference (in seconds) between the AIO-AFSATCOM observation and the corresponding DMSP/SSIES one. The bottom plot is the detrended SSIES/SM total ion density data. The SSIES/SM data is plotted in time-reverse order so that all three plots cover the same range of geomagnetic latitudes. The locations plotted with the SSIES/SM data are for the DMSP 350 km footprint locations.	6
4	Data derived from the DMSP SSIES/SM and DM sensor data for 17 January 1990. The top plot is of the RMS variance in ΔN_i from five-second SM sensor data samples centered on the time for which the data are plotted. The middle plot is of the C_L values derived from the ΔN_i data (solid lines) and from the WBMOD model (dotted line). The bottom plot is of five-second averages of the DM sensor horizontal cross-track drift velocity.	7

Figure

Caption

Page

- 5 Analysis results for the 17 January 1990 data sets. The top plot shows the variation of σ_ϕ (RMS phase) with geomagnetic latitude as calculated from the WBMOD model, from the SSIES C_kL and U_h data, and from the AIO-AFSATCOM phase data. The middle plot shows the variation of S_4 with geomagnetic latitude from the same sources. The bottom plot shows the variation of total ion density over the same latitude range. The arrows indicate the time/location of closest approach. 8
- 6 Locations of the DMSP F8 satellite traced down to 350 km altitude and the 350 km ionospheric penetration point (IPP) for the AIO-AFSATCOM link for the 23 January 1990 data set. The location marked by a cross-bar on both traces indicates the point where the two experiments were collecting data on the same geomagnetic latitude. The symbols are plotted at center-points for data samples used to generate various irregularity/scintillation parameters. The circled numbers on the AIO-AFSATCOM trace are used to identify individual data samples. 10
- 7 Plots from the DMSP SSIES/SM (total ion density) and SSIES/DM (horizontal cross-track ion drift velocity) sensors over the geomagnetic (apex) latitude range of 55° to 75° for 23 January 1990. The latitude range covered by the AIO-AFSATCOM data set (IPP) is indicated in both plots. These data are plotted in time-reverse order so that latitude increases from left to right, and the locations printed along the x-axis are for the DMSP 350 km footprint locations. 11
- 8 Data from the AIO-AFSATCOM link and the DMSP SSIES/SM sensor for the intervals shown in Figure 6. The top plot is the detrended intensity and the middle plot is the detrended phase from the AIO-AFSATCOM link. The times along the bottom of the phase plot are the time difference (in seconds) between the AIO-AFSATCOM observation and the corresponding DMSP/SSIES one. The bottom plot is the detrended SSIES/SM total ion density data. The SSIES/SM data is plotted in time-reverse order so that all three plots cover the same range of geomagnetic latitudes. The locations plotted with the SSIES/SM data are for the DMSP 350 km footprint locations. 12

DTIC QUALITY INSPECTED 3

For	
CRA&I	<input checked="" type="checkbox"/>
TAB	<input type="checkbox"/>
Unced	<input type="checkbox"/>
Justification	
By	
Distribution /	
Availability Codes	
Dist	Avail and / or Special
A-1	

Figure	Caption	Page
9	Data derived from the DMSP SSIES/SM and DM sensor data for 23 January 1990. The top plot is of the RMS variance in ΔN_i from five-second SM sensor data samples centered on the time for which the data are plotted. The middle plot is of the $C_k L$ values derived from the ΔN_i data (solid lines) and from the WBMOD model (dotted line). The bottom plot is of five-second averages of the DM sensor horizontal cross-track drift velocity.	13
10	Analysis results for the 23 January 1990 data sets. The top plot shows the variation of σ_ϕ (RMS phase) with geomagnetic latitude as calculated from the WBMOD model, from the SSIES $C_k L$ and U_h data, and from the AIO-AFSATCOM phase data. The middle plot shows the variation of S_4 with geomagnetic latitude from the same sources. The bottom plot shows the variation of total ion density over the same latitude range. The arrows indicate the time/location of closest approach.	14
11	Locations of the DMSP F8 satellite traced down to 350 km altitude and the 350 km ionospheric penetration point (IPP) for the AIO-AFSATCOM link for the 24 January 1990 data set. The location marked by a cross-bar on both traces indicates the point where the two experiments were collecting data on the same geomagnetic latitude. The symbols are plotted at center-points for data samples used to generate various irregularity/scintillation parameters. The circled numbers on the AIO-AFSATCOM trace are used to identify individual data samples.	16
12	Plots from the DMSP SSIES/SM (total ion density) and SSIES/DM (horizontal cross-track ion drift velocity) sensors over the geomagnetic (apex) latitude range of 55° to 75° for 24 January 1990. The latitude range covered by the AIO-AFSATCOM data set (IPP) is indicated in both plots. These data are plotted in time-reverse order so that latitude increases from left to right, and the locations printed along the x-axis are for the DMSP 350 km footprint locations.	17

Figure	Caption	Page
13	Data from the AIO-AFSATCOM link and the DMSP SSIES/SM sensor for the intervals shown in Figure 11. The top plot is the detrended intensity and the middle plot is the detrended phase from the AIO-AFSATCOM link. The times along the bottom of the phase plot are the time difference (in seconds) between the AIO-AFSATCOM observation and the corresponding DMSP/SSIES one. The bottom plot is the detrended SSIES/SM total ion density data. The SSIES/SM data is plotted in time-reverse order so that all three plots cover the same range of geomagnetic latitudes. The locations plotted with the SSIES/SM data are for the DMSP 350 km footprint locations.	18
14	Data derived from the DMSP SSIES/SM and DM sensor data for 24 January 1990. The top plot is of the RMS variance in ΔN_i from five-second SM sensor data samples centered on the time for which the data are plotted. The middle plot is of the $C_k L$ values derived from the ΔN_i data (solid lines) and from the WBMOD model (dotted line). The bottom plot is of five-second averages of the DM sensor horizontal cross-track drift velocity.	19
15	Analysis results for the 24 January 1990 data sets. The top plot shows the variation of σ_ϕ (RMS phase) with geomagnetic latitude as calculated from the WBMOD model, from the SSIES $C_k L$ and U_h data, and from the AIO-AFSATCOM phase data. The middle plot shows the variation of S_4 with geomagnetic latitude from the same sources. The bottom plot shows the variation of total ion density over the same latitude range. The arrows indicate the time/location of closest approach.	20
16	Locations of the DMSP F8 satellite traced down to 350 km altitude and the 350 km ionospheric penetration point (IPP) for the AIO-AFSATCOM link for the 25 January 1990 data set. The location marked by a cross-bar on both traces indicates the point where the two experiments were collecting data on the same geomagnetic latitude. The symbols are plotted at center-points for data samples used to generate various irregularity/scintillation parameters. The circled numbers on the AIO-AFSATCOM trace are used to identify individual data samples.	22

Figure	Caption	Page
17	Plots from the DMSP SSIES/SM (total ion density) and SSIES/DM (horizontal cross-track ion drift velocity) sensors over the geomagnetic (apex) latitude range of 55° to 75° for 25 January 1990. The latitude range covered by the AIO-AFSATCOM data set (IPP) is indicated in both plots. These data are plotted in time-reverse order so that latitude increases from left to right, and the locations printed along the x-axis are for the DMSP 350 km footprint locations.	23
18	Data from the AIO-AFSATCOM link and the DMSP SSIES/SM sensor for the intervals shown in Figure 16. The top plot is the detrended intensity and the middle plot is the detrended phase from the AIO-AFSATCOM link. The times along the bottom of the phase plot are the time difference (in seconds) between the AIO-AFSATCOM observation and the corresponding DMSP/SSIES one. The bottom plot is the detrended SSIES/SM total ion density data. The SSIES/SM data is plotted in time-reverse order so that all three plots cover the same range of geomagnetic latitudes. The locations plotted with the SSIES/SM data are for the DMSP 350 km footprint locations.	24
19	Data derived from the DMSP SSIES/SM and DM sensor data for 25 January 1990. The top plot is of the RMS variance in ΔN_i from five-second SM sensor data samples centered on the time for which the data are plotted. The middle plot is of the $C_k L$ values derived from the ΔN_i data (solid lines) and from the WBMOD model (dotted line). The bottom plot is of five-second averages of the DM sensor horizontal cross-track drift velocity.	25
20	Analysis results for the 25 January 1990 data sets. The top plot shows the variation of σ_ϕ (RMS phase) with geomagnetic latitude as calculated from the WBMOD model, from the SSIES $C_k L$ and U_h data, and from the AIO-AFSATCOM phase data. The middle plot shows the variation of S_4 with geomagnetic latitude from the same sources. The bottom plot shows the variation of total ion density over the same latitude range. The arrows indicate the time/location of closest approach.	26

Figure	Caption	Page
21	Locations of the DMSP F8 satellite traced down to 350 km altitude and the 350 km ionospheric penetration point (IPP) for the AIO-AFSATCOM link for the 28 January 1990 data set. The location marked by a cross-bar on both traces indicates the point where the two experiments were collecting data on the same geomagnetic latitude. The symbols are plotted at center-points for data samples used to generate various irregularity/scintillation parameters. The circled numbers on the AIO-AFSATCOM trace are used to identify individual data samples.	28
22	Plots from the DMSP SSIES/SM (total ion density) and SSIES/DM (horizontal cross-track ion drift velocity) sensors over the geomagnetic (apex) latitude range of 55° to 75° for 28 January 1990. The latitude range covered by the AIO-AFSATCOM data set (IPP) is indicated in both plots. These data are plotted in time-reverse order so that latitude increases from left to right, and the locations printed along the x-axis are for the DMSP 350 km footprint locations.	29
23	Data from the AIO-AFSATCOM link and the DMSP SSIES/SM sensor for the intervals shown in Figure 21. The top plot is the detrended intensity and the middle plot is the detrended phase from the AIO-AFSATCOM link. The times along the bottom of the phase plot are the time difference (in seconds) between the AIO-AFSATCOM observation and the corresponding DMSP/SSIES one. The bottom plot is the detrended SSIES/SM total ion density data. The SSIES/SM data is plotted in time-reverse order so that all three plots cover the same range of geomagnetic latitudes. The locations plotted with the SSIES/SM data are for the DMSP 350 km footprint locations.	30
24	Data derived from the DMSP SSIES/SM and DM sensor data for 28 January 1990. The top plot is of the RMS variance in ΔN_i from five-second SM sensor data samples centered on the time for which the data are plotted. The middle plot is of the $C_k L$ values derived from the ΔN_i data (solid lines) and from the WBMOD model (dotted line). The bottom plot is of five-second averages of the DM sensor horizontal cross-track drift velocity.	31

Figure	Caption	Page
25	Analysis results for the 28 January 1990 data sets. The top plot shows the variation of σ_ϕ (RMS phase) with geomagnetic latitude as calculated from the WBMOD model, from the SSIES C_kL and U_h data, and from the AIO-AFSATCOM phase data. The middle plot shows the variation of S_4 with geomagnetic latitude from the same sources. The bottom plot shows the variation of total ion density over the same latitude range. The arrows indicate the time/location of closest approach.	32
26	Locations of the DMSP F8 satellite traced down to 350 km altitude and the 350 km ionospheric penetration point (IPP) for the AIO-AFSATCOM link for the 17 January 1990 data set. The AIO-AFSATCOM data have been mapped into the plasma frame as defined by the DMSP observations using drift velocity measurements as described in the text. The location marked by a cross-bar on both traces indicates the point where the two experiments were collecting data on the same geomagnetic latitude. The symbols are plotted at center-points for data samples used to generate various irregularity/scintillation parameters. The circled numbers on the AIO-AFSATCOM trace are used to identify individual data samples.	34
27	The same locations as in Figure 26, now plotted in a fixed-earth frame. All labels are as in Figure 26.	35
28	Plots from the DMSP SSIES/SM (total ion density) and SSIES/DM (horizontal cross-track ion drift velocity) sensors over the geomagnetic (apex) latitude range of 55° to 75° for 17 January 1990. The latitude range covered by the AIO-AFSATCOM data set (IPP) <i>as mapped into the DMSP-based plasma frame</i> (see Figure 26) is indicated in both plots. These data are plotted in time-reverse order so that latitude increases from left to right, and the locations printed along the x-axis are for the DMSP 350 km footprint locations.	36
29	Data from the AIO-AFSATCOM link and the DMSP SSIES/SM sensor for the intervals in Figure 26. The top plot is the detrended intensity and the middle plot is the detrended phase from the AIO-AFSATCOM link. The times along the bottom of the phase plot are the time difference (in seconds) between the AIO-AFSATCOM observation and the corresponding DMSP/SSIES one. The bottom plot is the SSIES/SM total ion density data. The SSIES/SM data is plotted in time-reverse order so that all three plots cover the same range of geomagnetic latitudes. The locations plotted with the SSIES/SM data are for the DMSP 350 km footprint locations.	37

Figure	Caption	Page
30	The top two plots are as in Figure 29. The bottom plot is the detrended SSIES/SM total ion density data. This plot is labeled as in Figure 29.	38
31	Analysis results for the 17 January 1990 data sets as mapped into the plasma frame defined in Figure 26. The top plot shows the variation of σ_ϕ (RMS phase) with geomagnetic latitude as calculated from the WBMOD model, from the SSIES C_kL and U_h data, and from the AIO-AFSATCOM phase data. The middle plot shows the variation of S_4 with geomagnetic latitude from the same sources. The bottom plot shows the variation of total ion density over the same latitude range. The arrows indicate the time/location of closest approach.	39
32	Latitude scan of electron density profiles generated from the <i>in-situ</i> density measured by the DMSP SSIES Scintillation Meter. The segment labeled "Results Plots Coverage" is the latitude range covered in the scintillation index plots in Figure 31.	41
33	Latitude scan of electron density profiles from the EISCAT radar.	42
34	Latitude variation of f_oF2 for the 17 January 1990 campaign as derived from AIO ionosonde measurements (diamonds) and from the EISCAT latitude scan (triangles). The times at the ends of the two data segments indicate the end times of each segment. The vertical bar indicates the location and time of coincidence of the two data sets.	44
35	Analysis results for the 17 January 1990 data sets using f_oF2 values from the AIO ionosonde. The top plot shows the variation of σ_ϕ (RMS phase) with geomagnetic latitude as calculated from the WBMOD model, from the SSIES C_kL data, and from the AIO-AFSATCOM phase data. The middle plot shows the variation of S_4 with geomagnetic latitude from the same sources. The bottom plot shows the variation of total ion density over the same latitude range. The arrows indicate the time/location of closest approach.	46
36	Analysis results for the 17 January 1990 data set using ΔN constant with height (see explanation and caveats in text). The format of this figure is identical to Figure 35.	47

Figure	Caption	Page
37a	Locations of the DMSP F8 satellite traced down to 350 km altitude and the 350 km ionospheric penetration point (IPP) for the AIO-AFSATCOM link for the 24 January 1990 data set. The location marked by a cross-bar on both traces indicates the point where the two experiments were collecting data on the same geomagnetic latitude. The symbols are plotted at center-points for data samples used to generate various irregularity/scintillation parameters. The circled numbers on the AIO-AFSATCOM trace are used to identify individual data samples.	49
37b	Data from the AIO-AFSATCOM link and the DMSP SSIES/SM sensor for the intervals shown in Figure 37a. The top plot is the detrended intensity and the middle plot is the detrended phase from the AIO-AFSATCOM link (both detrended using a low-pass filter with a 0.1 Hz cutoff), and the bottom plot is the SSIES/SM total ion density data. The SSIES/SM data is plotted in time-reverse order so that all three plots cover the same range of geomagnetic latitudes. The locations plotted with the SSIES/SM data are for the DMSP 350 km footprint locations.	50
38a	Locations of the DMSP F8 satellite traced down to 350 km altitude and the 350 km IPP for the Tromso-Polar BEAR (PB) link for the 24 January 1990 data set. The location marked by a cross-bar on both traces indicates the point where the two experiments were collecting data on the same geomagnetic latitude. The symbols are plotted at center-points for data samples used to generate various irregularity/scintillation parameters. The location of Tromso is indicated, as is the latitude range covered by the AIO-AFSATCOM data set.	51
38b	Data from the DMSP SSIES/SM and SSIES/DM sensors and the Tromso-PB VHF link for the intervals shown in Figure 38a. The top plot is the SSIES/SM total ion density data and the bottom plot is the SSIES/DM horizontal cross-track ion drift velocity. Both are plotted in time-reverse order. The middle plot is the T parameter derived from the Tromso-PB VHF phase spectra.	52

Figure	Caption	Page
39a	Locations of the 350 km IPP for the AIO-AFSATCOM link and the 350 km IPP for the Tromso-PB link for the 24 January 1990 data set. The location marked by a cross-bar on both traces indicates the point where the two experiments were collecting data on the same geomagnetic latitude. The symbols are plotted at center-points for data samples used to generate various irregularity/scintillation parameters. The circled numbers on the AIO-AFSATCOM trace are used to identify individual data samples.	53
39b	Data from the AIO-AFSATCOM link and the Tromso-PB VHF link for the intervals shown in Figure 39a. The top plot is the detrended intensity and the middle plot is the detrended phase from the AIO-AFSATCOM link (both detrended using a low-pass filter with a 0.1 Hz cutoff), and the bottom plot is the T parameter derived from the Tromso-PB VHF phase spectra.	54
40	The top plot is $C_k L$ derived from the SSIES/SM data and the bottom plot is of five-minute averages of the SSIES/DM horizontal cross-track ion drift velocity. The middle plot shows the Tromso-PB VHF T values (solid curve) plotted with T values generated for the Tromso-PB geometry using the $C_k L$ values shown in the top plot (dashed curve).	57
41	This figure is identical to Figure 40, except that the $C_k L$ values and the drift velocity have been generated from the standard WBMOD model. The dashed curve in the middle plot was also generated from the standard WBMOD.	58
42	The top plot shows comparisons of the variation of $C_k L$ as a function of geomagnetic latitude from the DMSP SSIES data (dotted line), the Tromso-PB VHF T data (thin solid line), and from the standard WBMOD model (thick solid line). The bottom plot shows comparisons of the variation of the phase spectral slope parameter, p , as a function of geomagnetic latitude from the DMSP SSIES data (dotted line), the Tromso-PB VHF phase data (thin solid line), and from WBMOD (thick solid line).	59
43	The top plot shows a comparison of T calculate from the SSIES/SM data (dotted line) and from the Tromso-PB VHF data (solid line) over the latitude range coincident with the AIO-AFSATCOM trace (i.e., the same coverage as shown in Figure 39a). The bottom plot shows the same comparison of the SSIES/SM T (dashed line) with that calculated from the AIO-AFSATCOM phase data (solid line).	61

Figure	Caption	Page
44	The top plot shows the variation of $C_{\mu}L$ from all data sources as a function of geomagnetic latitude, and the bottom plot shows the variation of p as a function of geomagnetic latitude.	62
45	Comparison of S_4 values from the WBMOD model, the AIO-AFSATCOM data, and the DMSP/SSIES data for all five days included in the analysis.	64
46	Comparison of σ_{ϕ} values from the WBMOD model, the AIO-AFSATCOM data, and the DMSP/SSIES data for all five days included in the analysis.	66
47	Comparison of σ_{ϕ} values from the WBMOD model, the AIO-AFSATCOM data, and the DMSP/SSIES data for all five days included in the analysis using different modifications to the drift velocities used in the calculation.	69
A-1	Sample detrended AIO/AFSATCOM intensity record.	75
A-2	Sample detrended AIO/AFSATCOM phase record.	76
B-1	Resampled VHF phase spectra from the Tromso-Polar BEAR data set overplotted with the linear fits used to calculate T and p .	80
B-2	Detrended VHF phase data records from the AIO-AFSATCOM data set and the spectra generated from them. The linear fits used to calculate T and p are plotted over the phase spectra.	83

TABLES

Table	Caption	Page
1	Data for the January 1990 campaign	2
2	Data from the AIO sounder for 17 January 1990.	43

PREFACE

This report summarizes the work completed during a three-year investigation into methods for updating computer-based models of ionospheric scintillation using *in-situ* observations of the ionosphere from the DMSP SSIES sensors. This work is part of a larger effort with an overall objective of providing the USAF Air Weather Service with the capability of observing ionospheric scintillations, and the plasma density irregularities that cause the scintillations, in near real-time and updating models of ionospheric scintillation with these observations.

The following individuals provided invaluable assistance during the course of the investigation: Dr. Fred Rich (PL/GPSG; provided the SSIES data), Dr. Santimay Basu (PL/GPIA; discussions on the issue of scaling the *in situ* C_k to height-integrated C_kL), Dr. Bob Livingston (SRII; provided the AIO-AFSATCOM intensity and phase data), Dr. Jurgen Buchau (PL/GPIA; provided the AIO digisonde data), and Dr. Ed Weber (PL/GPIA; guidance, encouragement, and assorted odd-ends of data).

1. Introduction

Many modern military systems used for communications, command and control, navigation, and surveillance depend on reliable and relatively noise-free transmission of radiowave signals through the earth's ionosphere. Small-scale irregularities in the ionospheric density can cause severe distortion, known as radiowave scintillation, of both the amplitude and phase of these signals. A basic tool used in estimating these effects on systems is a computer program, WBMOD, based on a single-scatter phase-screen propagation model and a number of empirical models of the global morphology of ionospheric density irregularities. An inherent weakness of WBMOD is that the irregularity models provide median estimates for parameters with large dynamic ranges, which can lead to large under- and over-estimation of the effects of the ionospheric irregularities on a system.

One solution to this problem, at least for near real-time estimates, is to update the WBMOD irregularity models with observations of the various parameters modeled. One proposed source for these observations is from the *in-situ* plasma density monitor to be flown on the Defense Meteorology Satellite Program (DMSP) satellites. A previous study assessed the applicability of these data to real-time updates of the WBMOD models [Secan *et al.*, 1990]. (This study will be denoted the assessment study throughout this report). In the present study, techniques developed in the assessment study for characterizing scintillation level in the high latitude ionosphere will be improved, and further techniques for using these data to characterize scintillation levels in the equatorial and mid latitude ionosphere will be developed.

During the assessment study, a set of data was collected in a multi-instrument experiment conducted in the auroral zone near Tromso, Norway, during the month of January 1988. Scintillation measurements were made from the USAF Airborne Ionospheric Observatory (AIO) aircraft on a propagation path to one of the USAF AFSATCOM satellites timed and located to coincide with a DMSP F8 satellite pass. At nearly the same time, the EISCAT incoherent radar (located near Tromso) was measuring the background electron density profiles and *in-situ* plasma drifts up to an altitude of roughly 600 km along a geomagnetic meridian. Data from one pass in that data set were analyzed in detail in the assessment study, which found that the estimates of the level of intensity scintillation calculated from the DMSP *in-situ* plasma density measurements matched the levels observed on the AIO-AFSATCOM link fairly well.

That campaign was run just after solar minimum, so the background plasma-density levels were fairly low. It was decided to repeat the experiments later in the cycle when the density levels would be much higher. The second data collection campaign was conducted in January 1990 when the sunspot number was roughly a factor of three higher than in January 1988, and the observed plasma densities at DMSP altitude were a factor of two to four higher than those observed in the earlier campaign. In addition, since the DMSP F9 satellite had been launched with an SSIES instrument, data was collected from the pre-midnight sector from F9 as well as from the early evening sector from F8.

This report summarizes the findings of that study.

2. Summary of the 1990 Campaign

Analysis of data collected on five days from the 1990 SSIES/AIO/EISCAT campaign has been completed. Table 1 lists the dates and time periods covered by the analysis. The procedures used in processing the DMSP/SSIES and AIO-AFSATCOM data presented in this section are described in Appendix A. The data for each day will be presented with a discussion of the results for that day. Detailed analyses of the data collected on 17 January and 24 January will be presented in Sections 3 and 4.

Table 1. Data for the January 1990 campaign.

Date	AIO RR#	DMSP	Time Period(DMSP)	Time Period (AIO)
17 Jan	1	F8	18:31:28 - 18:36:28	18:19:28 - 18:43:52
23 Jan	3	F9	21:50:59 - 21:55:59	21:57:21 - 22:07:45
24 Jan	4	F8	18:40:28 - 18:45:28	18:33:24 - 18:52:12
25 Jan	5	F8	18:27:24 - 18:32:24	18:22:34 - 18:38:34
28 Jan	7	F9	21:48:47 - 21:53:47	21:43:56 - 21:57:08

The following plots will be presented for each day:

1. A plot of the locations of the 350-km ionospheric penetration point (IPP) for the AIO-AFSATCOM link and the 350-km field-line footprint for the DMSP/SSIES observations for the data analyzed on that day.

2. A context plot of the total ion density (N_i) from the DMSP/SSIES Scintillation Meter (SM) instrument and the horizontal cross-track ion drift velocity (U_h) from the DMSP/SSIES Drift Meter (DM) instrument for an eight-minute period covering the latitude range of 55° to 75° geomagnetic (apex).

3. A plot of the AIO-AFSATCOM intensity and phase data and the DMSP/SM N_i data used in the analysis.

4. Plots of the RMS variation in ΔN_i and $C_k L$ values calculated from the DMSP/SM data and the 5-second average U_h data from the DMSP/DM data.

5. Plots of the results of the analysis, including values of the phase scintillation index (σ_ϕ) and the intensity scintillation index (S_4) calculated (1) from the AIO-AFSATCOM data, (2) from the WBMOD model using only the date, time, SSN, and K_p as inputs, and (3) from the WBMOD model using $C_k L$ and U_h observations from the DMSP/SM and DMSP/DM data sets. A plot of the DMSP/SM N_i data is included to place the results shown in the top two plots in context.

2.1 17 January 1990 — DMSP F8 — AIO RR#1

The time of closest approach (TCA, defined as the time that both the DMSP 350 km footprint and the AIO-AFSATCOM 350 km IPP are at the same geomagnetic (apex) latitude) for this data set was at 18:34:05 GMT. The sunspot number (SSN) for this date was 150, and the K_p values for the three-hour period prior to, including, and after the TCA were 2, 2-, and 3. The nominal separation between the DMSP footprint and the AIO-AFSATCOM IPP was roughly 1.0° of longitude (40 km), and the nominal elevation angle of the AIO-AFSATCOM link was 78° . The plots showing the data for this day are given in Figures 1 through 5.

As can be seen in Figure 2, the latitude range covered by the AIO-AFSATCOM data set analyzed started well poleward of the location of the transition from the smooth (mid-latitude) ionosphere to the irregular (auroral) ionosphere at 62.6° geomagnetic (apex) latitude, and ended just equatorward of several large density-enhancement features seen in the density data co-located with enhancements in the cross-track drift velocity. The detrended intensity and phase AIO-AFSATCOM records (top two plots in Figure 3) both show low scintillation levels at the southern end of the data set with a fairly sharp increase roughly halfway through the set. The detrended *in situ* density (bottom plot in Figure 3) shows roughly the same subjective "roughness" throughout the data set with the exception of two features located at times 66843 and 66837.

Figure 4 shows the results of the first stage of the analysis of the DMSP/SSIES data. The average C_kL level is roughly a factor of two greater than that specified by WBMOD, and the cross-track velocity is fairly constant at approximately 500 m/s in the sunward direction. The differences in behavior of the $\text{RMS } \Delta N_i$ and $\log(C_kL)$ variations are due largely to the stronger effect of large-scale irregularities on $\text{RMS } \Delta N_i$.

Figure 5 summarizes the comparison between the scintillation indices derived from the AIO-AFSATCOM data and those derived from the DMSP/SSIES data. The wide discrepancy between the S_4 values at the southern end of the data is quite a bit larger than that seen in the analysis of data from the January 1988 campaign [Secan and Reinleitner, 1989]. The C_kL values which would match the low AIO-AFSATCOM S_4 values south of 67.5° are 1.5 to 2.0 orders of magnitude lower than that calculated from the DMSP/SSIES data. Comparison of the two sets of σ_p estimates lead to similar, though smaller, differences.

Note: A more detailed analysis of this data set is presented in Section 3.

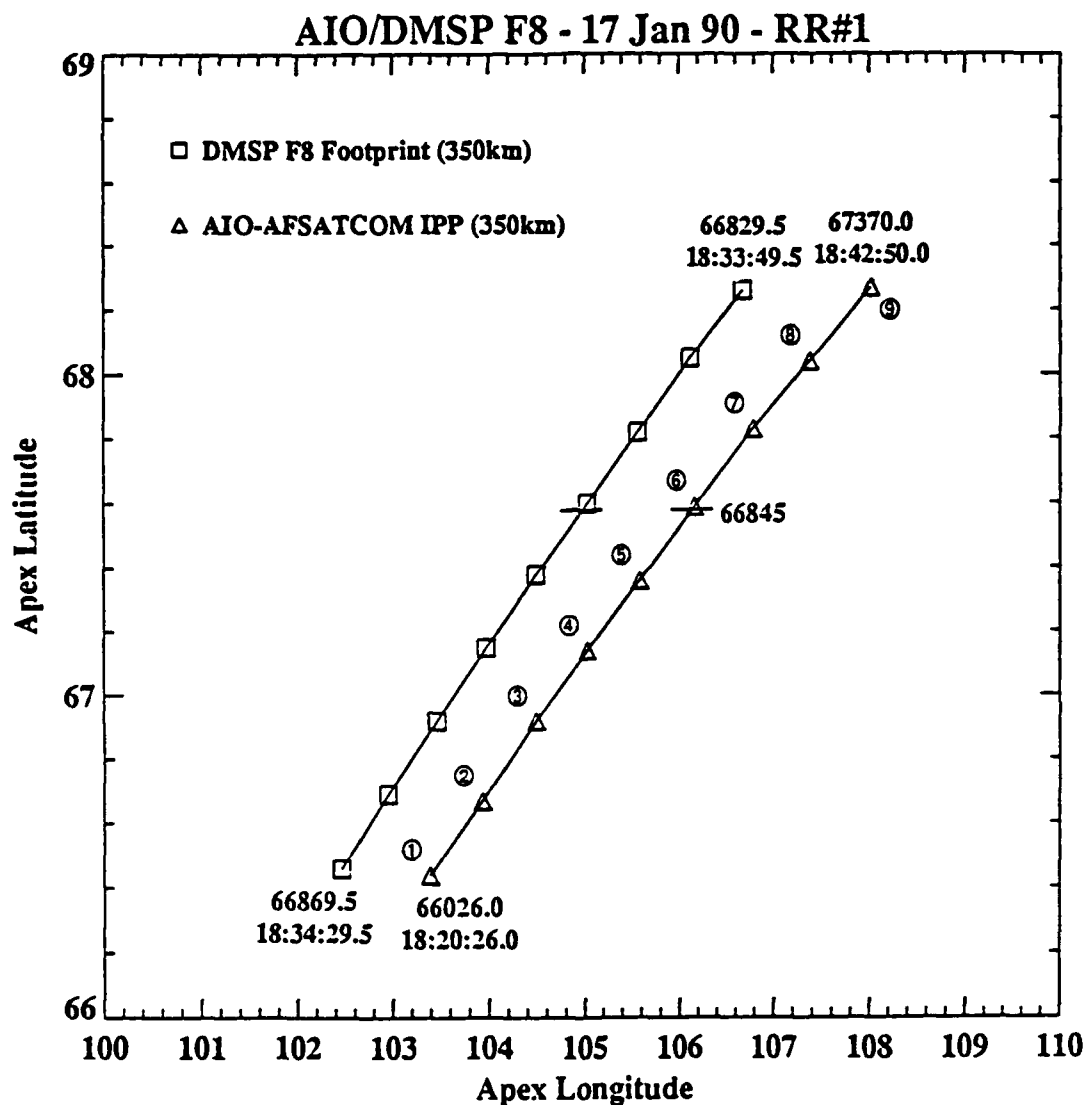


Figure 1. Locations of the DMSP F8 satellite traced down to 350 km altitude and the 350 km ionospheric penetration point (IPP) for the AIO-AFSATCOM link for the 17 January 1990 data set. The location marked by a cross-bar on both traces indicates the point where the two experiments were collecting data on the same geomagnetic latitude. The symbols are plotted at center-points for data samples used to generate various irregularity/scintillation parameters. The circled numbers on the AIO-AFSATCOM trace are used to identify individual data samples.

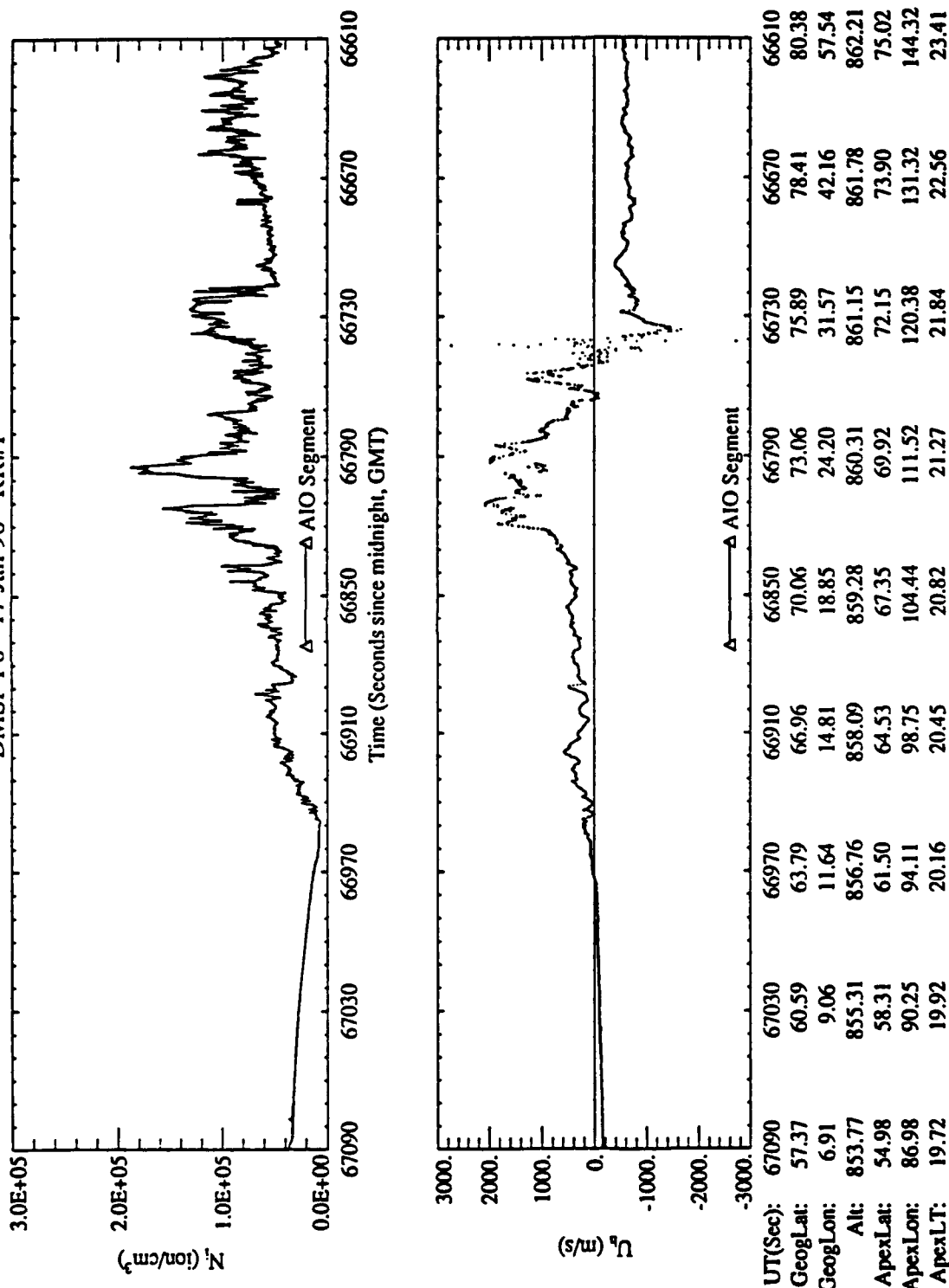


Figure 2. Plots from the DMSP SSIES/SM (total ion density) and SSIES/DM (horizontal cross-track ion drift velocity) sensors over the geomagnetic (apex) latitude range of 55° to 75° for 17 January 1990. The latitude range covered by the AIO-AFSATCOM data set (IPP) is indicated in both plots. These data are plotted in time-reverse order so that latitude increases from left to right, and the locations printed along the x-axis are for the DMSP 350 km footprint locations.

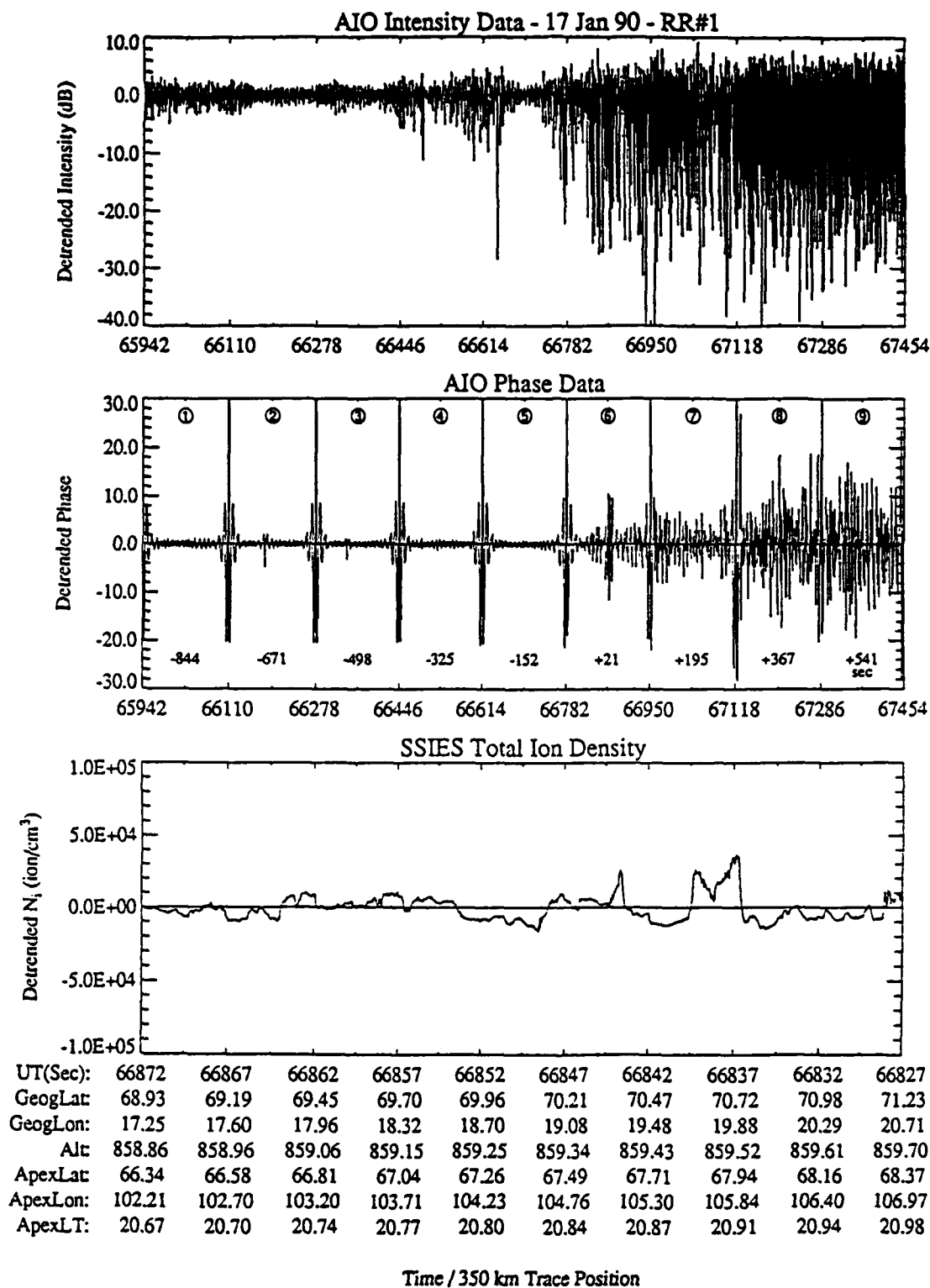


Figure 3. Data from the AIO-AFSATCOM link and the DMSP SSIES/SM sensor for the intervals shown in Figure 1. The top plot is the detrended intensity and the middle plot is the detrended phase from the AIO-AFSATCOM link. The times along the bottom of the phase plot are the time difference (in seconds) between the AIO-AFSATCOM observation and the corresponding DMSP/SSIES one. The bottom plot is the detrended SSIES/SM total ion density data. The SSIES/SM data is plotted in time-reverse order so that all three plots cover the same range of geomagnetic latitudes. The locations plotted with the SSIES/SM data are for the DMSP 350 km footprint locations.

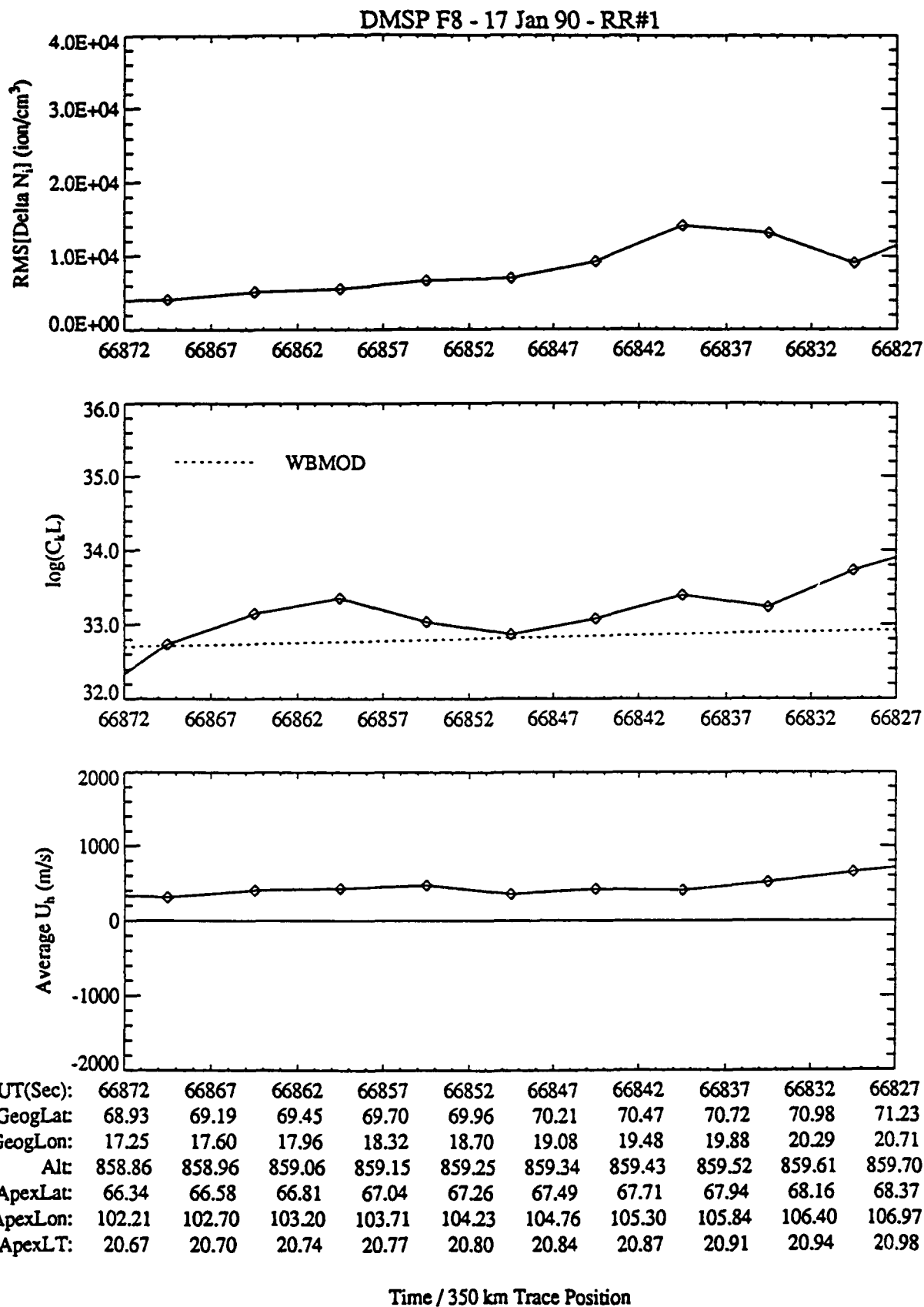


Figure 4. Data derived from the DMSP SSIES/SM and DM sensor data for 17 January 1990. The top plot is of the RMS variance in ΔN_i from five-second SM sensor data samples centered on the time for which the data are plotted. The middle plot is of the $C_L L$ values derived from the ΔN_i data (solid lines) and from the WBMOD model (dotted line). The bottom plot is of five-second averages of the DM sensor horizontal cross-track drift velocity.

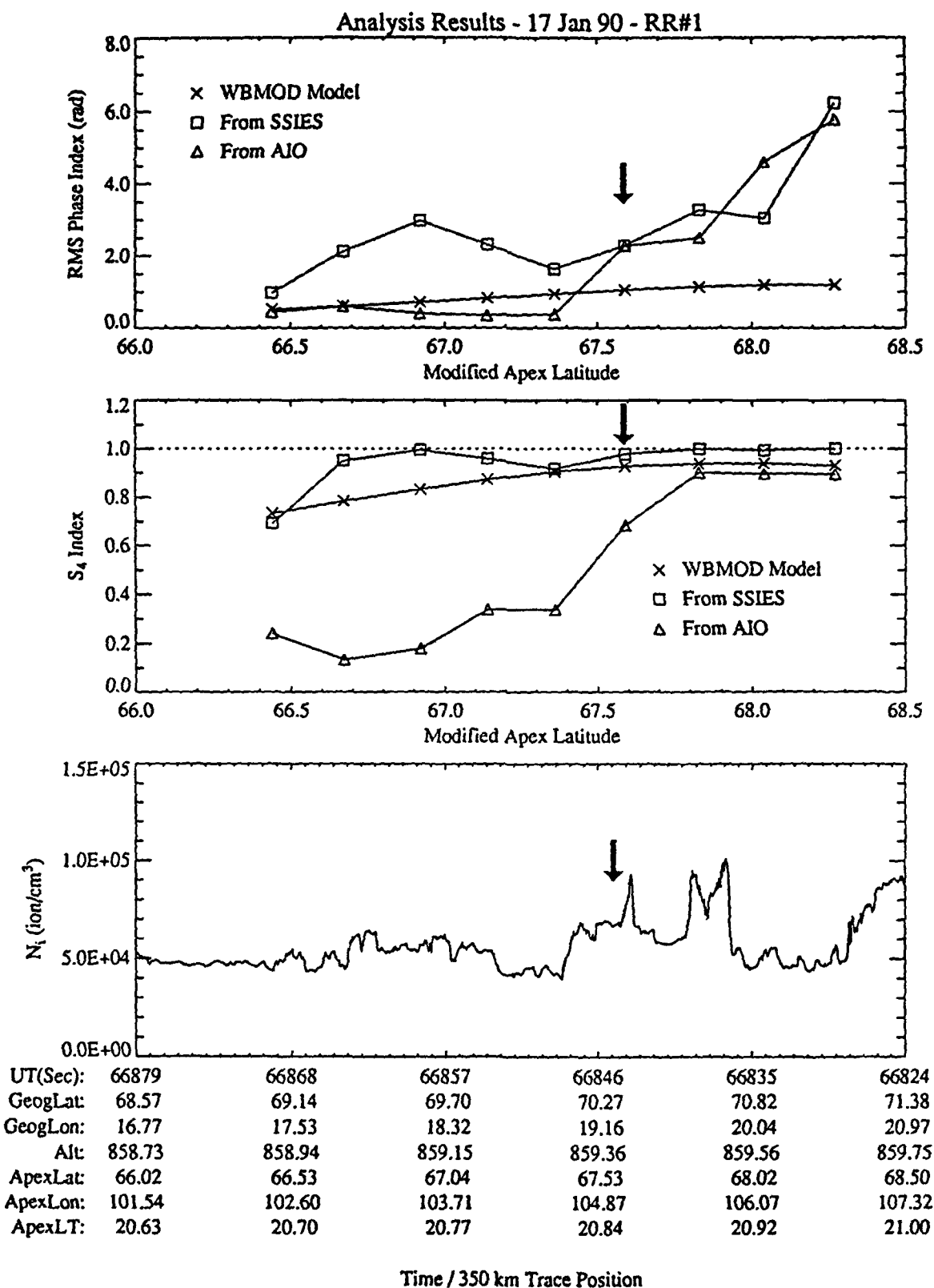


Figure 5. Analysis results for the 17 January 1990 data sets. The top plot shows the variation of σ_ϕ (RMS phase) with geomagnetic latitude as calculated from the WBMOD model, from the SSIES C_kL and U_h data, and from the AIO-AFSATCOM phase data. The middle plot shows the variation of S_4 with geomagnetic latitude from the same sources. The bottom plot shows the variation of total ion density over the same latitude range. The arrows indicate the time/location of closest approach.

2.2 23 January 1990 — DMSP F9 — AIO RR#3

The time of closest approach for this data set was at a time prior to the start of usable data from the AIO-AFSATCOM link (approximately 21:54 GMT). The SSN for this date was 196, and the K_p values for the three-hour period prior to, including, and after the TCA were 3+, 4, and 5. The nominal separation between the DMSP footprint and the AIO-AFSATCOM IPP was roughly 3.5° of longitude (115 km), and the nominal elevation angle of the AIO-AFSATCOM link was 37° . The plots showing the data for this day are given in Figures 6 through 10.

As can be seen in Figure 7, the *in situ* density over latitude range covered by the AIO-AFSATCOM data set analyzed was relatively high (2.5×10^5 ion/cm³) and contained several large irregularity structures. The AIO-AFSATCOM data in Figure 8 shows high scintillation levels throughout the pass. Note that the time difference between the DMSP and the AIO-AFSATCOM data ranges from just over 2 minutes to almost 14 minutes (see middle plot in Figure 8). With geomagnetic activity at storm levels, it is not clear that we can assume (1) that the ionosphere has remained unchanged over the time interval between the collection of the two data sets, or (2) that ionospheric structures (both in density and in drift velocity) will map zonally along geomagnetic latitudes.

Figure 9 shows the results of the first stage of the analysis of the DMSP/SSIES data. The average $C_k L$ level is roughly an order of magnitude greater than that specified by WBMOD, and the cross-track velocity is fairly constant at approximately 500 m/s in the sunward direction. Again, the differences in behavior of the RMS ΔN_i and $\log(C_k L)$ variations are due largely to the stronger effect of large-scale irregularities on RMS ΔN_i .

Figure 10 summarizes the comparison between the scintillation indices derived from the AIO-AFSATCOM data and those derived from the DMSP/SSIES data. The general level of phase scintillation (σ_ϕ) is similar between the two observations across the latitude range, but the trends do not match well at all. Both data sets show essentially saturation in the S_4 index.

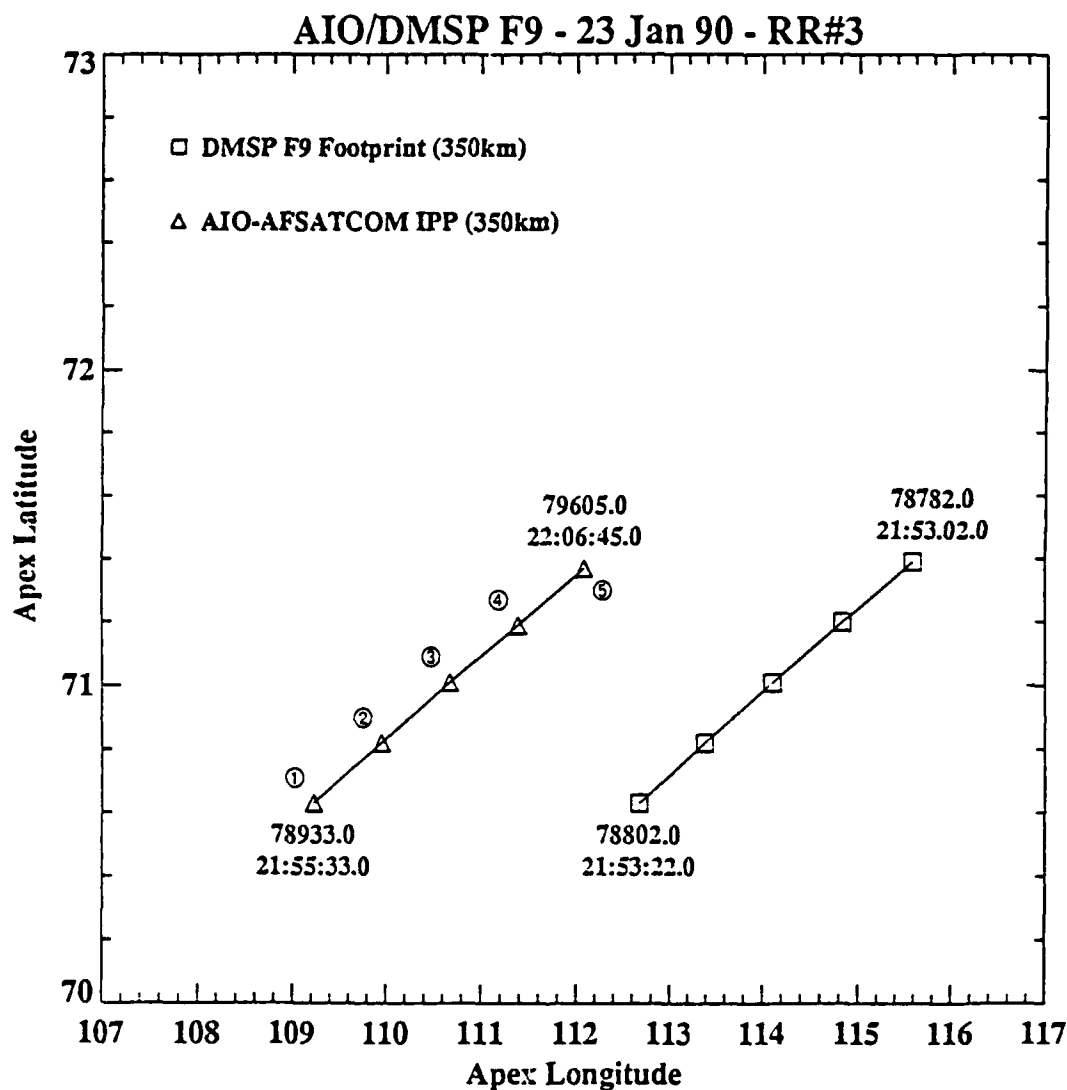
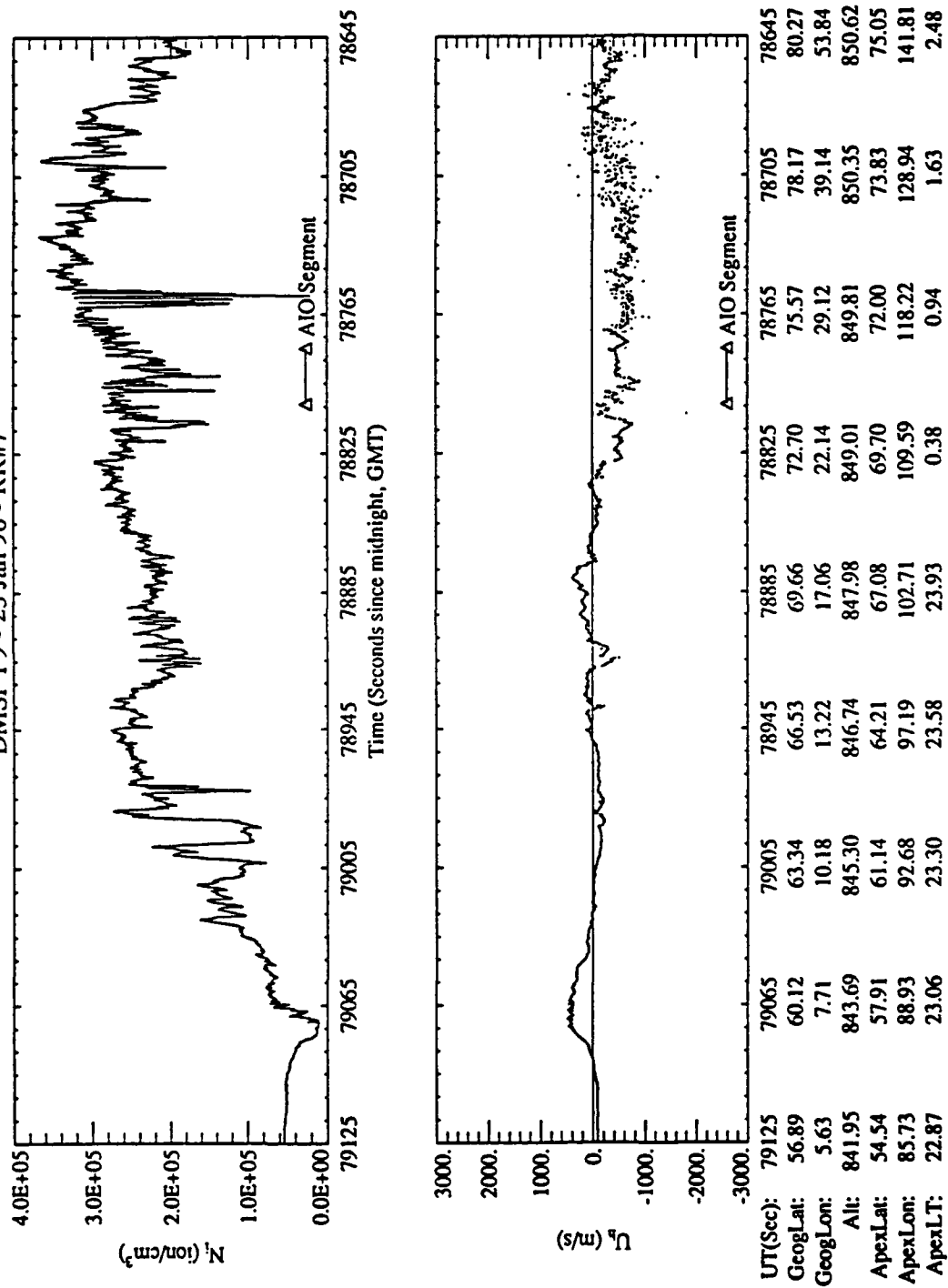


Figure 6. Locations of the DMSP F8 satellite traced down to 350 km altitude and the 350 km ionospheric penetration point (IPP) for the AIO-AFSATCOM link for the 23 January 1990 data set. The location marked by a cross-bar on both traces indicates the point where the two experiments were collecting data on the same geomagnetic latitude. The symbols are plotted at center-points for data samples used to generate various irregularity/scintillation parameters. The circled numbers on the AIO-AFSATCOM trace are used to identify individual data samples.



Time / 350 km Trace Position

Figure 7. Plots from the DMSP SSIES/SM (total ion density) and SSIES/DM (horizontal cross-track ion drift velocity) sensors over the geomagnetic (apex) latitude range of 55° to 75° for 23 January 1990. The latitude range covered by the AIO-AFSATCOM data set (IPP) is indicated in both plots. These data are plotted in time-reverse order so that latitude increases from left to right, and the locations printed along the x-axis are for the DMSP 350 km footprint locations.

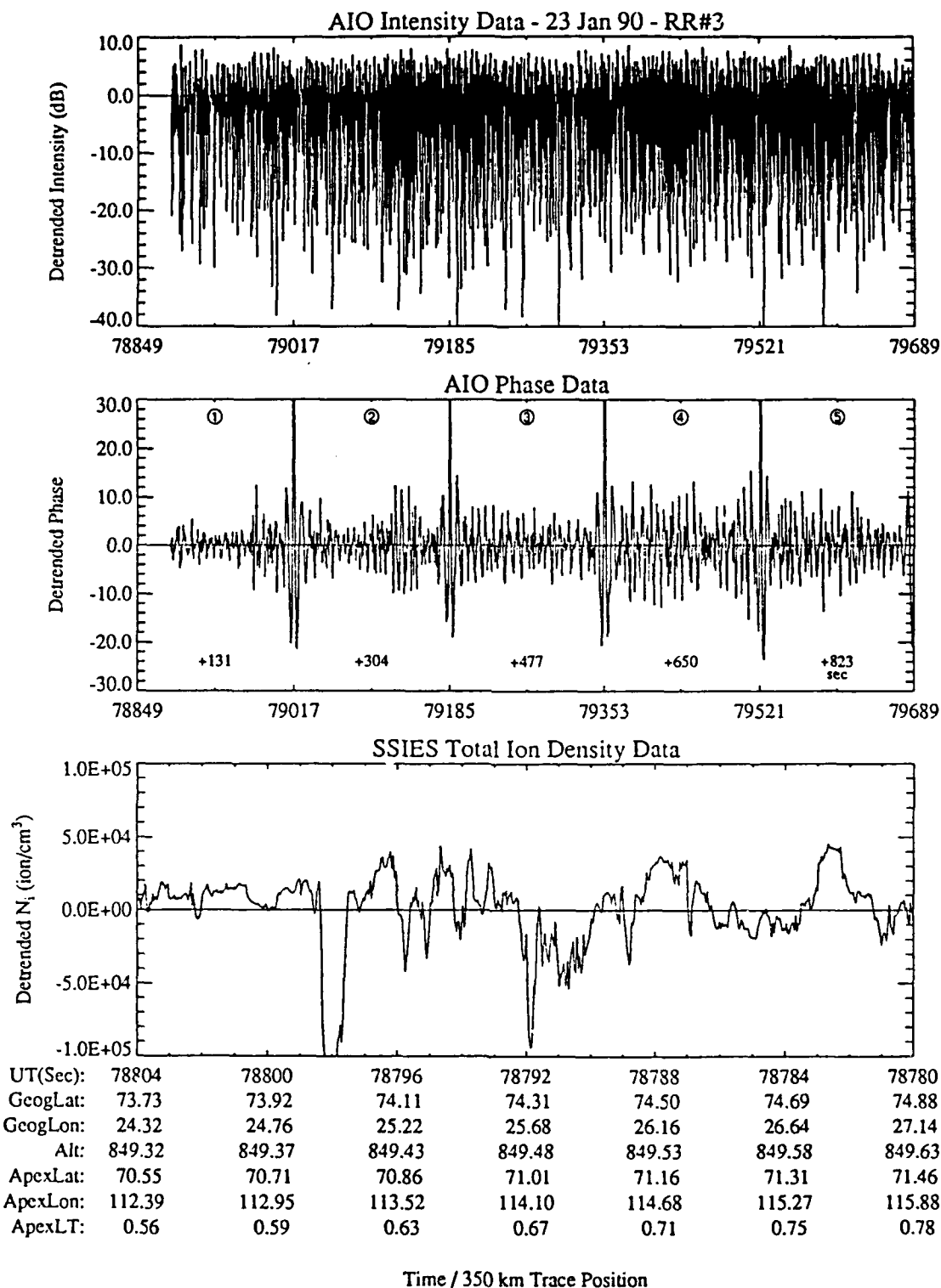


Figure 8. Data from the AIO-AFSATCOM link and the DMSP SSIES/SM sensor for the intervals shown in Figure 6. The top plot is the detrended intensity and the middle plot is the detrended phase from the AIO-AFSATCOM link. The times along the bottom of the phase plot are the time difference (in seconds) between the AIO-AFSATCOM observation and the corresponding DMSP/SSIES one. The bottom plot is the detrended SSIES/SM total ion density data. The SSIES/SM data is plotted in time-reverse order so that all three plots cover the same range of geomagnetic latitudes. The locations plotted with the SSIES/SM data are for the DMSP 350 km footprint locations.

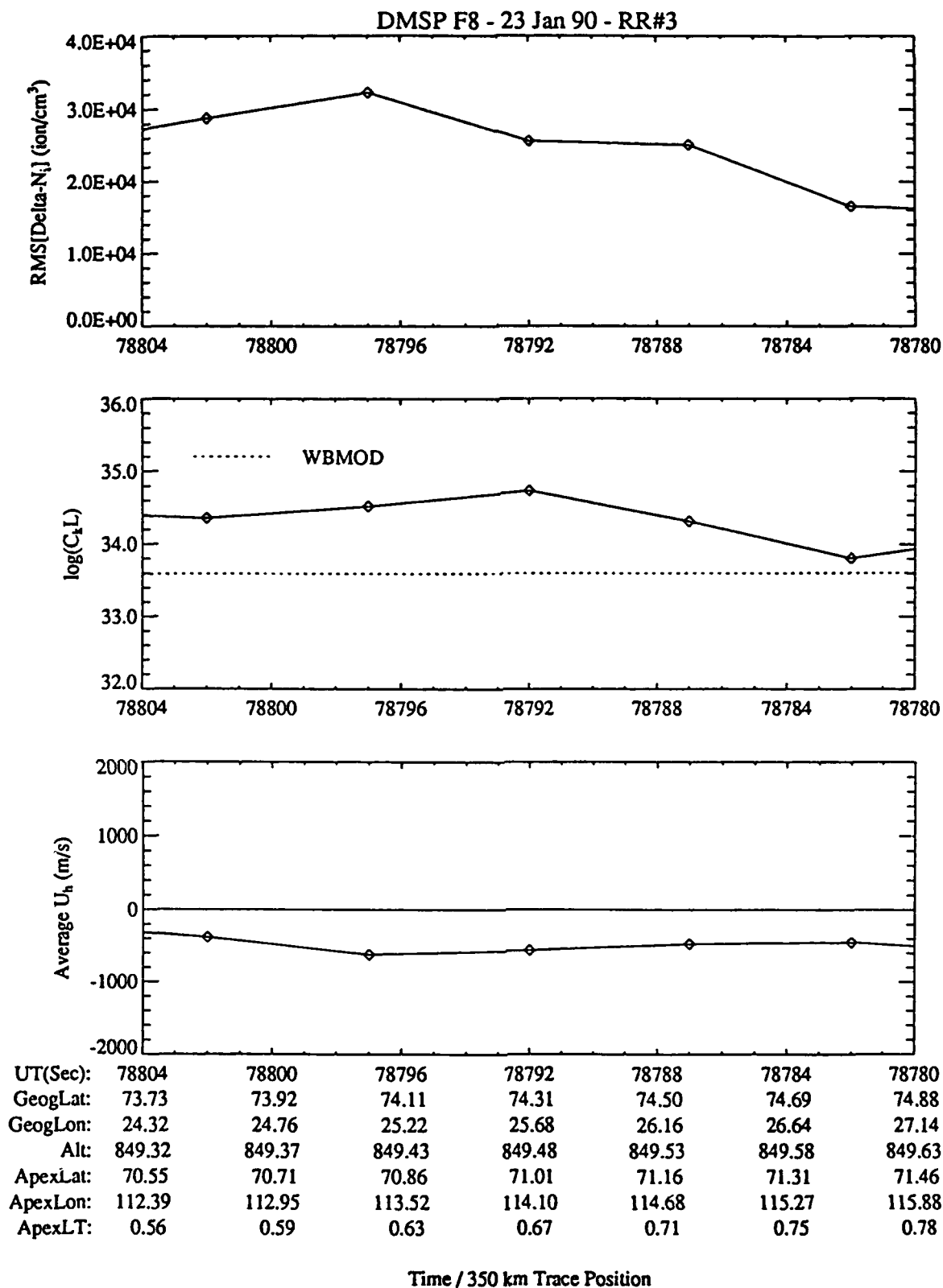


Figure 9. Data derived from the DMSP SSIES/SM and DM sensor data for 23 January 1990. The top plot is of the RMS variance in ΔN_i from five-second SM sensor data samples centered on the time for which the data are plotted. The middle plot is of the $C_k L$ values derived from the ΔN_i data (solid lines) and from the WBMOD model (dotted line). The bottom plot is of five-second averages of the DM sensor horizontal cross-track drift velocity.

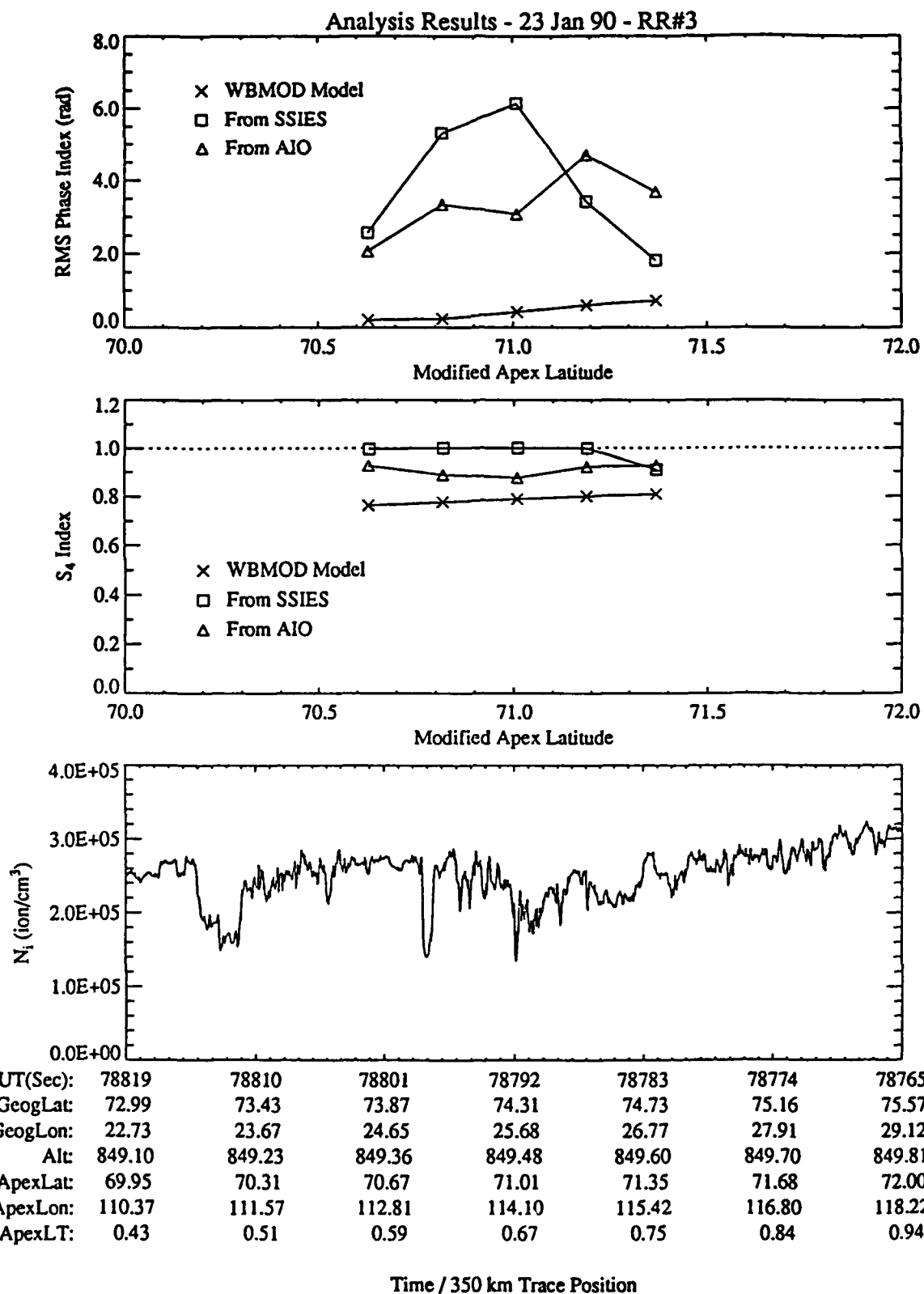


Figure 10. Analysis results for the 23 January 1990 data sets. The top plot shows the variation of σ_ϕ (RMS phase) with geomagnetic latitude as calculated from the WBMOD model, from the SSIES C_kL and U_h data, and from the AIO-AFSATCOM phase data. The middle plot shows the variation of S_4 with geomagnetic latitude from the same sources. The bottom plot shows the variation of total ion density over the same latitude range. The arrows indicate the time/location of closest approach.

2.3 24 January 1990 — DMSP F8 — AIO RR#4

The time of closest approach for this data set was at 18:43:00 GMT. The SSN for this date was 202, and the K_p values for the three-hour period prior to, including, and after the TCA were 3+, 5, and 5. The nominal separation between the DMSP footprint and the AIO-AFSATCOM IPP was roughly 3.0° of longitude (120 km), and the nominal elevation angle of the AIO-AFSATCOM link was 67° . The plots showing the data for this day are given in Figures 11 through 15.

As can be seen in Figure 12, the latitude range covered by the AIO-AFSATCOM data set analyzed started well poleward of the location of the transition from the smooth (mid-latitude) ionosphere to the irregular (auroral) ionosphere at 57.9° geomagnetic (apex) latitude, and just poleward of several large density-enhancement features seen in the density data. The detrended intensity and phase AIO-AFSATCOM records (top two plots in Figure 13) both show patches of enhanced scintillation, while the detrended *in situ* density (bottom plot in Figure 13) shows relatively low irregularity strength throughout the data segment. This is reflected in the plots in Figure 14 which show low values for both $\text{RMS}(\Delta N_i)$ and $C_k L$. Also note the relatively low cross-track drift velocities (less than 150 m/s).

This difference between the AIO-AFSATCOM and DMSP records is reflected in the analyses shown in Figure 15. The σ_o values generated from the DMSP data are markedly lower than the corresponding AIO-AFSATCOM values, due partly to log $C_k L$ values and partly to the low *in situ* drift velocities, and most of the DMSP-derived S_4 values are too low as well. The results from this data set will be discussed in more detail in Section 4.

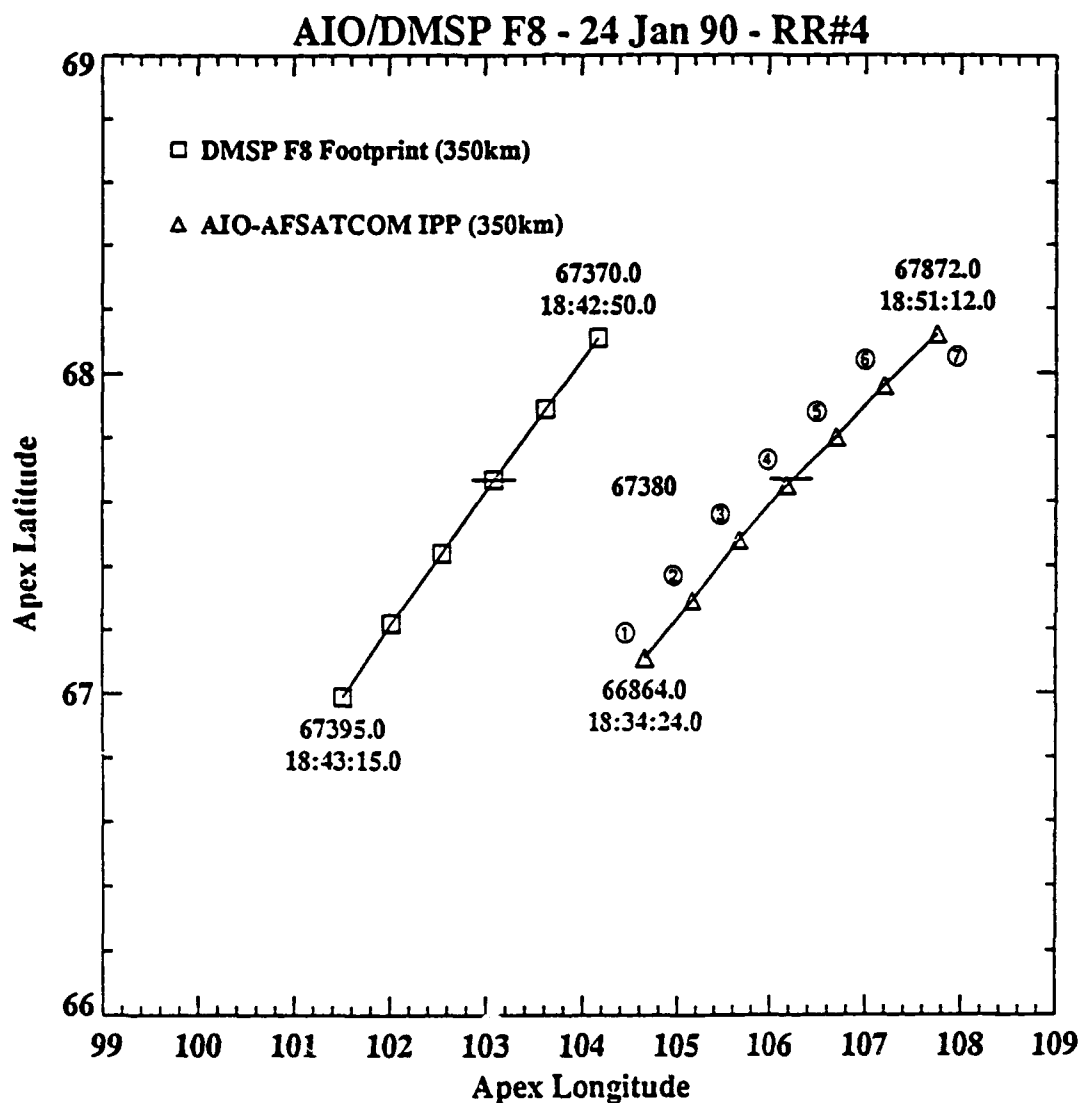


Figure 11. Locations of the DMSP F8 satellite traced down to 350 km altitude and the 350 km ionospheric penetration point (IPP) for the AIO-AFSATCOM link for the 24 January 1990 data set. The location marked by a cross-bar on both traces indicates the point where the two experiments were collecting data on the same geomagnetic latitude. The symbols are plotted at center-points for data samples used to generate various irregularity/scintillation parameters. The circled numbers on the AIO-AFSATCOM trace are used to identify individual data samples.

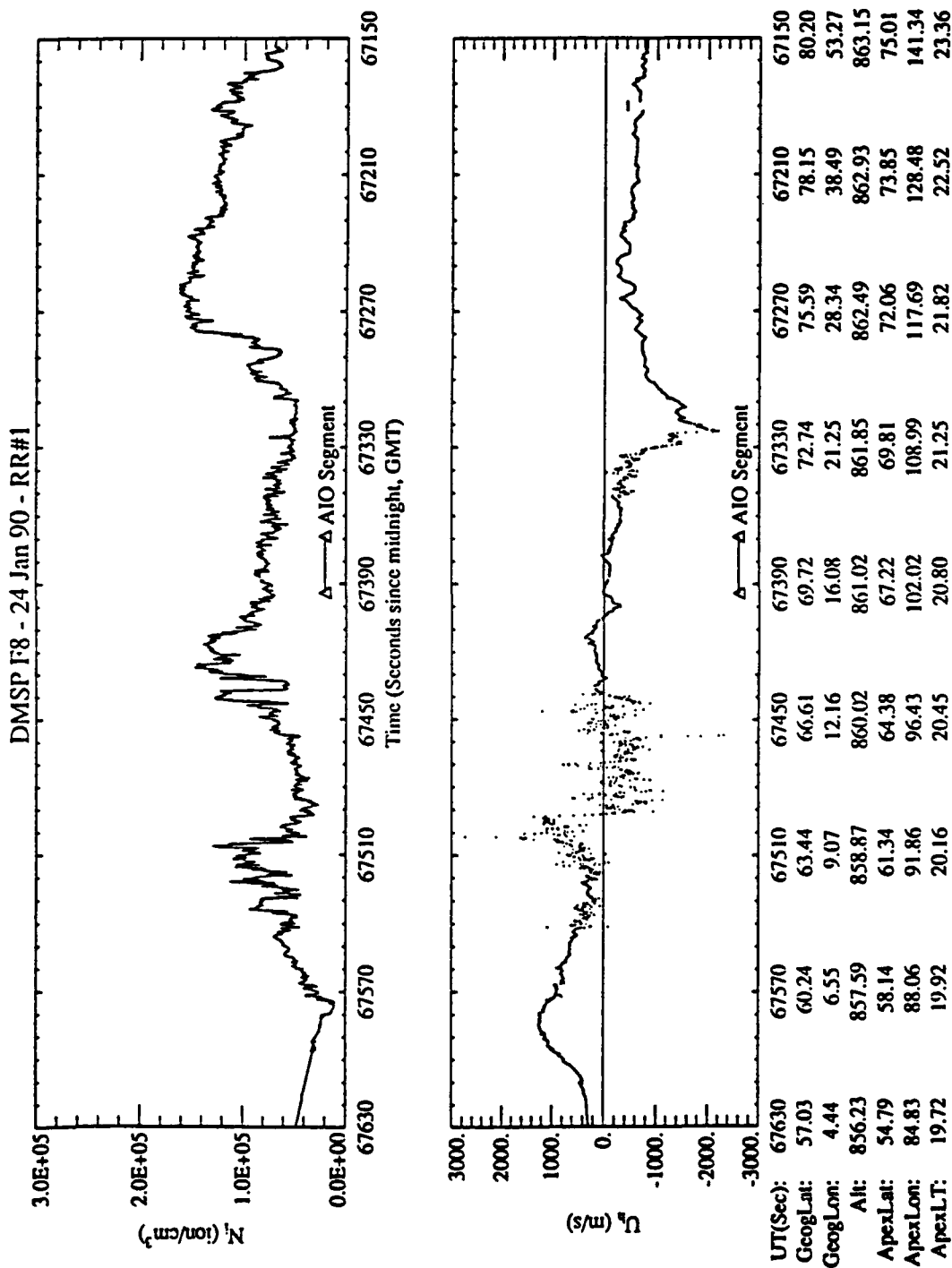
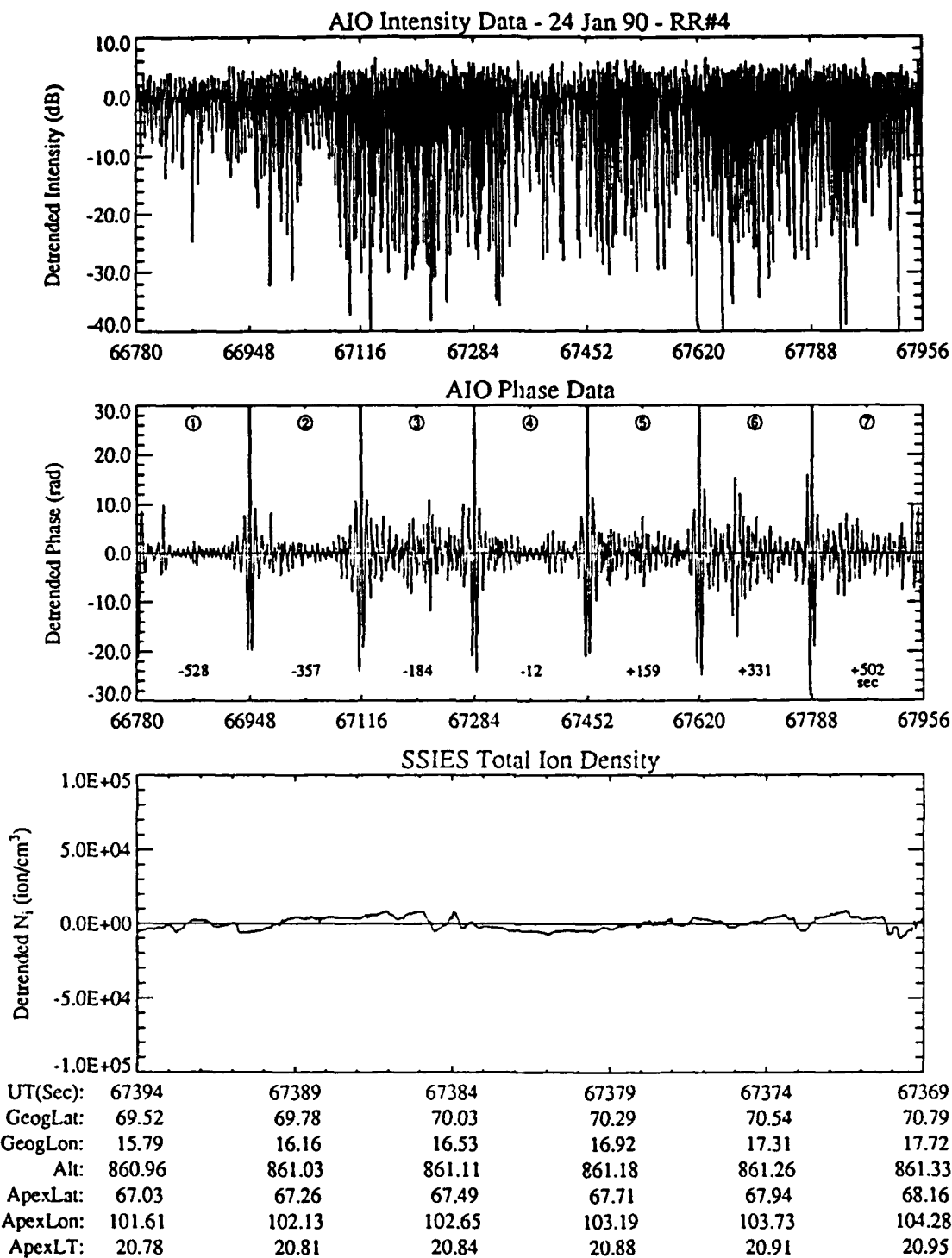


Figure 12. Plots from the DMSP SSIES/SM (total ion density) and SSIES/DM (horizontal cross-track ion drift velocity) sensors over the geomagnetic (apex) latitude range of 55° to 75° for 24 January 1990. The latitude range covered by the AIO-AFSATCOM data set (IPP) is indicated in both plots. These data are plotted in time-reverse order so that latitude increases from left to right, and the locations printed along the x-axis are for the DMSP 350 km footprint locations.



Time / 350 km Trace Position

Figure 13. Data from the AIO-AFSATCOM link and the DMSP SSIES/SM sensor for the intervals shown in Figure 11. The top plot is the detrended intensity and the middle plot is the detrended phase from the AIO-AFSATCOM link. The times along the bottom of the phase plot are the time difference (in seconds) between the AIO-AFSATCOM observation and the corresponding DMSP/SSIES one. The bottom plot is the detrended SSIES/SM total ion density data. The SSIES/SM data is plotted in time-reverse order so that all three plots cover the same range of geomagnetic latitudes. The locations plotted with the SSIES/SM data are for the DMSP 350 km footprint locations.

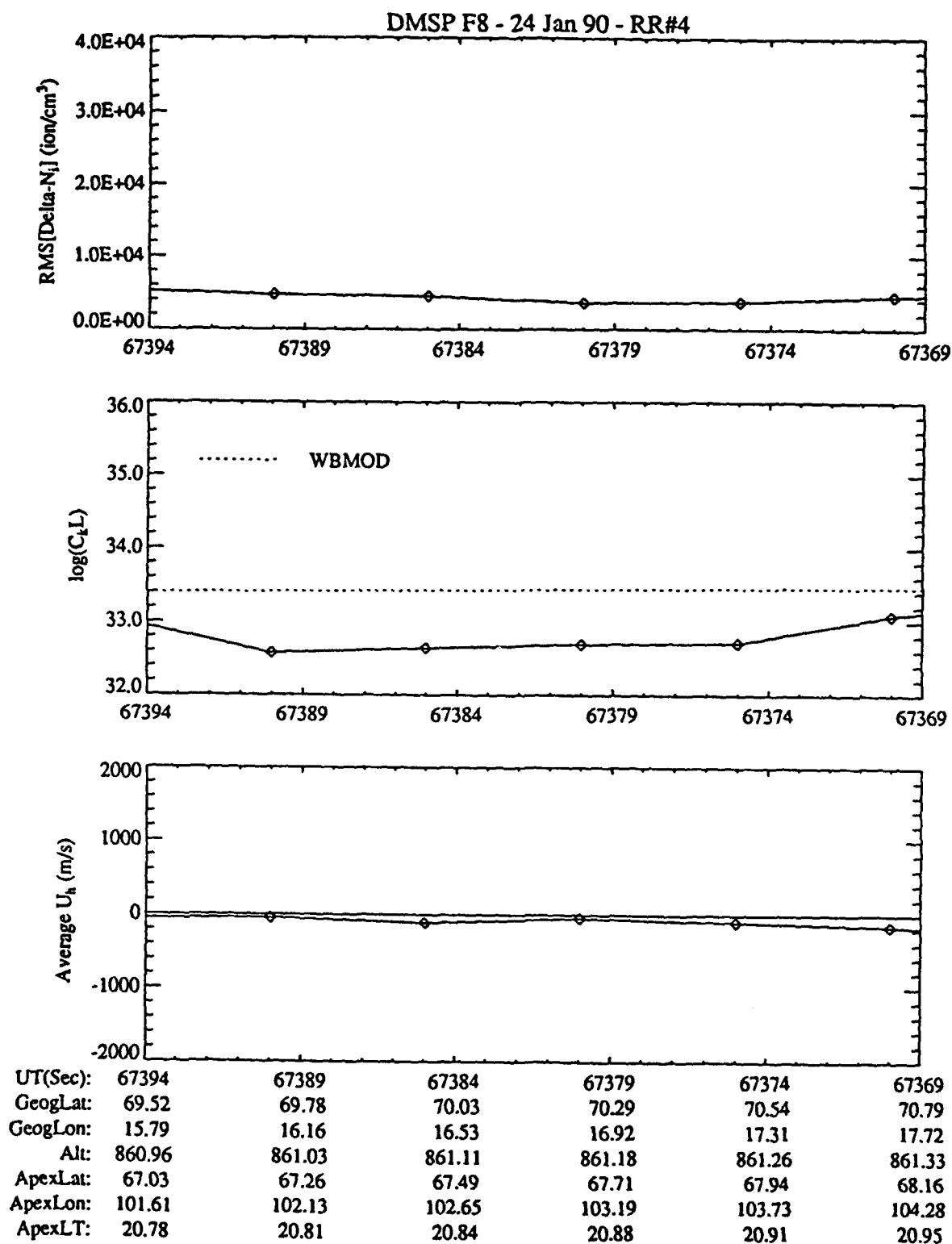


Figure 14. Data derived from the DMSP SSIES/SM and DM sensor data for 24 January 1990. The top plot is of the RMS variance in ΔN_i from five-second SM sensor data samples centered on the time for which the data are plotted. The middle plot is of the $C_k L$ values derived from the ΔN_i data (solid lines) and from the WBMOD model (dotted line). The bottom plot is of five-second averages of the DM sensor horizontal cross-track drift velocity.

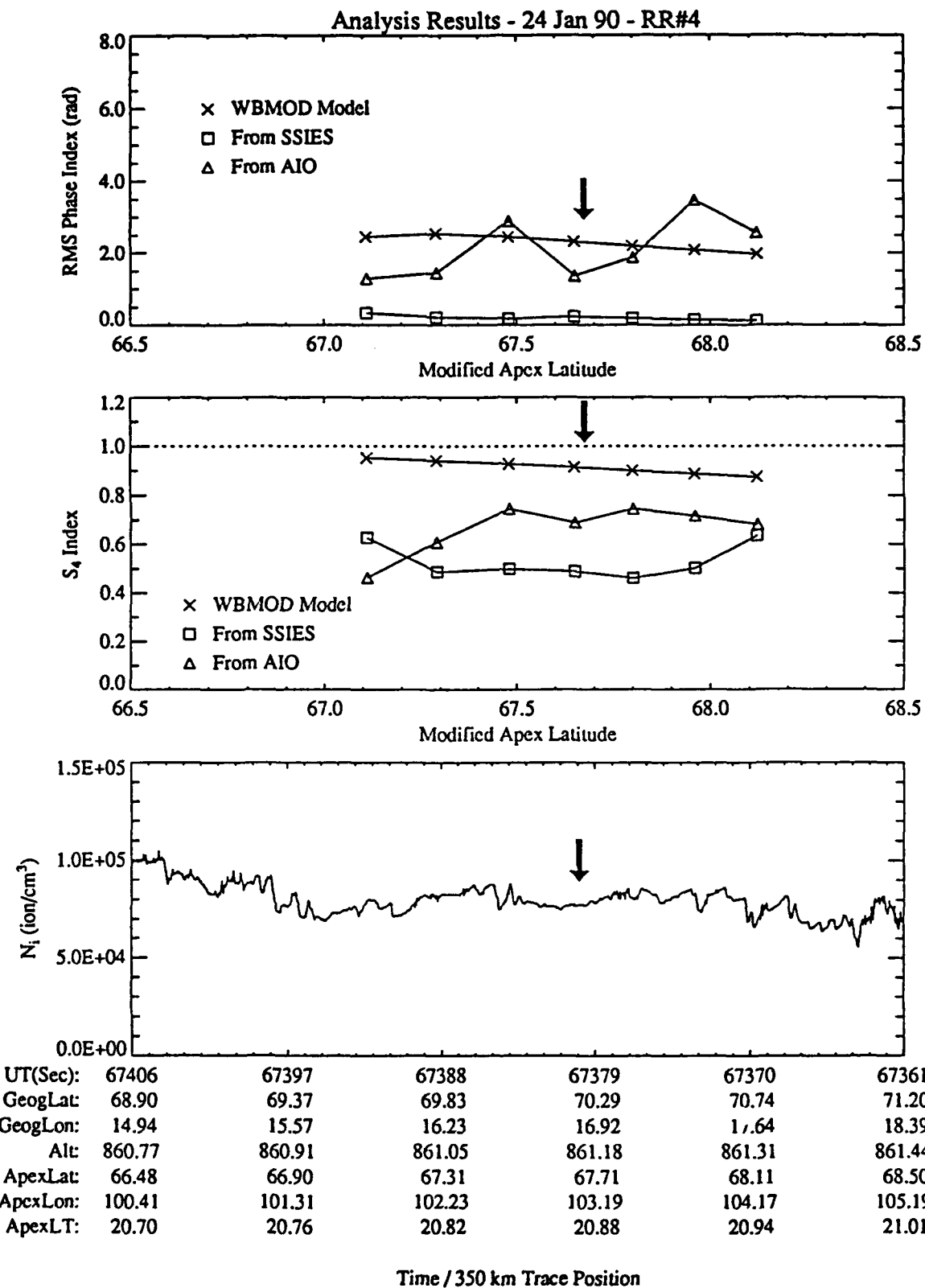


Figure 15. Analysis results for the 24 January 1990 data sets. The top plot shows the variation of σ_p (RMS phase) with geomagnetic latitude as calculated from the WBMOD model, from the SSIES $C_k L$ and U_h data, and from the AIO-AFSATCOM phase data. The middle plot shows the variation of S_4 with geomagnetic latitude from the same sources. The bottom plot shows the variation of total ion density over the same latitude range. The arrows indicate the time/location of closest approach.

2.4 25 January 1990 — DMSP F8 — AIO RR#5

The time of closest approach for this data set was at 18:29:56 GMT. The SSN for this date was 197, and the K_p values for the three-hour period prior to, including, and after the TCA were 3+, 2, and 2. The nominal separation between the DMSP footprint and the AIO-AFSATCOM IPP was roughly 2.5° of longitude (105 km), and the nominal elevation angle of the AIO-AFSATCOM link was 67° . The plots showing the data for this day are given in Figures 16 through 20.

As can be seen in Figure 17, the latitude range covered by the AIO-AFSATCOM data set analyzed started just poleward of the location of the transition from the smooth (mid-latitude) ionosphere to the irregular (auroral) ionosphere at 62.6° geomagnetic (apex) latitude. The detrended intensity and phase AIO-AFSATCOM records (top two plots in Figure 18) both show patches of enhanced scintillation, while the detrended *in situ* density (bottom plot in Figure 18) shows moderately-low irregularity strength throughout the data segment. The $C_k L$ values derived from the DMSP data are roughly the same as those derived from WBMOD for existing conditions (Figure 19).

The plots in Figure 20 show that the match between the two σ_ϕ data sets was quite good throughout the pass, but that the DMSP-derived S_4 values were generally higher than the corresponding AIO-AFSATCOM values by roughly the same amount that the AIO-AFSATCOM values exceeded the DMSP values in the 24 January 1990 analysis.

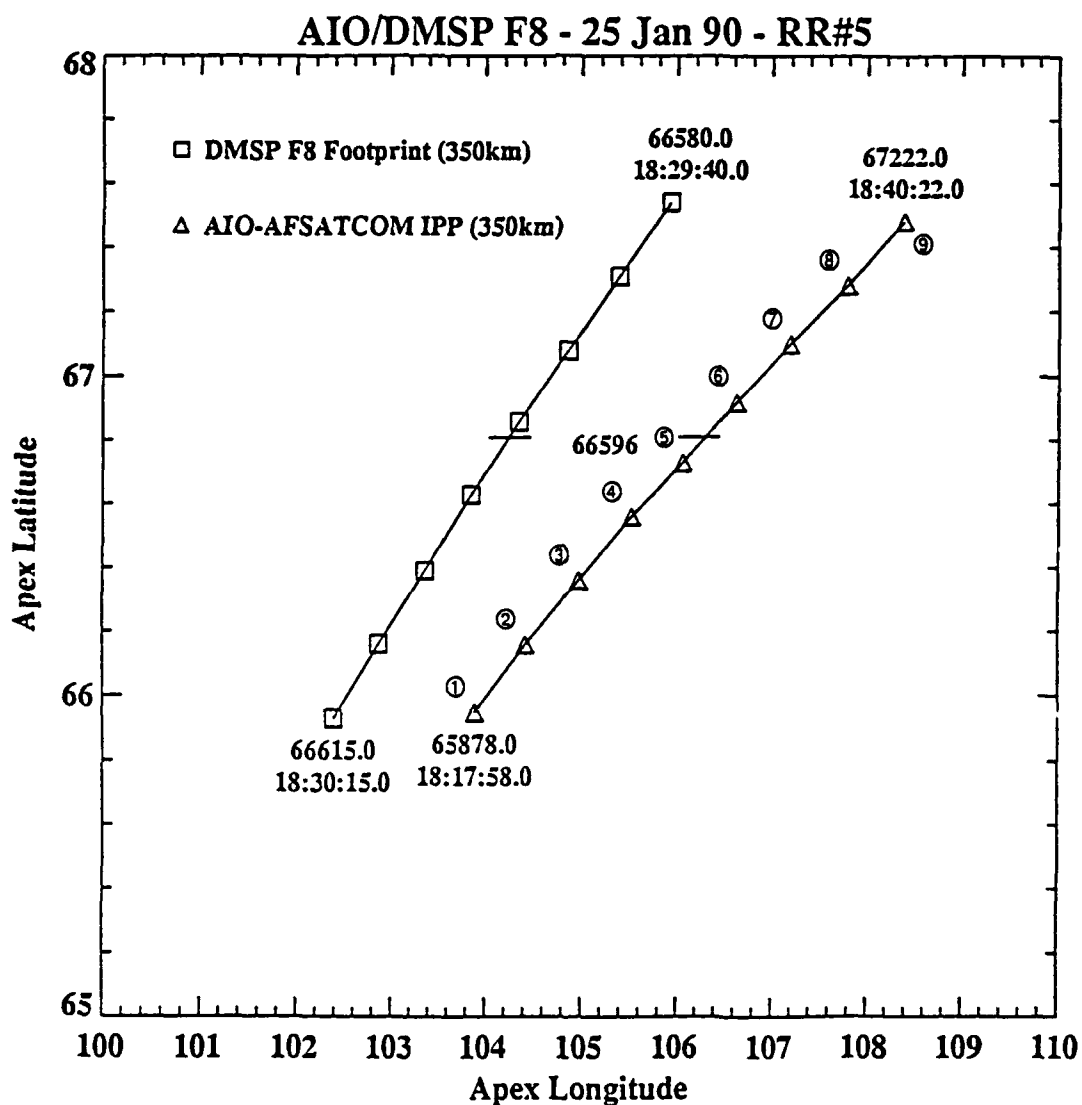


Figure 16. Locations of the DMSP F8 satellite traced down to 350 km altitude and the 350 km ionospheric penetration point (IPP) for the AIO-AFSATCOM link for the 25 January 1990 data set. The location marked by a cross-bar on both traces indicates the point where the two experiments were collecting data on the same geomagnetic latitude. The symbols are plotted at center-points for data samples used to generate various irregularity/scintillation parameters. The circled numbers on the AIO-AFSATCOM trace are used to identify individual data samples.

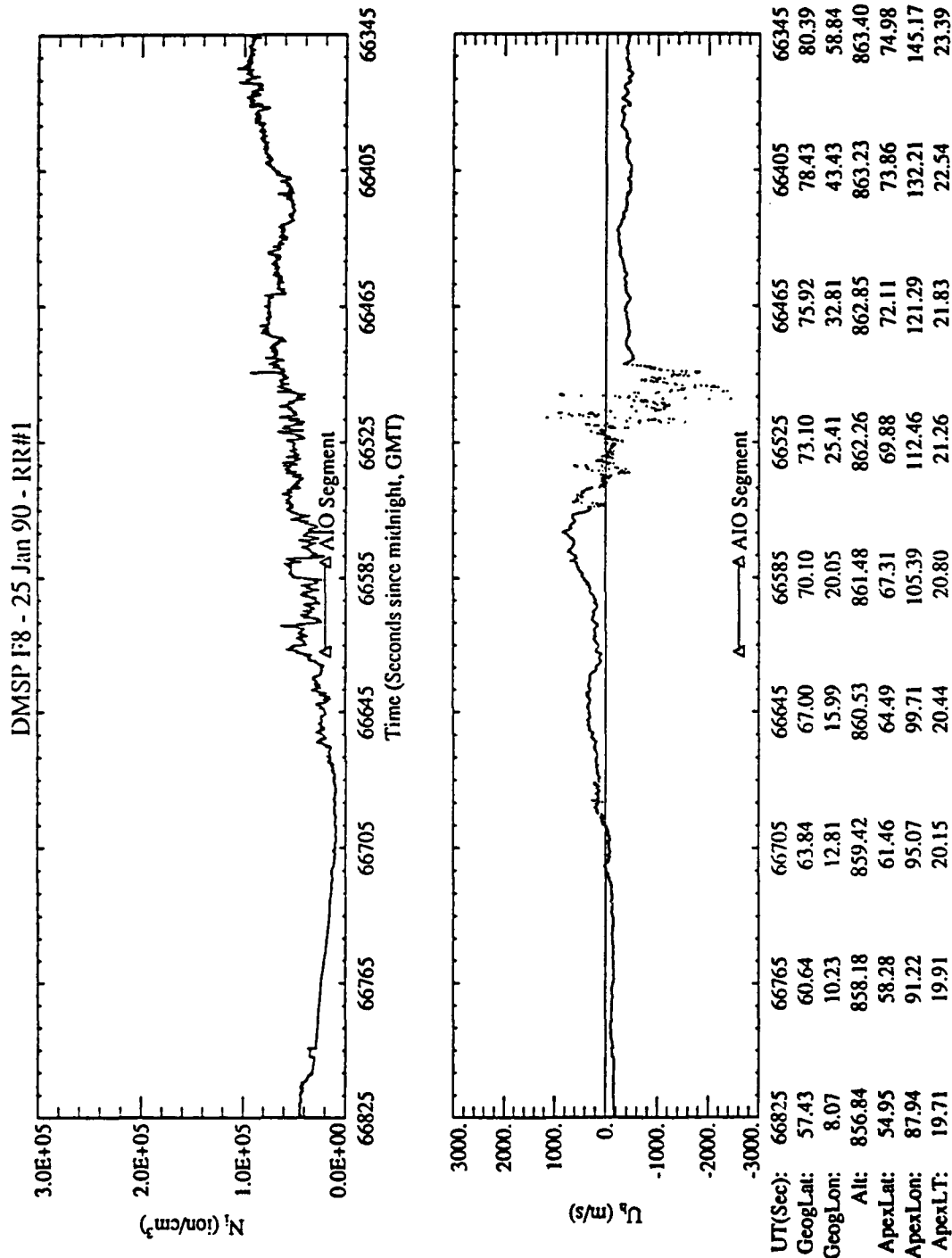


Figure 17. Plots from the DMSP SSIES/SM (total ion density) and SSIES/DM (horizontal cross-track ion drift velocity) sensors over the geomagnetic (apex) latitude range of 55° to 75° for 25 January 1990. The latitude range covered by the AIO-AFSATCOM data set (IPP) is indicated in the plots. These data are plotted in time-reverse order so that latitude increases from left to right, and the locations printed along the x-axis are for the DMSP 350 km footprint locations.

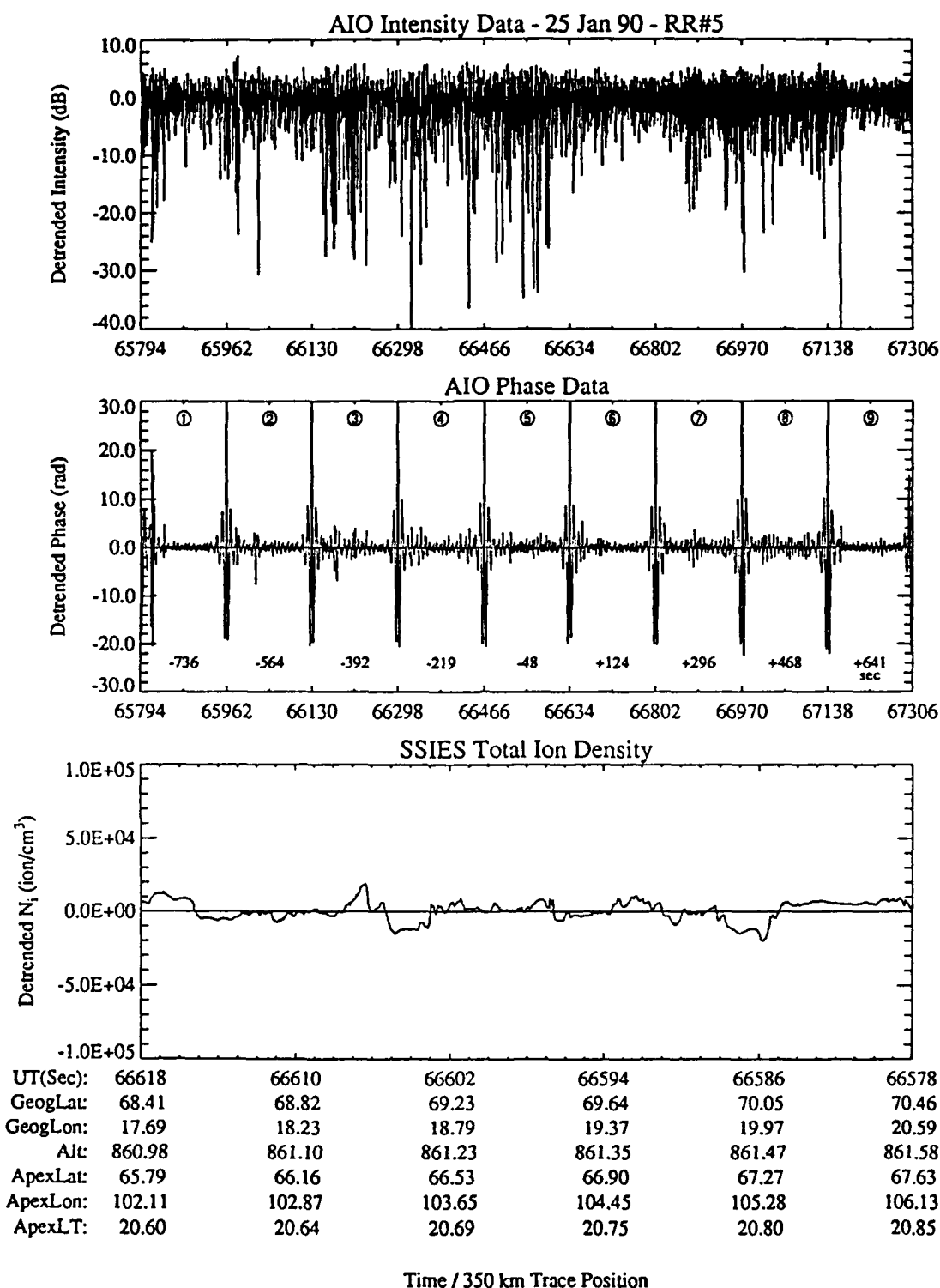


Figure 18. Data from the AIO-AFSATCOM link and the DMSP SSIES/SM sensor for the intervals shown in Figure 16. The top plot is the detrended intensity and the middle plot is the detrended phase from the AIO-AFSATCOM link. The times along the bottom of the phase plot are the time difference (in seconds) between the AIO-AFSATCOM observation and the corresponding DMSP/SSIES one. The bottom plot is the detrended SSIES/SM total ion density data. The SSIES/SM data is plotted in time-reverse order so that all three plots cover the same range of geomagnetic latitudes. The locations plotted with the SSIES/SM data are for the DMSP 350 km footprint locations.

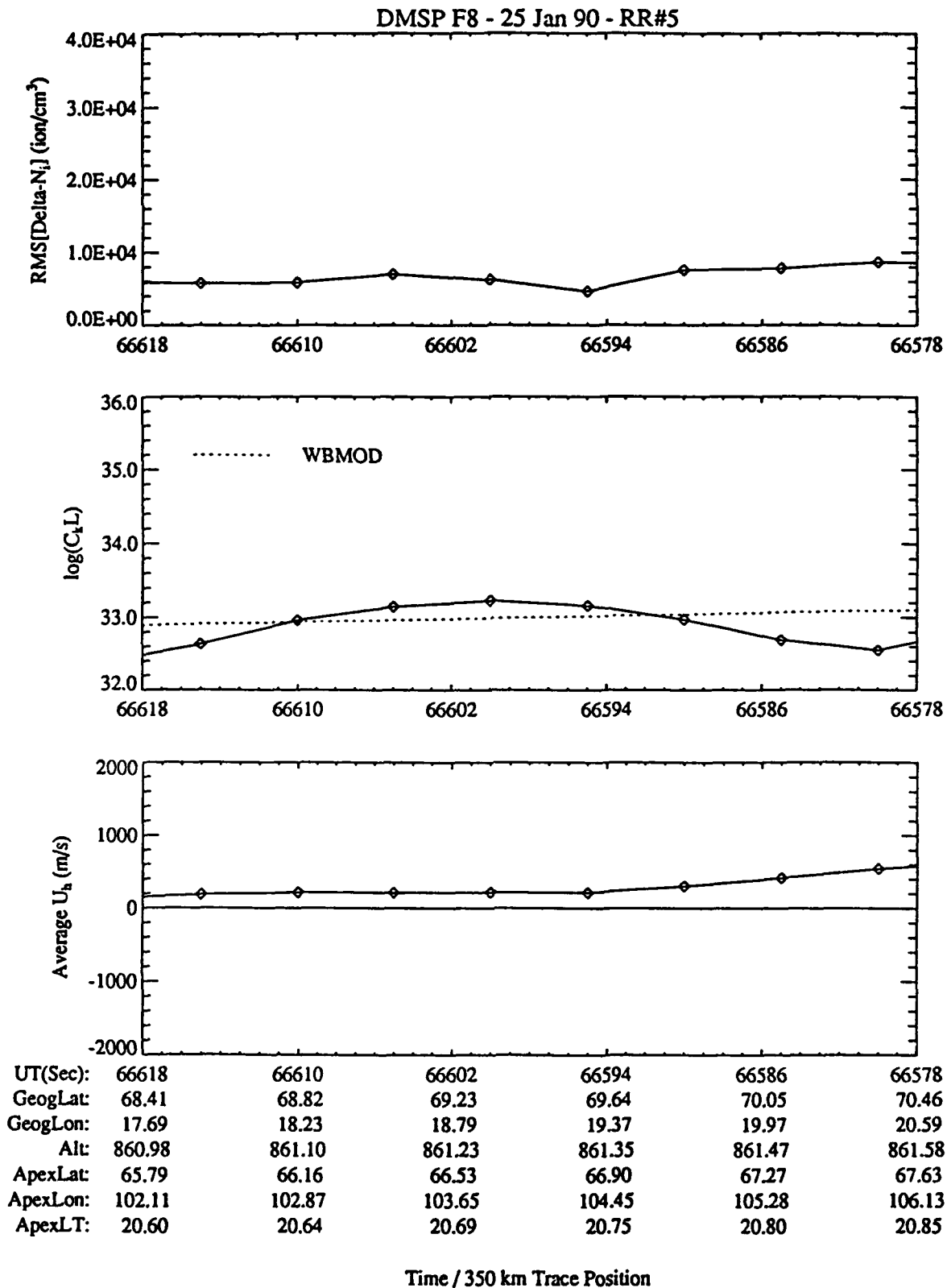


Figure 19. Data derived from the DMSP SSIES/SM and DM sensor data for 25 January 1990. The top plot is of the RMS variance in ΔN_i from five-second SM sensor data samples centered on the time for which the data are plotted. The middle plot is of the $C_i L$ values derived from the ΔN_i data (solid lines) and from the WBMOD model (dotted line). The bottom plot is of five-second averages of the DM sensor horizontal cross-track drift velocity.

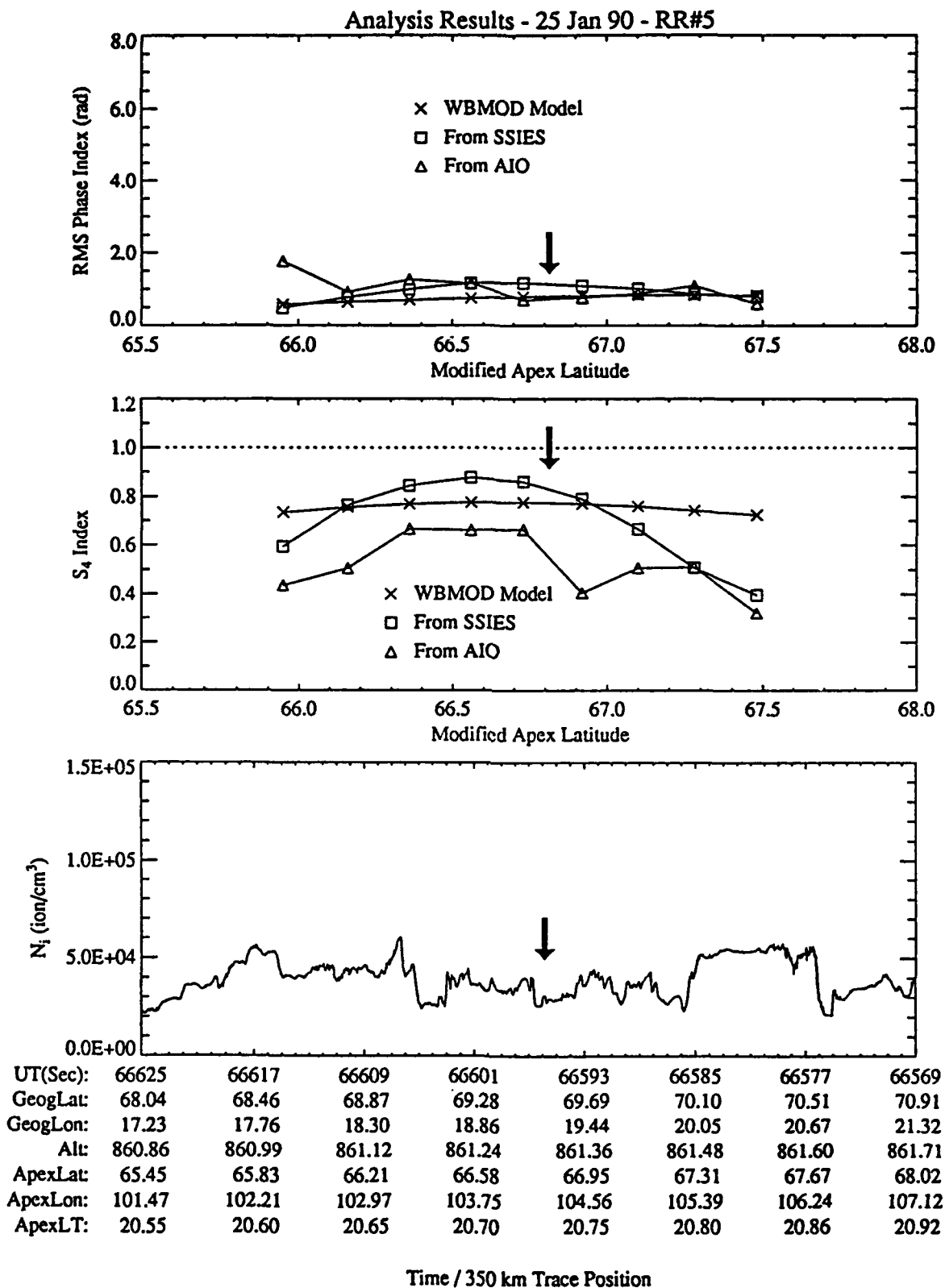


Figure 20. Analysis results for the 25 January 1990 data sets. The top plot shows the variation of σ_ϕ (RMS phase) with geomagnetic latitude as calculated from the WBMOD model, from the SSIES C_kL and U_h data, and from the AIO-AFSATCOM phase data. The middle plot shows the variation of S_4 with geomagnetic latitude from the same sources. The bottom plot shows the variation of total ion density over the same latitude range. The arrows indicate the time/location of closest approach.

2.5 28 January 1990 — DMSP F9 — AIO RR#7

The time of closest approach for this data set was at 21:51:13 GMT. The SSN for this date was 193, and the K_p values for the three-hour period prior to, including, and after the TCA were 3-, 3, and 4+. The nominal separation between the DMSP footprint and the AIO-AFSATCOM IPP was roughly 4.0° of longitude (165 km), and the nominal elevation angle of the AIO-AFSATCOM link was 37° . The plots showing the data for this day are given in Figures 21 through 25.

As can be seen in Figure 22, the latitude range covered by the AIO-AFSATCOM data set analyzed started just poleward of the location of the transition from the smooth (mid-latitude) ionosphere to the irregular (auroral) ionosphere at 62.8° geomagnetic (apex) latitude and spanned a small density enhancement feature on the poleward side of the auroral zone. The detrended intensity and phase AIO-AFSATCOM records (top two plots in Figure 23) both show patches of enhanced scintillation, while the detrended *in situ* density (bottom plot in Figure 23) shows relatively high irregularity strength at the equatorward edge of the data set tending to lower strength levels at the poleward edge. The C_kL values derived from the DMSP data are about an order of magnitude higher than the WBMOD values at the equatorward edge of the set dropping to about an order of magnitude lower at the poleward edge (Figure 19). The $\text{RMS}(\Delta N_i)$ data in Figure 19 shows this same trend, and the *in situ* drift velocity peaks at a value of roughly 1 km/sec a third of the way into the set, dropping to near zero near the poleward edge.

The results for this date are shown in Figure 25. The agreement between the two data sets is not that good. While the phase results (σ_ϕ) would be in general agreement if the DMSP data were shifted northward slightly, the intensity results (S_4) do not agree at all. The AIO-AFSATCOM data shows a roughly constant S_4 of about 0.8, while the DMSP data shows a steady drop in S_4 from near saturation at the equatorward edge to 0.3 at the poleward edge. [Note: A close inspection of the AIO-AFSATCOM data indicates that the large phase excursions in the first half of the data sets labeled 4 and 5 in the middle plot of Figure 23 are somewhat suspect, particularly those in set 5 which were accompanied by a very large spike-enhancement in the signal intensity. The results shown in Figure 25 for the last two AIO-AFSATCOM data points were calculated using data from the last half of the 120-second data samples only.]

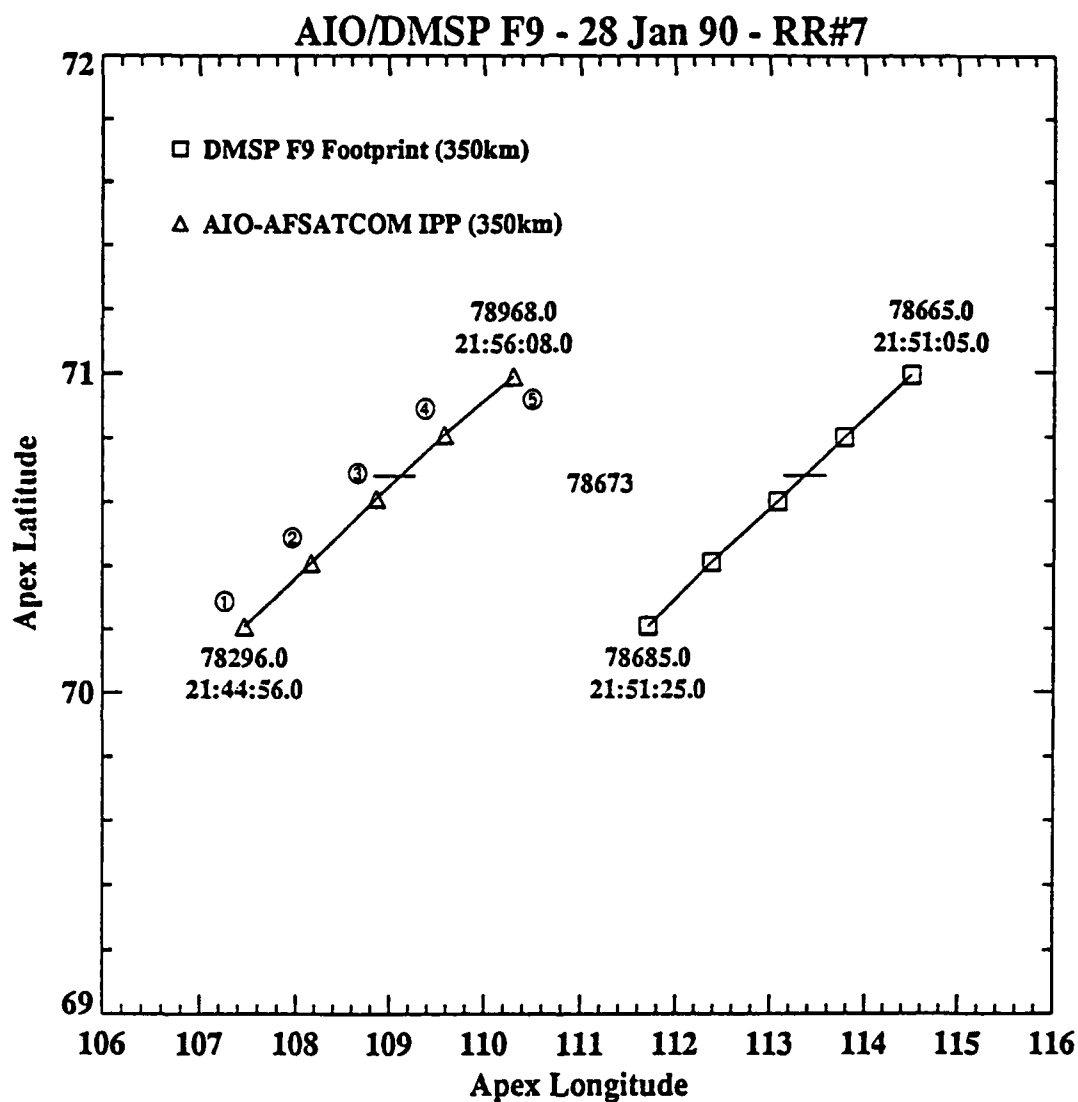


Figure 21. Locations of the DMSP F8 satellite traced down to 350 km altitude and the 350 km ionospheric penetration point (IPP) for the AIO-AFSATCOM link for the 28 January 1990 data set. The location marked by a cross-bar on both traces indicates the point where the two experiments were collecting data on the same geomagnetic latitude. The symbols are plotted at center-points for data samples used to generate various irregularity/scintillation parameters. The circled numbers on the AIO-AFSATCOM trace are used to identify individual data samples.

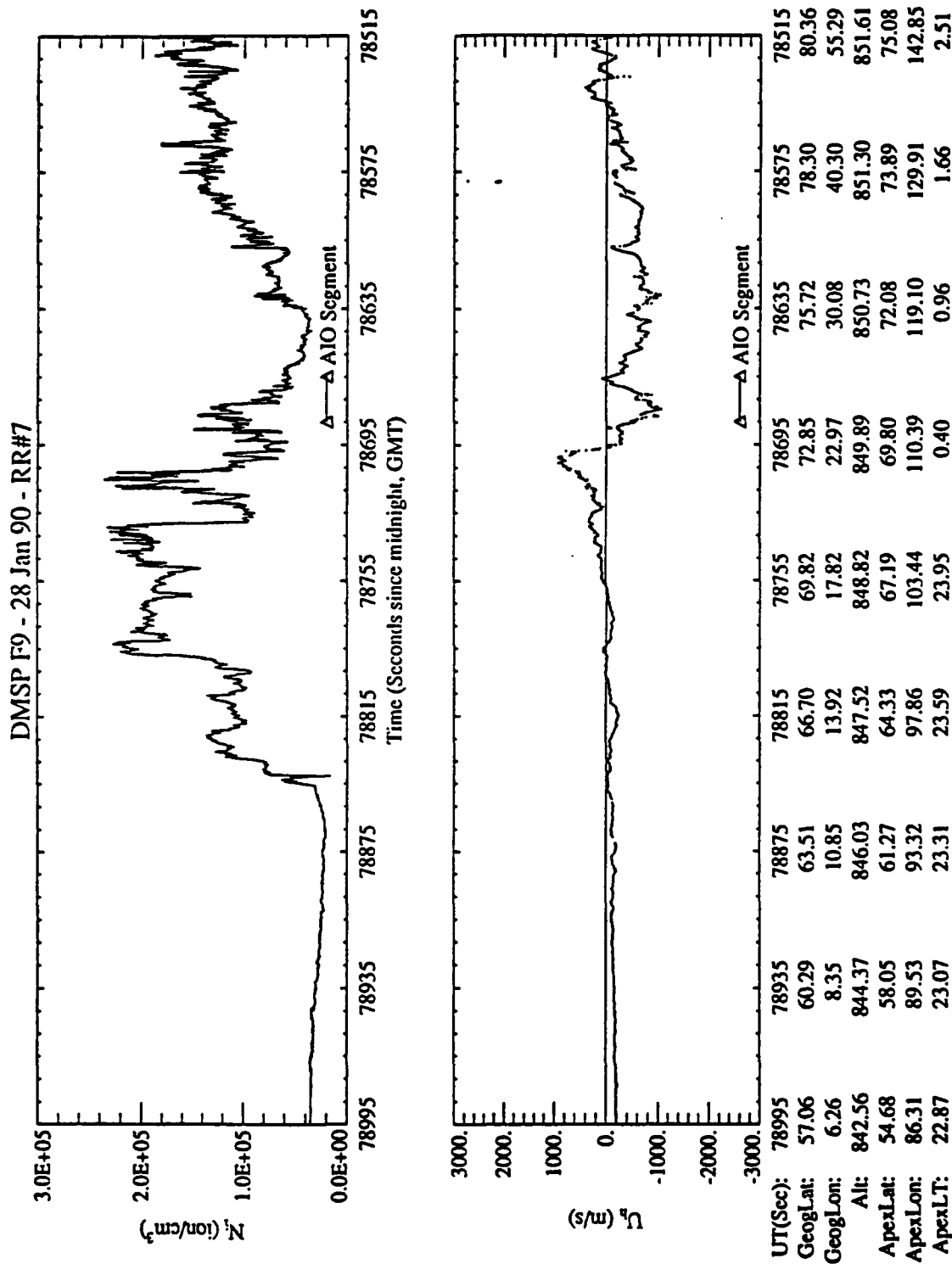
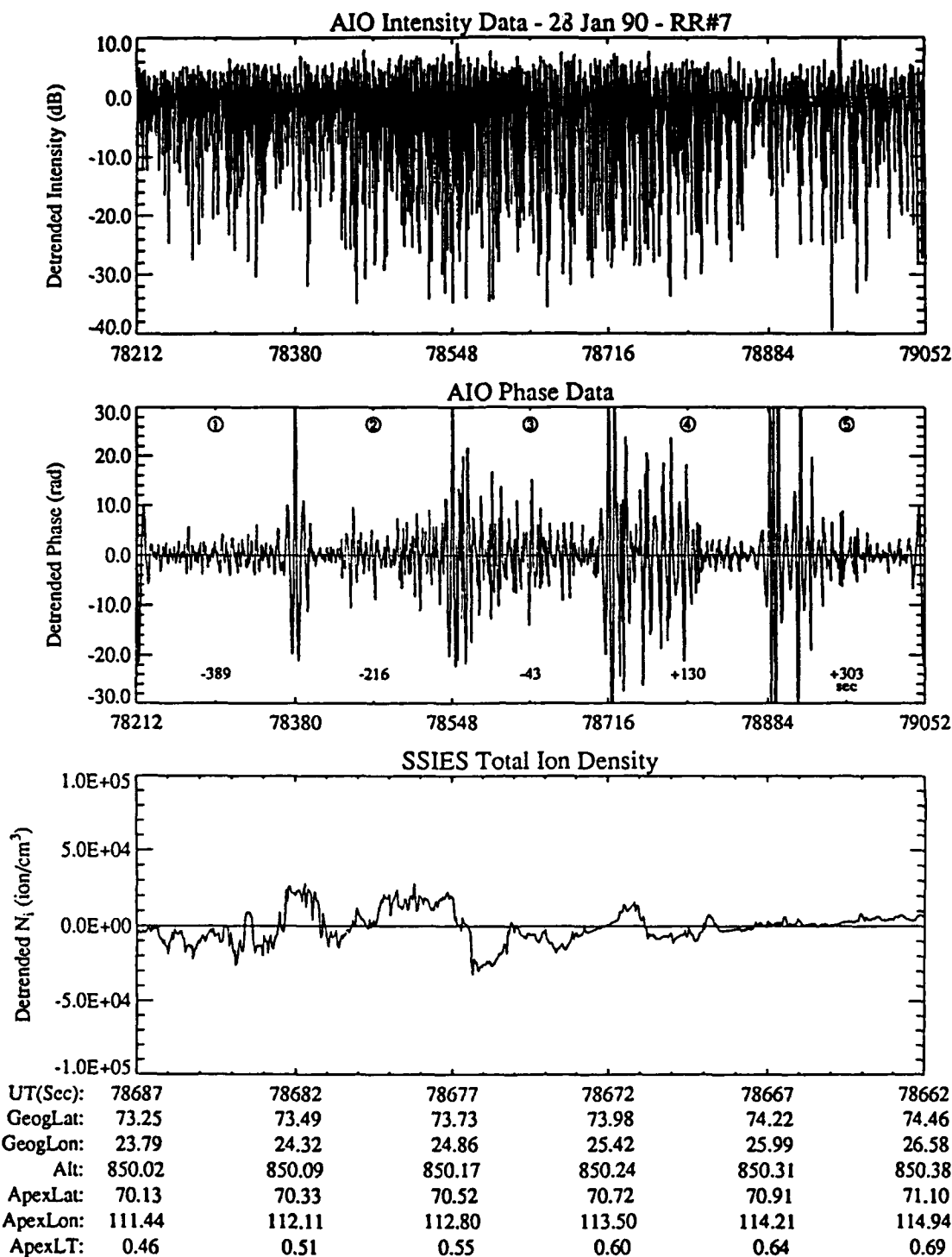


Figure 22. Plots from the DMSP SSIES/SM (total ion density) and SSIES/DM (horizontal cross-track ion drift velocity) sensors over the geomagnetic (apex) latitude range of 55° to 75° for 28 January 1990. The latitude range covered by the AIO-AFSATCOM data set (IPP) is indicated in both plots. These data are plotted in time-reverse order so that latitude increases from left to right, and the locations printed along the x-axis are for the DMSP 350 km footprint locations.



Time / 350 km Trace Position

Figure 23. Data from the AIO-AFSATCOM link and the DMSP SSIES/SM sensor for the intervals shown in Figure 21. The top plot is the detrended intensity and the middle plot is the detrended phase from the AIO-AFSATCOM link. The times along the bottom of the phase plot are the time difference (in seconds) between the AIO-AFSATCOM observation and the corresponding DMSP/SSIES one. The bottom plot is the detrended SSIES/SM total ion density data. The SSIES/SM data is plotted in time-reverse order so that all three plots cover the same range of geomagnetic latitudes. The locations plotted with the SSIES/SM data are for the DMSP 350 km footprint locations.

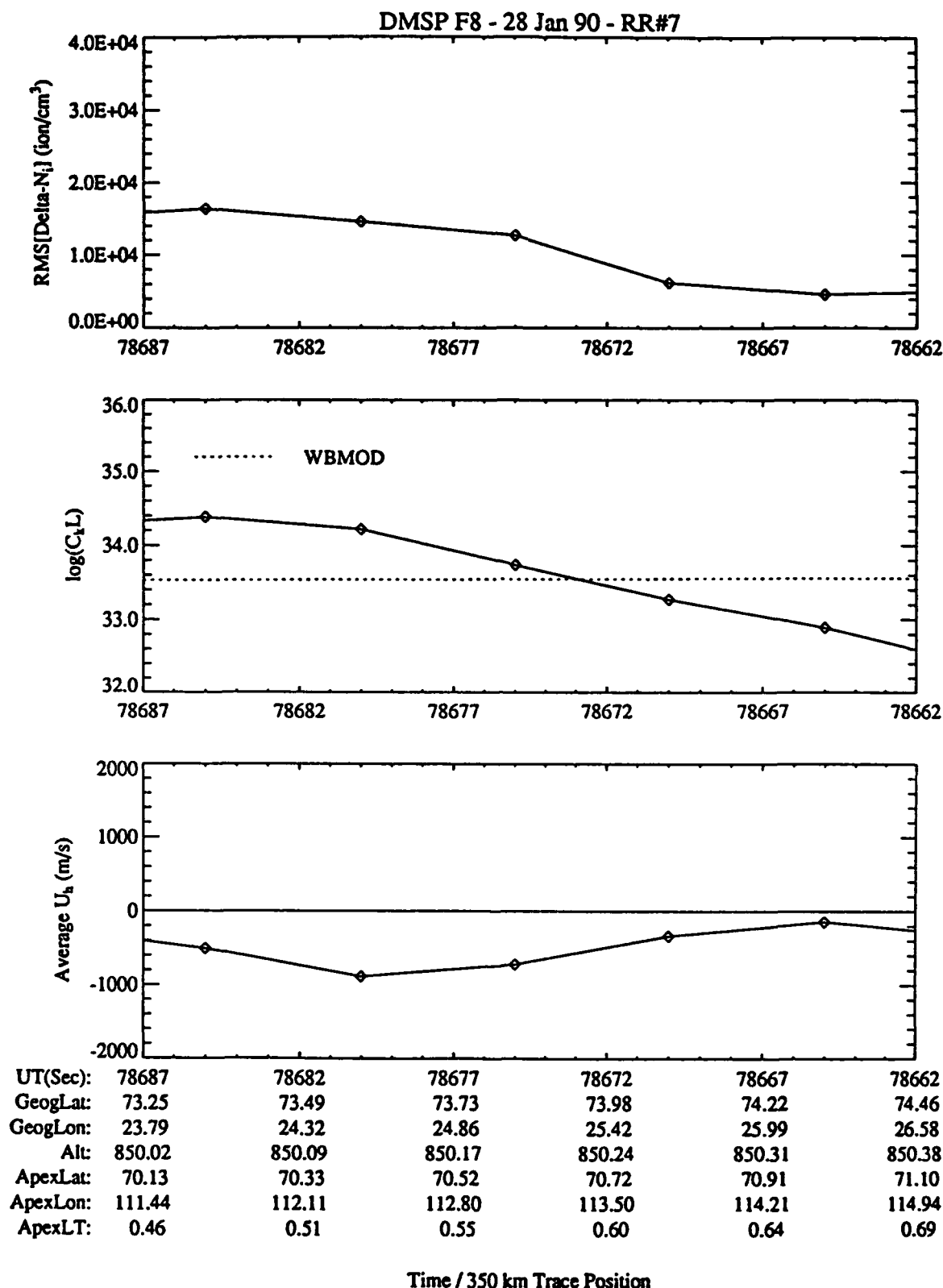


Figure 24. Data derived from the DMSP SSIES/SM and DM sensor data for 28 January 1990. The top plot is of the RMS variance in ΔN_i from five-second SM sensor data samples centered on the time for which the data are plotted. The middle plot is of the $C_p L$ values derived from the ΔN_i data (solid lines) and from the WBMOD model (dotted line). The bottom plot is of five-second averages of the DM sensor horizontal cross-track drift velocity.

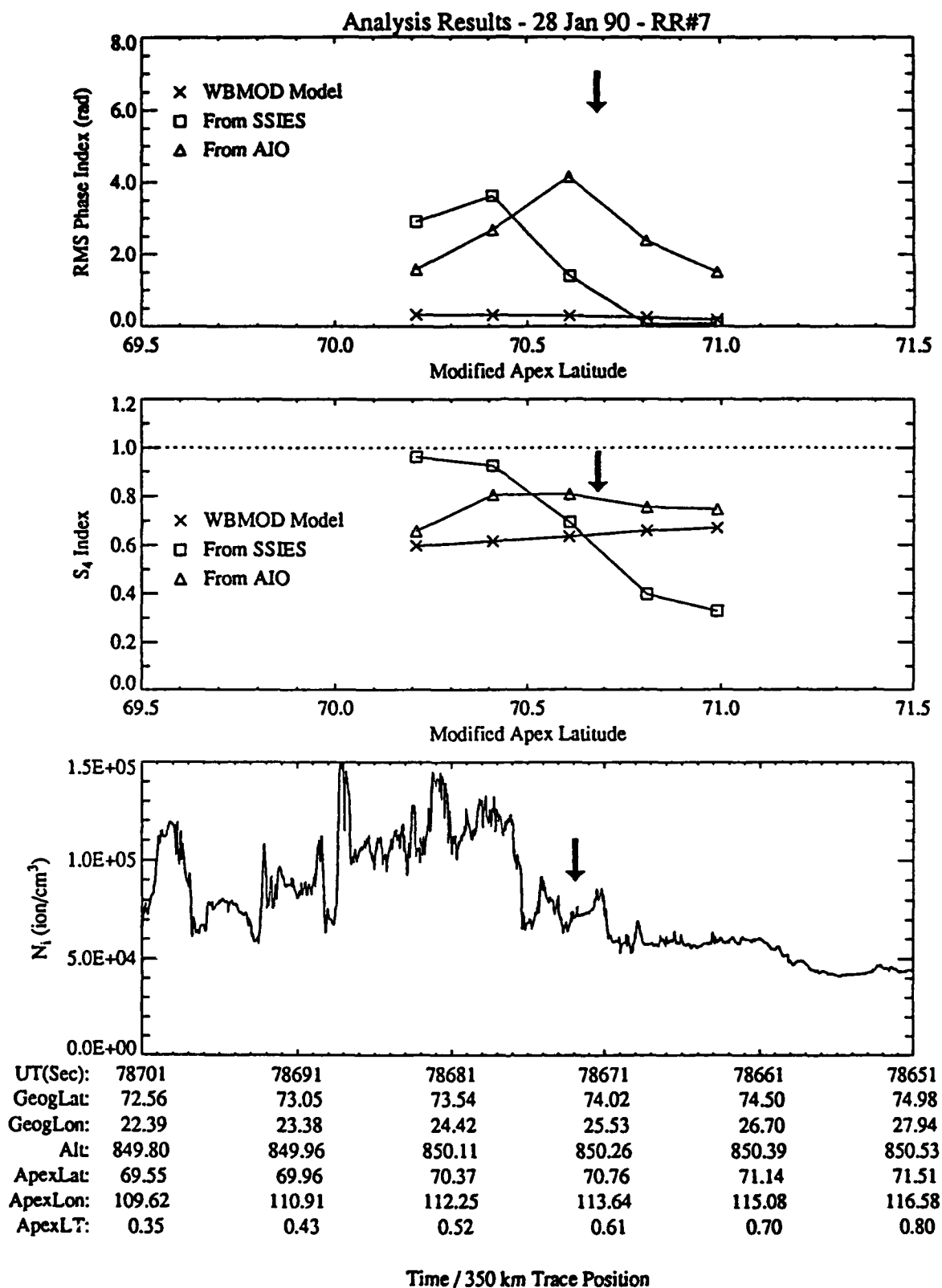


Figure 25. Analysis results for the 28 January 1990 data sets. The top plot shows the variation of σ_p (RMS phase) with geomagnetic latitude as calculated from the WBMOD model, from the SSIES C_kL and U_h data, and from the AIO-AFSATCOM phase data. The middle plot shows the variation of S_4 with geomagnetic latitude from the same sources. The bottom plot shows the variation of total ion density over the same latitude range. The arrows indicate the time/location of closest approach.

3. Detailed Analysis — 17 January 1990

The 17 January set was discussed in some detail in the report for the first year of this project [Secan, 1991]. It was shown in that report that the "scintillation boundary" seen in the AIO-AFSATCOM data was probably not due to rapid equatorward movement of the auroral scintillation boundary just prior to the DMSP overflight since four sequential DMSP passes over the northern auroral region showed little change in the position of this boundary. In that report, it was stated that one possible explanation for the discrepancy might be a problem with the profiles used to scale the *in situ* C_k to $C_k L$ and that profile data from EISCAT could help resolve that issue. Since that report, we have investigated three aspects of this problem in more detail: (1) the effect of the *in situ* drift velocity on the comparison of the SSIES and AIO-AFSATCOM data, (2) the effect of uncertainties in the underlying electron density height profile, and (3) different assumptions about the height variation of ΔN .

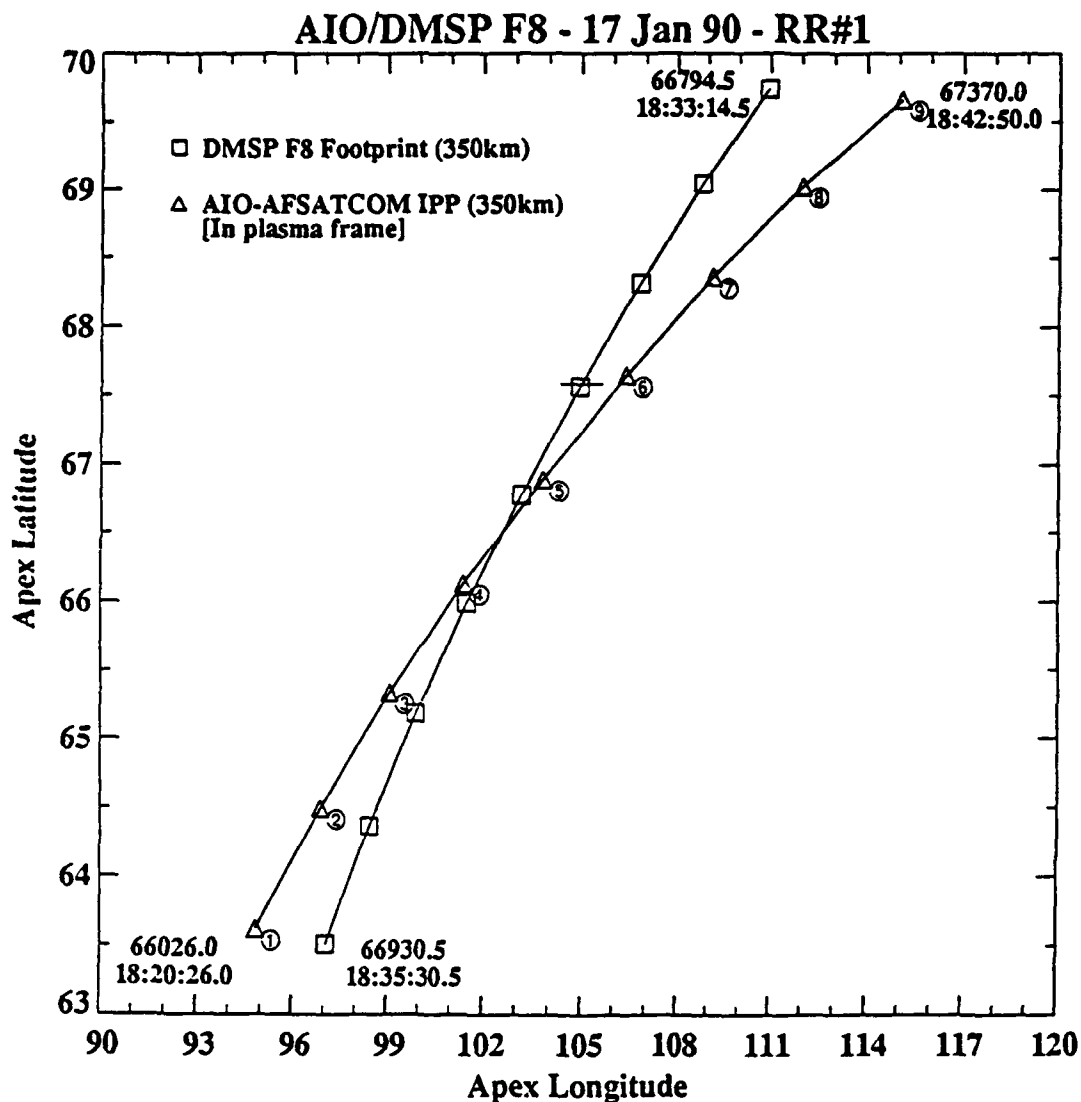
3.1 Drift Velocity Effects

The Retarding Potential Analyzer (RPA) sensor on DMSP satellites F8 and F9 have been non-functional since shortly after launch, so in the initial analysis of the DMSP SSIES data we had information only on the cross-track components of the drift. Analysis of data from the EISCAT radar shows a roughly 500 m/s meridional drift which was not included in the initial analyses of these data [Weber, private communication]. While this has some effect on the C_k and $C_k L$ values calculated from the *in situ* density measurements (see Section 5 for a further discussion of this), the largest effect in terms of the comparison with the AIO scintillation measurements is in deciding which DMSP observations to compare with which AIO observations.

Figures 26 and 27 show the relative locations of the DMSP and AIO observations in a "plasma" frame and in the fixed-earth frame. In the plasma-frame plot, the DMSP data is assumed to be a snapshot of the plasma distribution at the time of the pass. The location of the AIO observations are transformed into this frame using the cross-track drift velocities measured by the DMSP Drift Meter (DM) instrument and an assumed 500 m/s drift southward. Figure 28 is a "context" plot showing the range of the AIO-AFSATCOM observations in the plasma frame plotted with the SSIES density and cross-track velocity measurements.

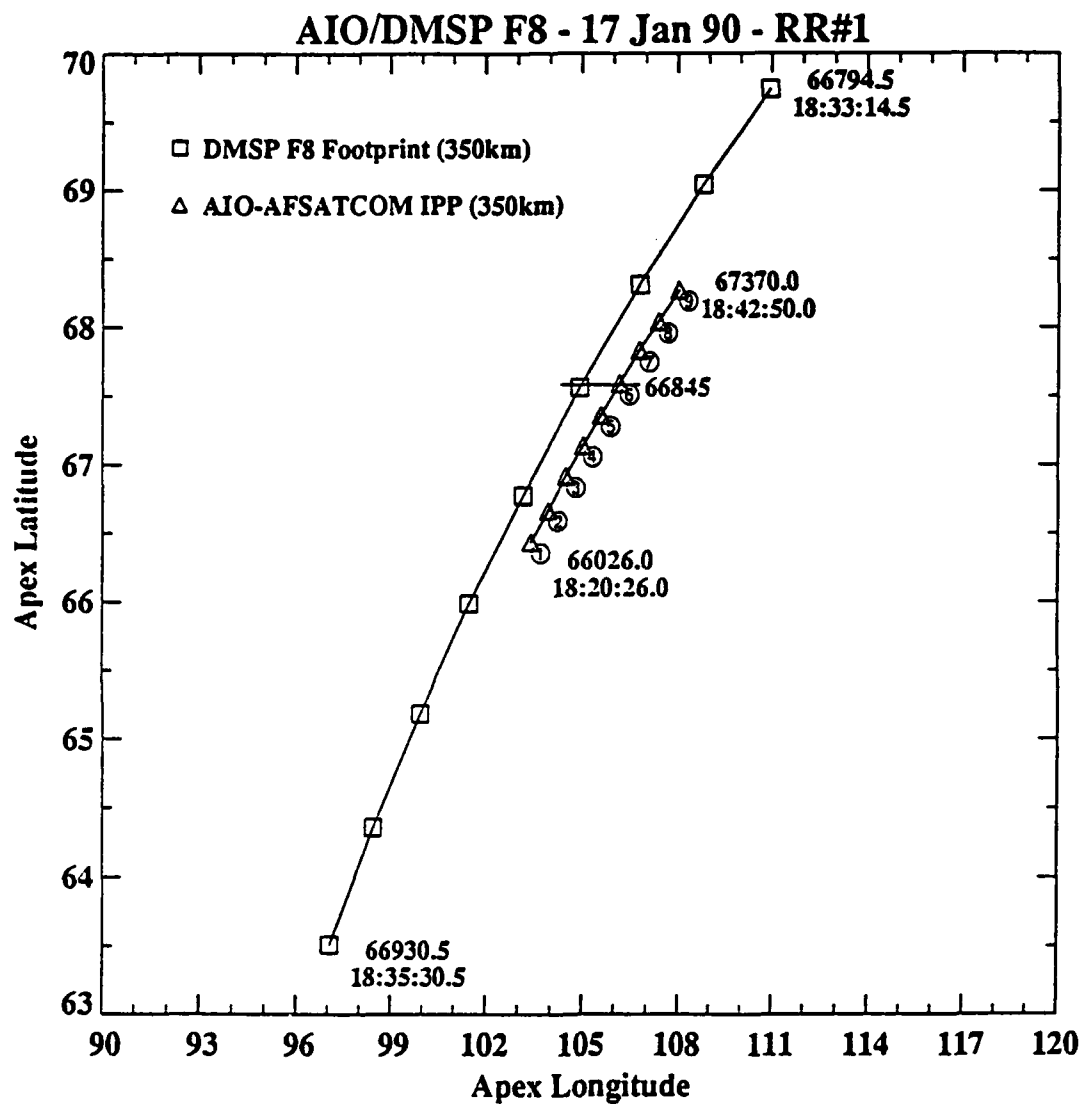
Figures 29 and 30 show the raw and detrended *in situ* density compared to the detrended AIO-AFSATCOM intensity and phase records using the mapping shown in Figure 26 (the plasma frame). Qualitatively, this is a definite improvement over previous comparisons of these data (see Figure 3). Both sets of data show a steady increase in structure from south to north, with fairly good matching in smaller-scale features such as that in data set #6 (between times 66782 and 66950 on the AIO phase plot and times 66837 and 66854 on the SSIES plot).

Unfortunately, we still have a problem with quantitative comparisons. Figure 31 shows the various scintillation indices calculated from the *in situ* and beacon data (compare to Figure 5). While the trends shown from the two data sets are similar, the indices calculated from the *in*



Thu May 14 09:42:59 1992

Figure 26. Locations of the DMSP F8 satellite traced down to 350 km altitude and the 350 km ionospheric penetration point (IPP) for the AIO-AFSATCOM link for the 17 January 1990 data set. The AIO-AFSATCOM data have been mapped into the plasma frame as defined by the DMSP observations using drift velocity measurements as described in the text. The location marked by a cross-bar on both traces indicates the point where the two experiments were collecting data on the same geomagnetic latitude. The symbols are plotted at center-points for data samples used to generate various irregularity/scintillation parameters. The circled numbers on the AIO-AFSATCOM trace are used to identify individual data samples.



Thu May 14 09:43:13 1992

Figure 27. The same locations as in Figure 26, now plotted in a fixed-earth frame. All labels are as in Figure 26.

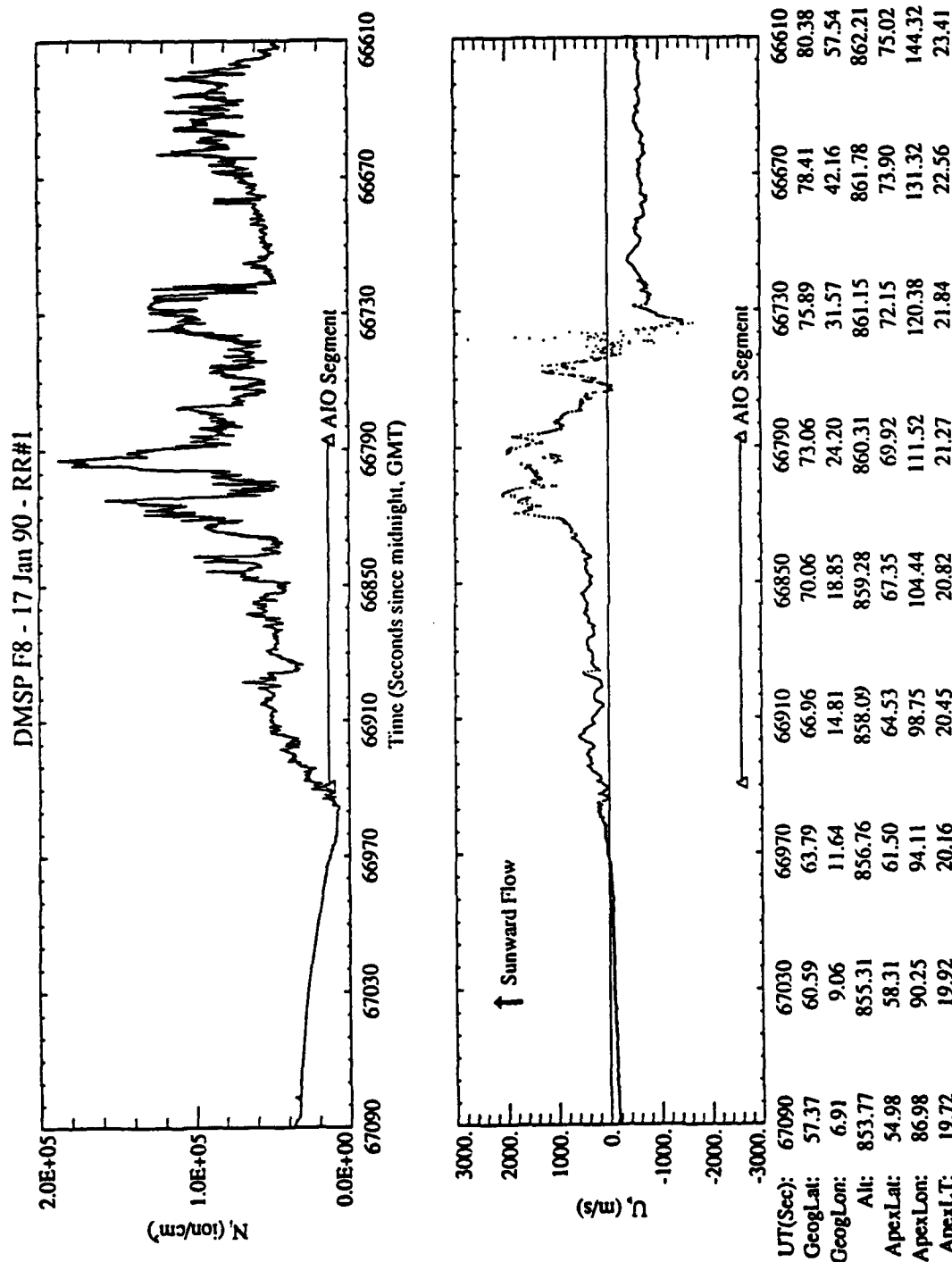


Figure 28. Plots from the DMSP SSIES/SM (total ion density) and SSIES/DM (horizontal cross-track ion drift velocity) sensors over the geomagnetic (apex) latitude range of 55° to 75° for 17 January 1990. The latitude range covered by the AIO-AFSATCOM data set (IPP) as mapped into the DMSP-based plasma frame (see Figure 26) is indicated in both plots. These data are plotted in time-reverse order so that latitude increases from left to right, and the locations printed along the x-axis are for the DMSP 350 km footprint locations.

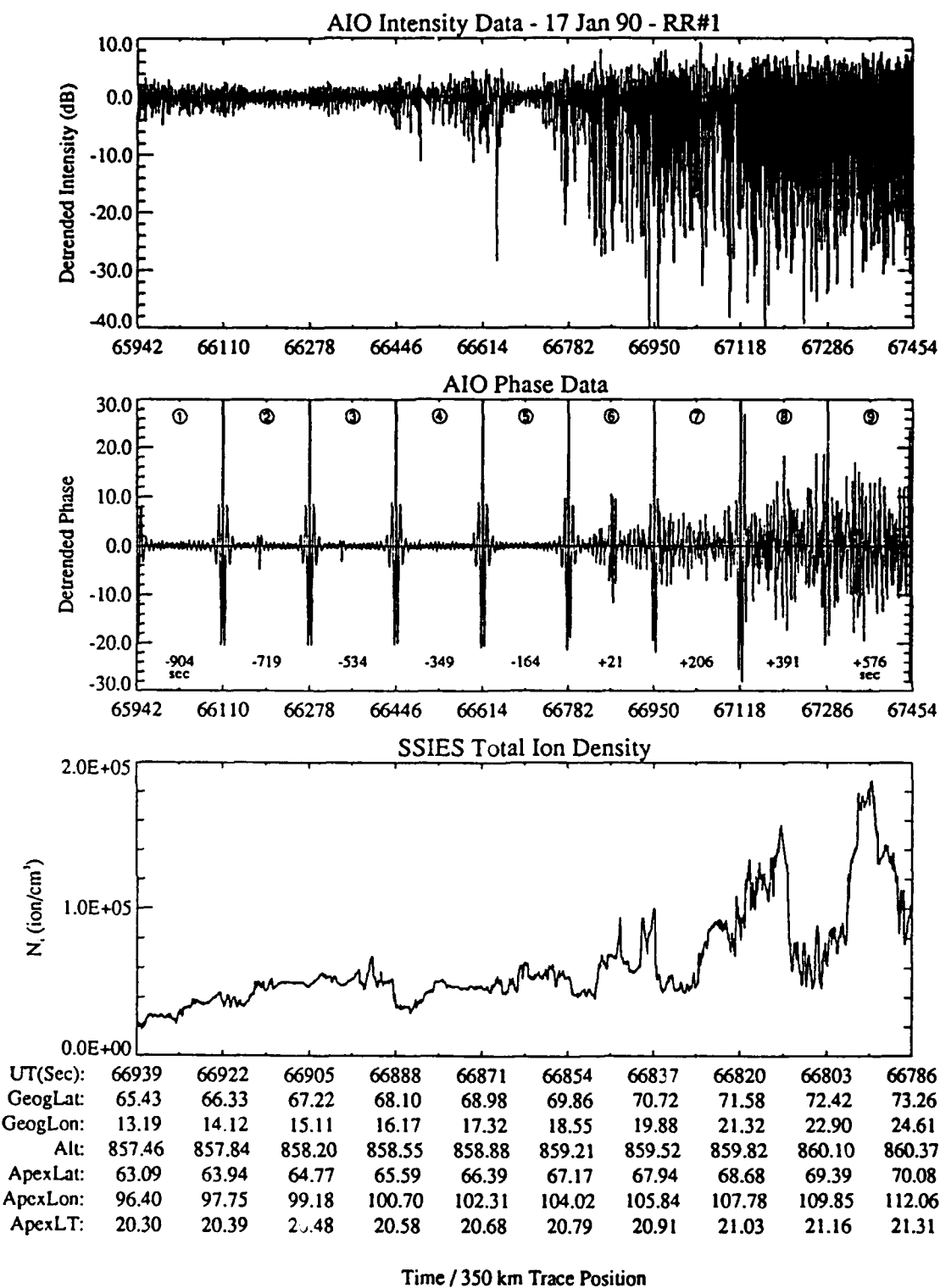


Figure 29. Data from the AIO-AFSATCOM link and the DMSP SSIES/SM sensor for the intervals in Figure 26. The top plot is the detrended intensity and the middle plot is the detrended phase from the AIO-AFSATCOM link. The times along the bottom of the phase plot are the time difference (in seconds) between the AIO-AFSATCOM observation and the corresponding DMSP/SSIES one. The bottom plot is the SSIES/SM total ion density data. The SSIES/SM data is plotted in time-reverse order so that all three plots cover the same range of geomagnetic latitudes. The locations plotted with the SSIES/SM data are for the DMSP 350 km footprint locations.

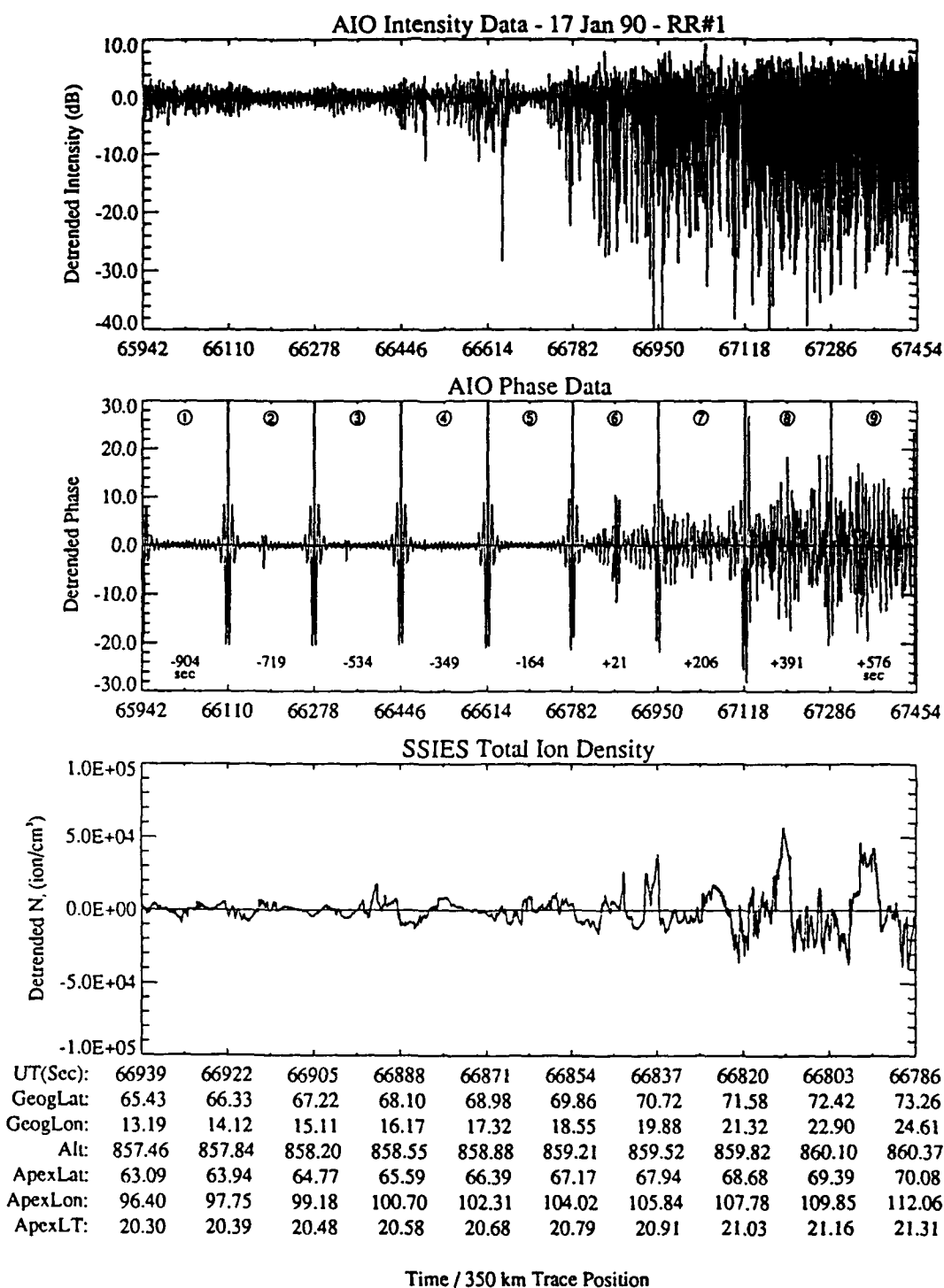
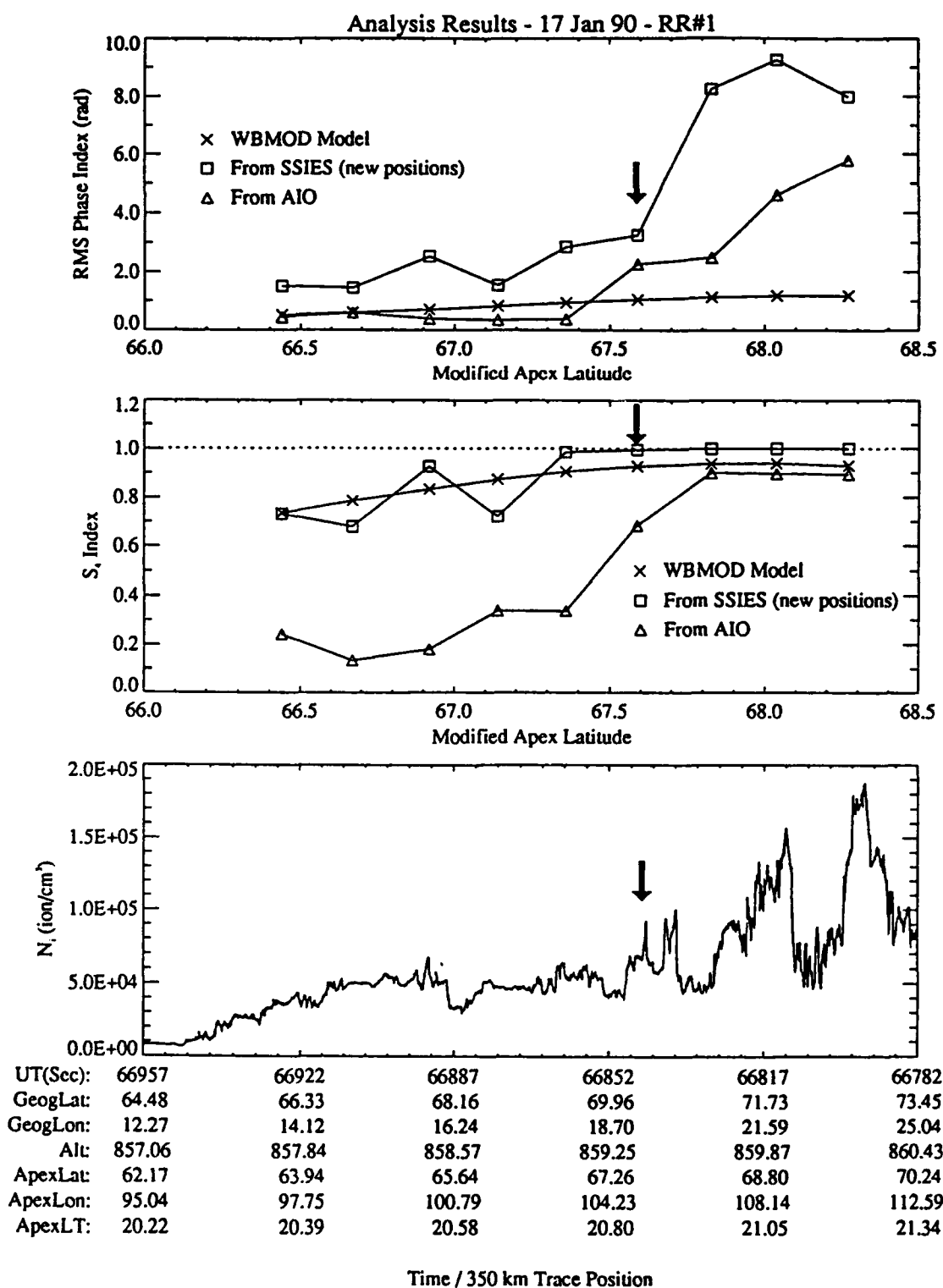


Figure 30. The top two plots are as in Figure 29. The bottom plot is the detrended SSIES/SM total ion density data. This plot is labeled as in Figure 29.



Thu May 14 09:44:49 1992

Figure 31. Analysis results for the 17 January 1990 data sets as mapped into the plasma frame defined in Figure 26. The top plot shows the variation of σ_p (RMS phase) with geomagnetic latitude as calculated from the WBMOD model, from the SSIES $C_k L$ and U_h data, and from the AIO-AFSATCOM phase data. The middle plot shows the variation of S_4 with geomagnetic latitude from the same sources. The bottom plot shows the variation of total ion density over the same latitude range. The arrows indicate the time/location of closest approach.

situ data are consistently higher than those calculated from the AIO-AFSATCOM data, particularly the S_4 values calculated for the southern end of the pass. The AIO-AFSATCOM values show a transition from a region of very low scintillation ($S_4 \leq 0.2$) to one of high scintillation ($S_4 > 0.8$), while the *in situ* data shows S_4 to be ≥ 0.7 for the entire pass. We may be able to resolve this discrepancy by adjusting the effective layer-thickness parameter (L_{eff}) used to convert the SSIES-derived C_k values to $C_k L$, but it may require L_{eff} values that are unrealistically low. This issue was addressed next.

3.2 Background Electron Density Profile

Specifying the background electron density profile, $N(h)$, is only necessary if the model for the height variation of ΔN assumes that ΔN is a function of $N(h)$. This is the case for the assumption we have been using that $\Delta N/N$ is a constant throughout the layer. This assumption leads to an L_{eff} which is proportional to the distance between the satellite and the peak of the layer, weakly dependent on the shape of the layer between the peak and the satellite, and proportional to the square of the ratio of the density at the peak ($N_m F2$) to the density at the satellite (N_s). In calculating L_{eff} in the analyses presented to this point, we have used a model of the topside ionosphere fit to the density at the satellite altitude to provide an estimate of $N_m F2$. The only constraint used was that the $N_m F2$ values be comparable with those derived from a latitude scan of electron density profiles from the EISCAT radar during the time of the DMSP pass.

Figures 32 and 33 show the profiles derived from the DMSP density data and profiles from the EISCAT scan. The DMSP data covers the time span 18:32:12 UT (northern end) to 18:35:56 UT (southern end) and the EISCAT data begins at 18:20:20 UT at the northern end and ends approximately 20 minutes later at the southern end. Note that the coordinate system used (modified apex (APXLat) defined at 350 km for the DMSP profiles, corrected-geomagnetic (CGLat) defined at the earth's surface for the EISCAT profiles) are nearly identical at these latitudes, with about a 0.5° offset ($CGLat = APXLat - 0.5^\circ$). The peak density values are not too different in these two latitude scans, at least in the region of interest shown in the DMSP plot (labeled "Results Plot Coverage"). In particular, note the feature at about 67.5° CGLat in the EISCAT data and 68.0° APXLat in the DMSP data. This appears to be the feature that is associated with the enhanced scintillation in the AIO-AFSATCOM records.

While the agreement between these two data sets is not too bad, it must be remembered that neither of these latitude scans is truly a "snapshot" of the ionosphere — the DMSP scan required 3.5 minutes and the EISCAT scan 20 minutes. There is evidence from the EISCAT drift measurements that there was a strong (500 m/s) equatorward flow throughout this period of interest. This is comparable to the equatorward scan velocity of the EISCAT radar, so the EISCAT scan cannot be used as a "frozen-in" (in the fixed-earth frame) specification of the ionosphere under which the AIO aircraft moved. In other words, the EISCAT $N_m F2$ values may not be representative of the values at the AIO-AFSATCOM IPP which are needed in order to specify $N(h)$ for the L_{eff} calculation.

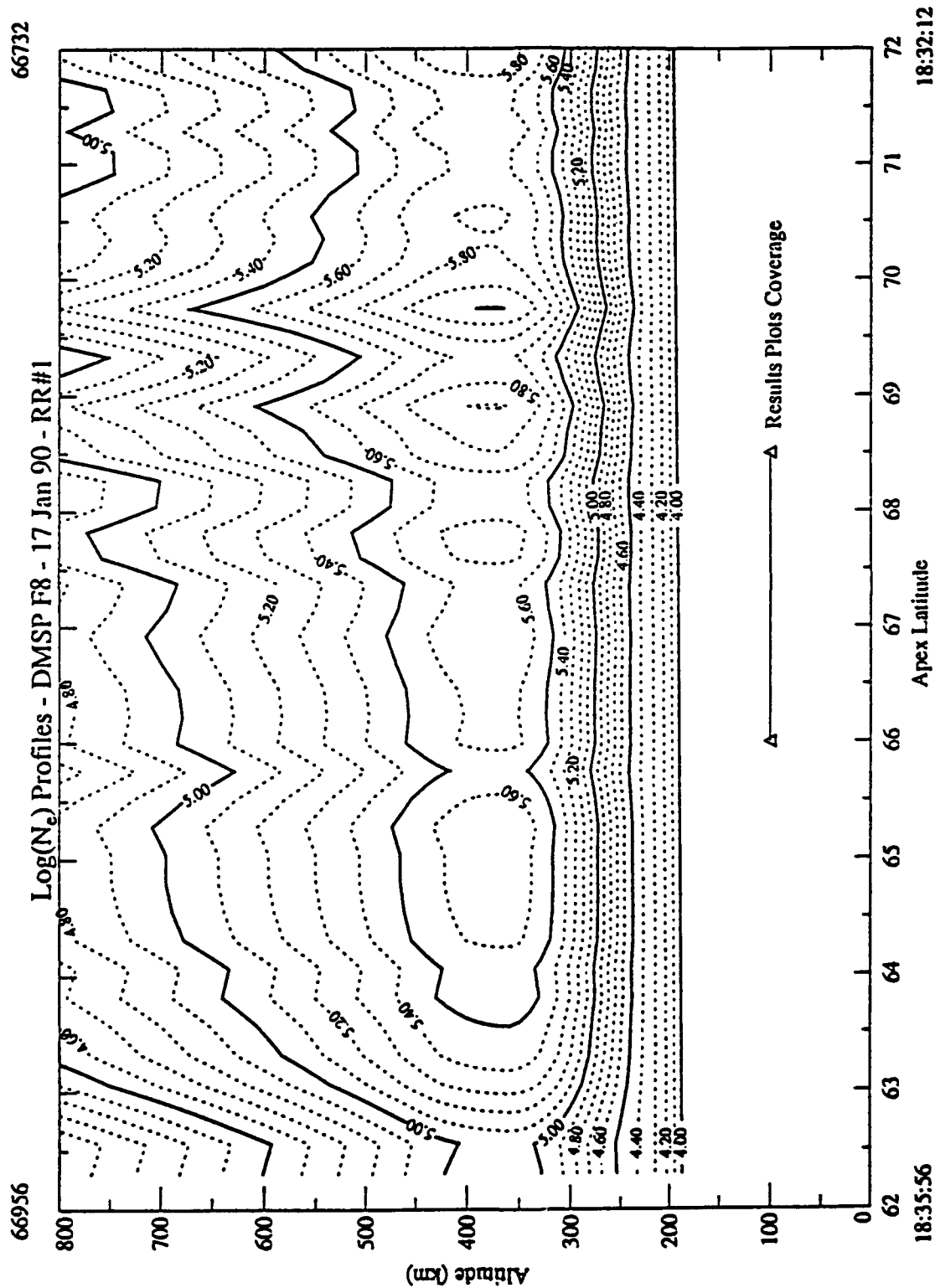


Figure 32. Latitude scan of electron density profiles generated from the *in-situ* density measured by the DMSP SSIES Scintillation Meter. The segment labeled "Results Plots Coverage" is the latitude range covered in the scintillation index plots in Figure 31.

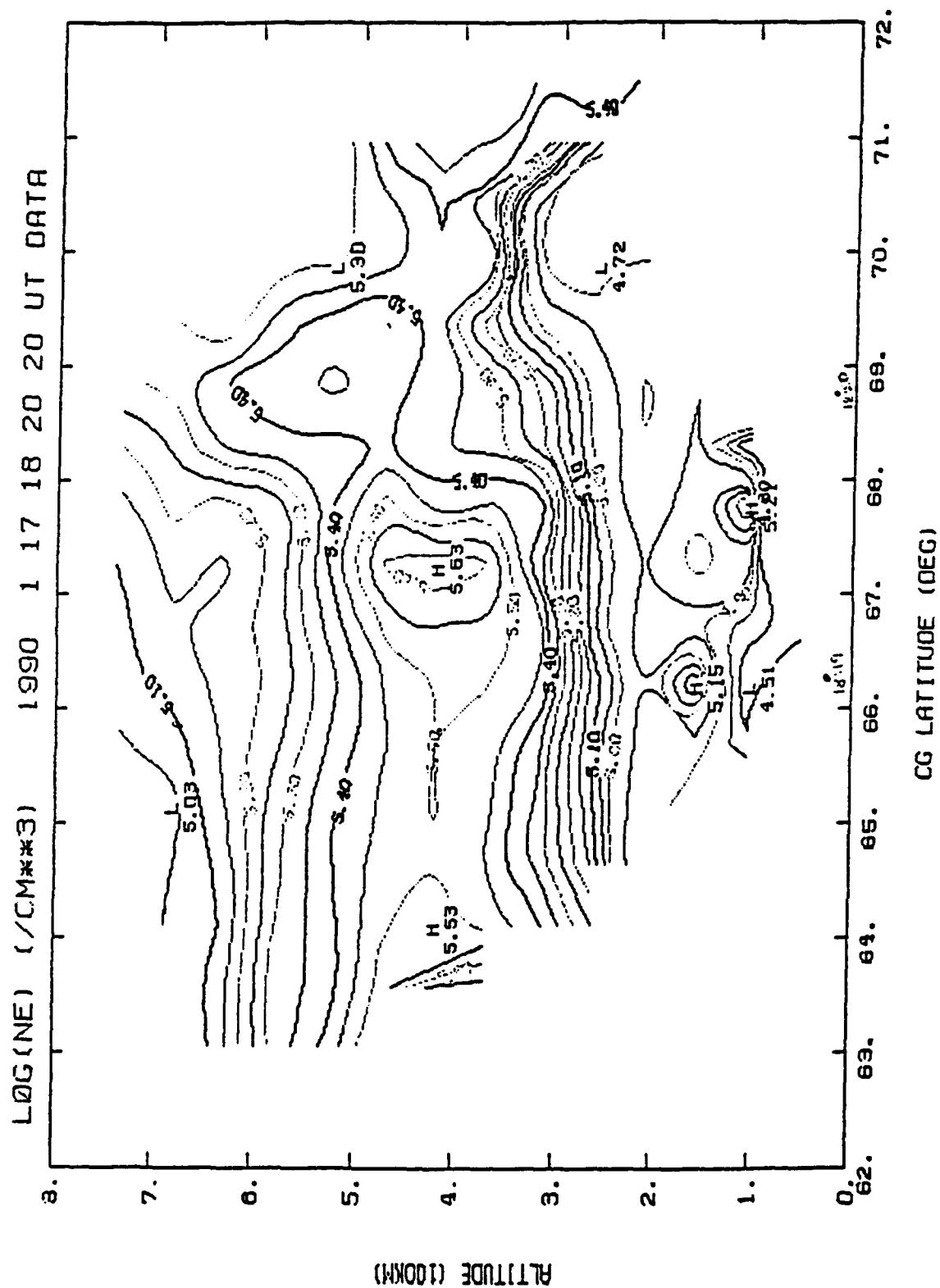


Figure 33. Latitude scan of electron density profiles from the EISCAT radar.

Table 2. Data from the AIO ionosonde for 17 January 1990.

HHMMSS	SEC	f _o F2	h _m F2	h _p F2	f _o E	f _o E _s	MLAT	MLON
-----	-----	-----	-----	-----	-----	-----	-----	-----
181411	65651	3.80	0.00	378.40	3.40	3.50	66.84	103.49
181641	65801	3.80	278.00	373.40	3.00	3.70	66.62	103.50
181911	65951	3.90	272.30	418.40	3.10	3.90	66.81	103.22
182141	66101	4.10	281.30	426.70	3.00	3.90	67.05	103.77
182411	66251	3.80	256.70	410.00	3.00	3.80	67.27	104.29
182641	66401	3.90	258.10	365.00	2.80	99.99	67.50	104.84
182911	66551	3.80	242.60	375.00	2.90	4.10	67.72	105.38
183141	66701	3.80	0.00	393.40	3.00	3.90	67.93	105.94
183411	66851	3.80	0.00	383.40	3.00	4.10	68.17	106.53
183641	67001	3.80	0.00	426.70	3.00	3.90	68.40	107.14
183911	67151	3.80	0.00	446.70	3.00	3.90	68.61	107.72
184141	67301	4.00	0.00	413.40	3.00	3.90	68.84	108.36
184411	67451	4.10	289.50	411.70	2.90	4.30	69.05	108.98
184641	67601	3.90	0.00	330.00	3.00	5.80	69.26	109.62
184911	67751	4.50	277.00	363.40	3.00	4.60	69.27	110.19

Legend: HHMMSS : GMT (HH:MM:SS)
SEC : GMT (seconds since midnight)
f_oF2 : f_oF2 (MHz)
h_mF2 : h_mF2 (km)
h_pF2 : h'F2 (km)
f_oE : f_oE (MHz)
f_oE_s : f_oE_s(MHz)
MLAT : Modified apex latitude (deg)
MLON : Modified apex longitude (deg)

The f_oF2 data from the AIO ionosonde have been folded into the analysis of the 17 Jan 90 data set. Table 2 is a listing of various profile parameters derived from the ionosonde, and is a subset of the data provided from PL/GPIA. Figure 34 shows the f_oF2 data from this list plotted as a function of geomagnetic (modified apex) latitude with f_oF2 estimates taken from the EISCAT scan shown in Figure 33. The times at either end of the two data segments plotted indicate the times at the ends of the two data sets, and the vertical line indicates the latitude and time of coincidence between the two data sets.

These new f_oF2 measurements were used to generate new S₄ and σ_p estimates from the DMSP SSIES data. Electron density profiles to be used in converting C_k to C_kL were built by

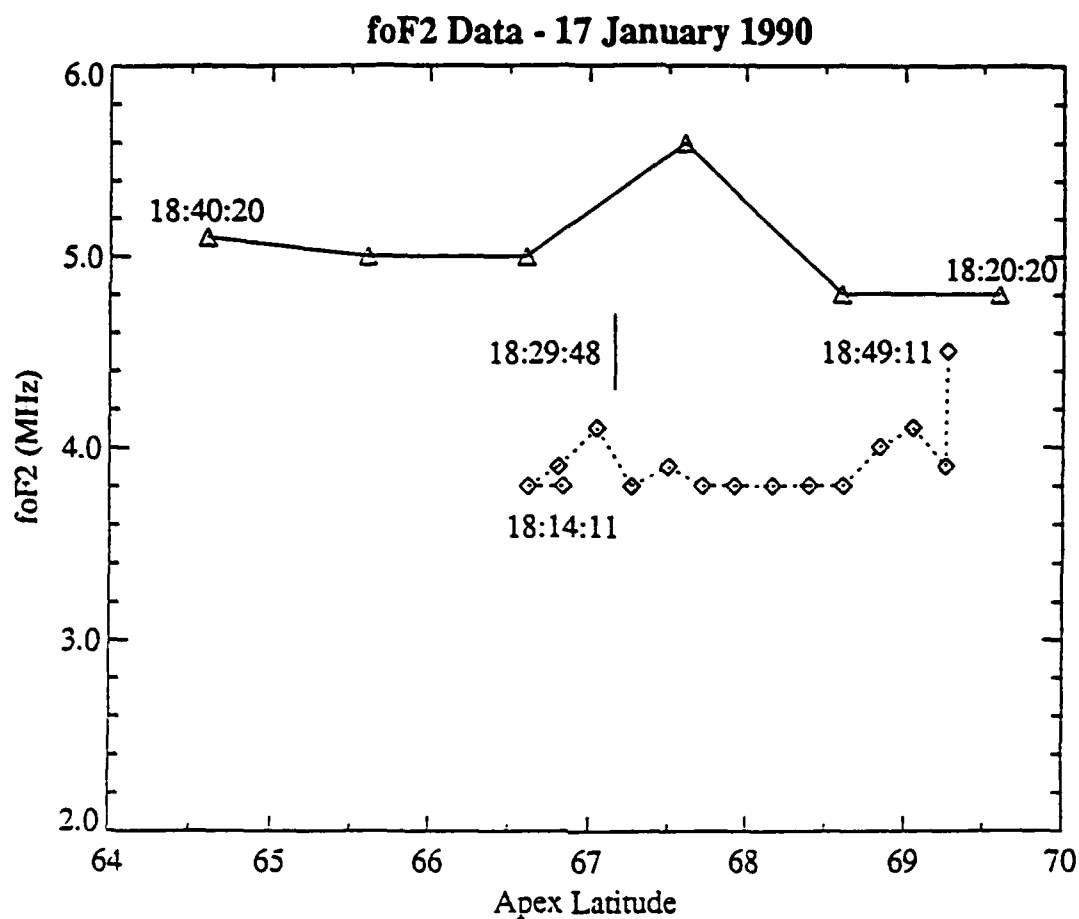


Figure 34. Latitude variation of f_oF2 for the 17 January 1990 campaign as derived from AIO ionosonde measurements (diamonds) and from the EISCAT latitude scan (triangles). The times at the ends of the two data segments indicate the end times of each segment. The vertical bar indicates the location and time of coincidence of the two data sets.

fitting a profile model to the *in-situ* density from the SSIES sensor and the density derived from the AIO f_oF2 measurements at the F2 peak. Figure 35 shows the new results compared to the AIO-AFSATCOM observations, which should be compared to Figure 31 which shows the results obtained using profiles fit only to the *in-situ* density and f_oF2 values comparable to those derived from the EISCAT scan. There is general improvement at all latitudes, although the SSIES-derived values are still significantly higher than those derived from the AIO-AFSATCOM data at the southern end of the pass. Note that the SSIES-derived values are significantly closer to the AIO-AFSATCOM values for the data set taken at the time of closest approach.

This demonstrates the importance of having accurate estimates for the electron density at the F2 peak in building the profiles to be used to convert C_k to $C_k L$. This reinforces the findings of the parametric studies completed in the early stages of this study [Secan, 1987] which found that $C_k L$ calculated from the SSIES C_k data will be very sensitive to inaccuracies in the F2 peak density used in the calculation. Peak electron densities derived from the planned DMSP SSUSI and SSULI UV sensors may be critical inputs for this calculation.

3.3 Height Variation of ΔN

The two critical assumptions made in calculating L_{eff} are (1) that the irregularity spectrum observed at the DMSP altitude is representative in some way of the spectrum within the bulk of the irregularity layer, and (2) that the irregularity strength scales in altitude in order to keep $\Delta N/N$ constant. The validity of the first assumption is central to the entire investigation. If it does not hold, then it severely limits the usefulness of the DMSP data for estimating $C_k L$. The second assumption, which specifies the details of the relationship between the spectral strength at DMSP altitude to that near the F2 peak, is simply one of several models which could apply to the situation.

Using a model that $\Delta N/N$ is constant throughout the layer leads to a value of 1.4×10^4 km for L_{eff} . An alternative representation for the height variation of ΔN , which could be looked on as a limiting case for the primary assumption, is that ΔN is constant throughout the layer. The equation for L_{eff} is then simply $L_{eff} = h_s - h_b$ where h_s is the satellite altitude and h_b is the height of the bottom of the layer. If we assume that the base of the layer is at 250 km and that the nominal height of the satellite is 850 km, this leads to an L_{eff} of 6.0×10^2 km, over a factor of 20 smaller than that calculated assuming $\Delta N/N$ is a constant. Figure 36 is a plot of the results for 17 January using this new definition for L_{eff} (compare this with Figure 31). The difference between the AIO-AFSATCOM values and the DMSP values are now much better at the southern end of the pass, but are much worse at the northern end. Note that this result is valid *regardless* of what $N_m F2$ is since the L_{eff} parameter is now a function solely of the thickness of the layer. But, one must accept the assumption that ΔN is constant throughout the layer from the satellite altitude down to the F2 peak.

What this tends to indicate is that we may not be able to use a simple "one size fits all" model for the way in which the irregularity strength maps in height along field lines. For this

Analysis Results - 17 Jan 90 - RR#1

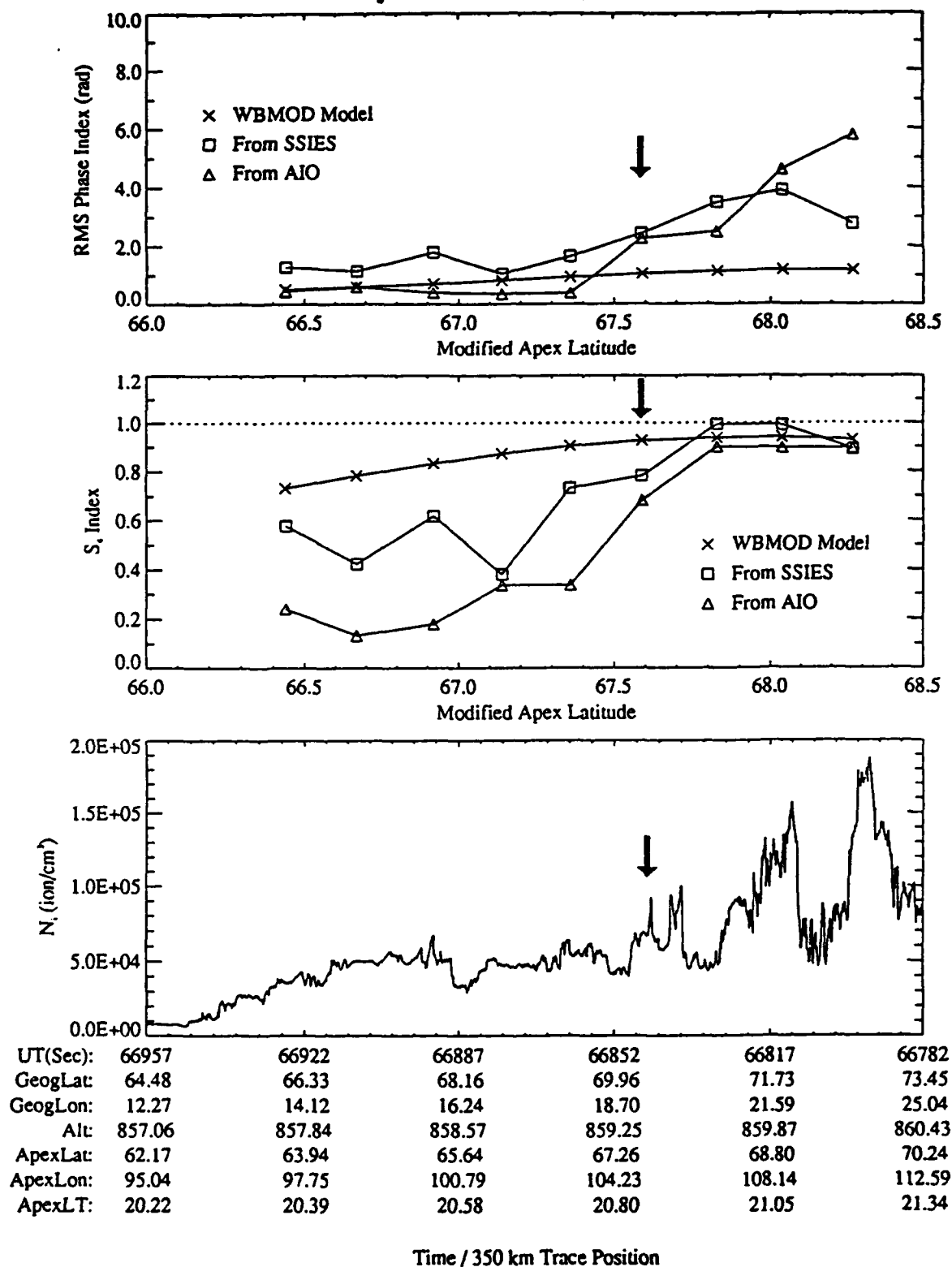


Figure 35. Analysis results for the 17 January 1990 data sets using f_oF_2 values from the AIO ionosonde. The top plot shows the variation of σ_ϕ (RMS phase) with geomagnetic latitude as calculated from the WBMOD model, from the SSIES C_kL data, and from the AIO-AFSATCOM phase data. The middle plot shows the variation of S_4 with geomagnetic latitude from the same sources. The bottom plot shows the variation of total ion density over the same latitude range. The arrows indicate the time/location of closest approach.

Analysis Results - 17 Jan 90 - RR#1

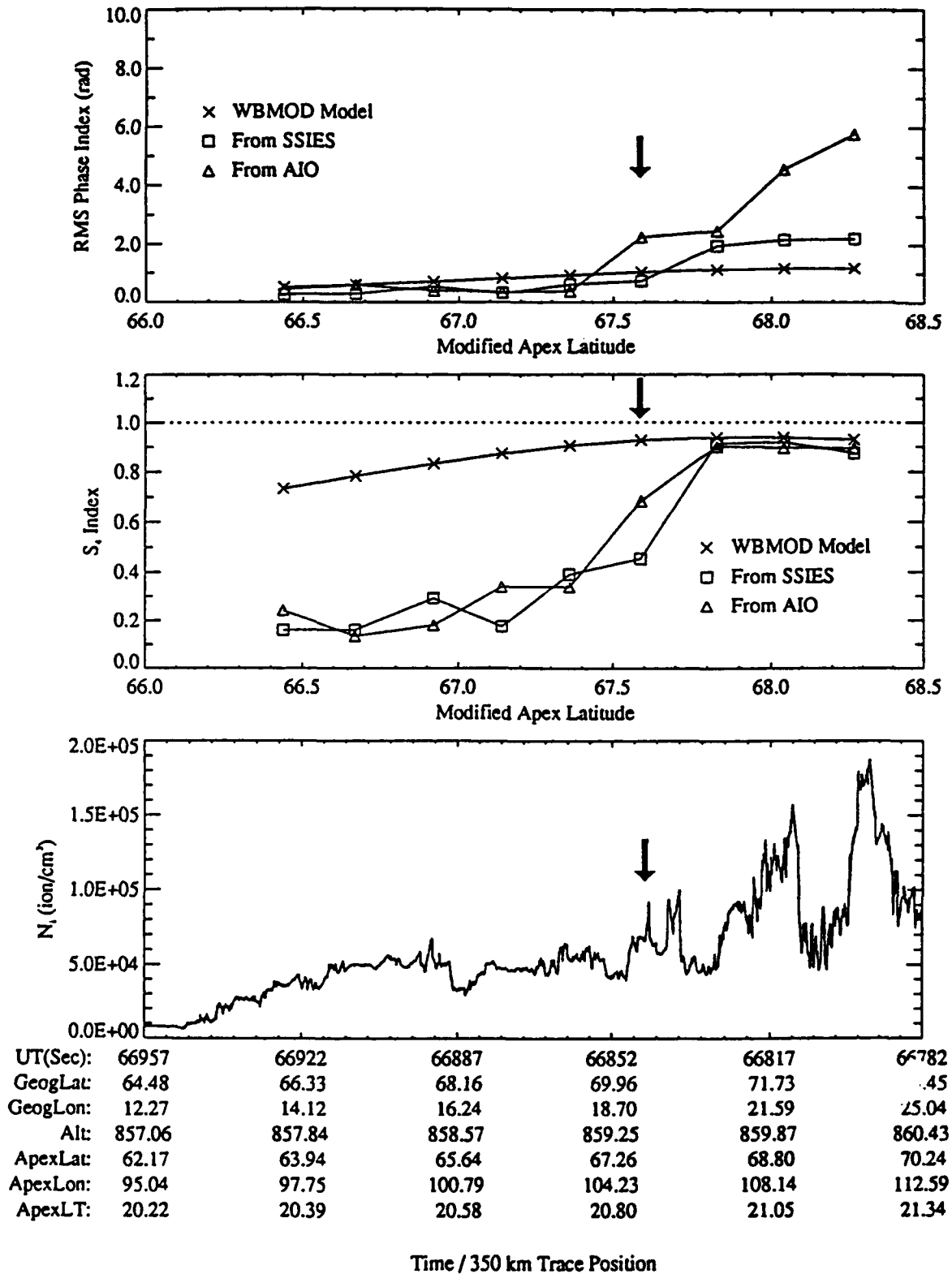


Figure 36. Analysis results for the 17 January 1990 data set using ΔN constant with height (see explanation and caveats in text). The format of this figure is identical to Figure 35.

particular case, it appears that the model assuming that ΔN (and C_k) are height-invariant is valid (fits best) for the southern section of the pass and the model assuming $\Delta N/N$ is height invariant is valid for the northern section. There is nothing inherently wrong or bad about needing a more complex model, but if these data are to be used operationally there must be a way to determine which model is valid for a particular case. This is something which will require further investigation.

[Note: Figure 36 should not be used as evidence that we are correctly scaling the DMSP data. It simply shows that we can obtain a reasonable fit to the observed scintillation levels using another model for the height variation of ΔN , a model which may or may not be valid.]

4. Detailed Analysis — 24 January 1990

There was a near-coincident pass of the Polar BEAR (PB) satellite during the 24 January 1990 DMSP/AIO-AFSATCOM data campaign (Round-robin (RR) #4). The DMSP (F8) F2-region footprint crossed the same geomagnetic latitude as the ionospheric penetration point (IPP) of the AIO-AFSATCOM link at 18:43:04, and the Tromso-PB IPP crossed the AIO-AFSATCOM IPP at 18:52:20. The DMSP footprint and the Tromso-PB IPP crossed at 18:46:11. While the longitude separations between the various data sets at the near-coincident times (defined as the times at which two of the experiments were sampling the ionosphere at the same geomagnetic latitude) were not as small as would be desired (3.4° for DMSP/AIO-AFSATCOM, 3.0° for Tromso-PB/AIO-AFSATCOM, and 10.5° for DMSP/Tromso-PB), these three sets provide a means for addressing concerns about the AIO-AFSATCOM phase data as well as an opportunity to compare SSIES-derived scintillation parameters to observed parameters over a larger latitude span in more of a "snapshot" sense than is available with just the AIO-AFSATCOM data. The geometry and data for each of the three inter-comparisons are shown in Figures 37 through 39.

Figure 37a shows the location of the DMSP 350 km F2-region footprint and the AIO-AFSATCOM 350 km IPP in modified apex latitude and longitude around the near-coincident time. The symbols plotted along the data-collection tracks indicate center-times/locations of the data subsets which were used in calculated irregularity/scintillation parameters. The cross-bars on the two traces labeled with the time 67384 indicate the near-coincident time/location. The data corresponding to these traces are shown in Figure 37b. The two top plots show the detrended (0.1 Hz cutoff) intensity and phase data from the AIO-AFSATCOM link, and the bottom plot shows the plasma-density data from the DMSP SSIES Scintillation Meter (SM) sensor. [Note that the DMSP data is plotted with time running from right to left so that latitude runs from left to right in all three plots in this figure.] The circled numbers on the AIO-AFSATCOM phase plot enumerate the data samples used in the analysis, centered between times at which the AFSATCOM satellite switched frequencies. These numbers correspond to those shown on the AIO-AFSATCOM track in Figure 37a. Note the very strong scintillation evident in both the intensity and phase records and the lack of any substantial irregularities in the *in-situ* density record.

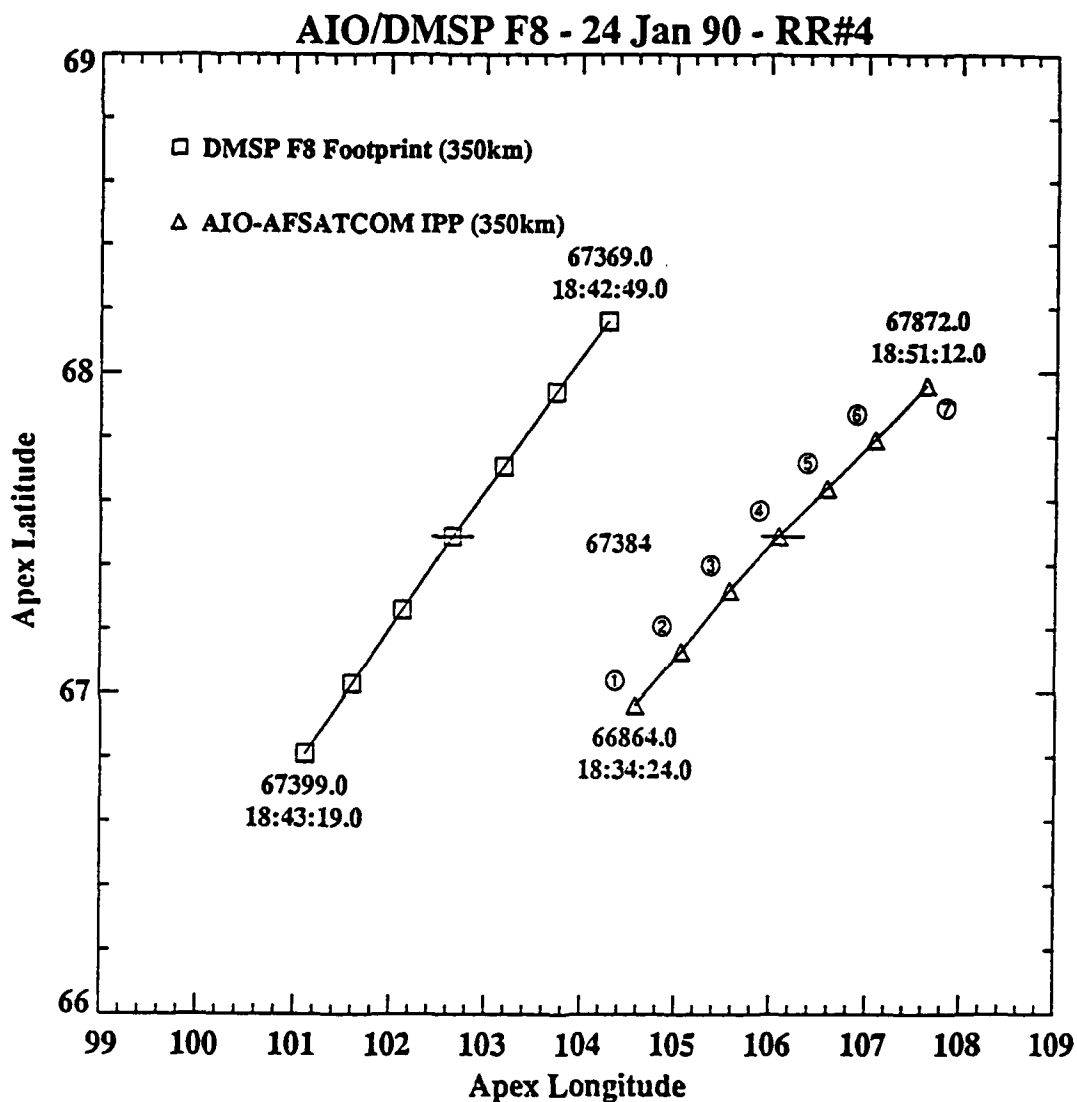


Figure 37a. Locations of the DMSP F8 satellite traced down to 350 km altitude and the 350 km ionospheric penetration point (IPP) for the AIO-AFSATCOM link for the 24 January 1990 data set. The location marked by a cross-bar on both traces indicates the point where the two experiments were collecting data on the same geomagnetic latitude. The symbols are plotted at center-points for data samples used to generate various irregularity/scintillation parameters. The circled numbers on the AIO-AFSATCOM trace are used to identify individual data samples.

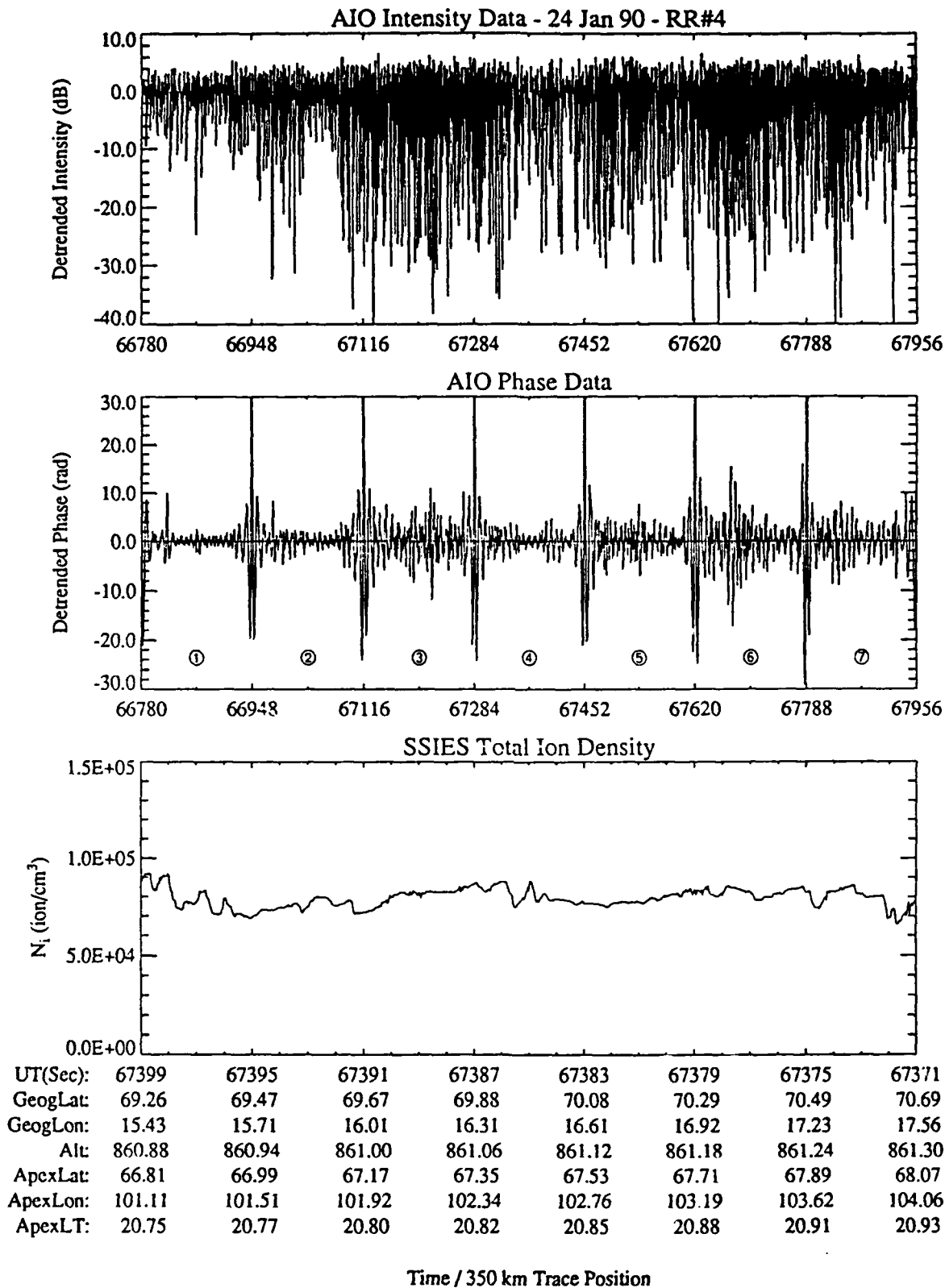


Figure 37b. Data from the AIO-AFSATCOM link and the DMSP SSIES/SM sensor for the intervals shown in Figure 37a. The top plot is the detrended intensity and the middle plot is the detrended phase from the AIO-AFSATCOM link (both detrended using a low-pass filter with a 0.1 Hz cutoff), and the bottom plot is the SSIES/SM total ion density data. The SSIES/SM data is plotted in time-reverse order so that all three plots cover the same range of geomagnetic latitudes. The locations plotted with the SSIES/SM data are for the DMSP 350 km footprint locations.

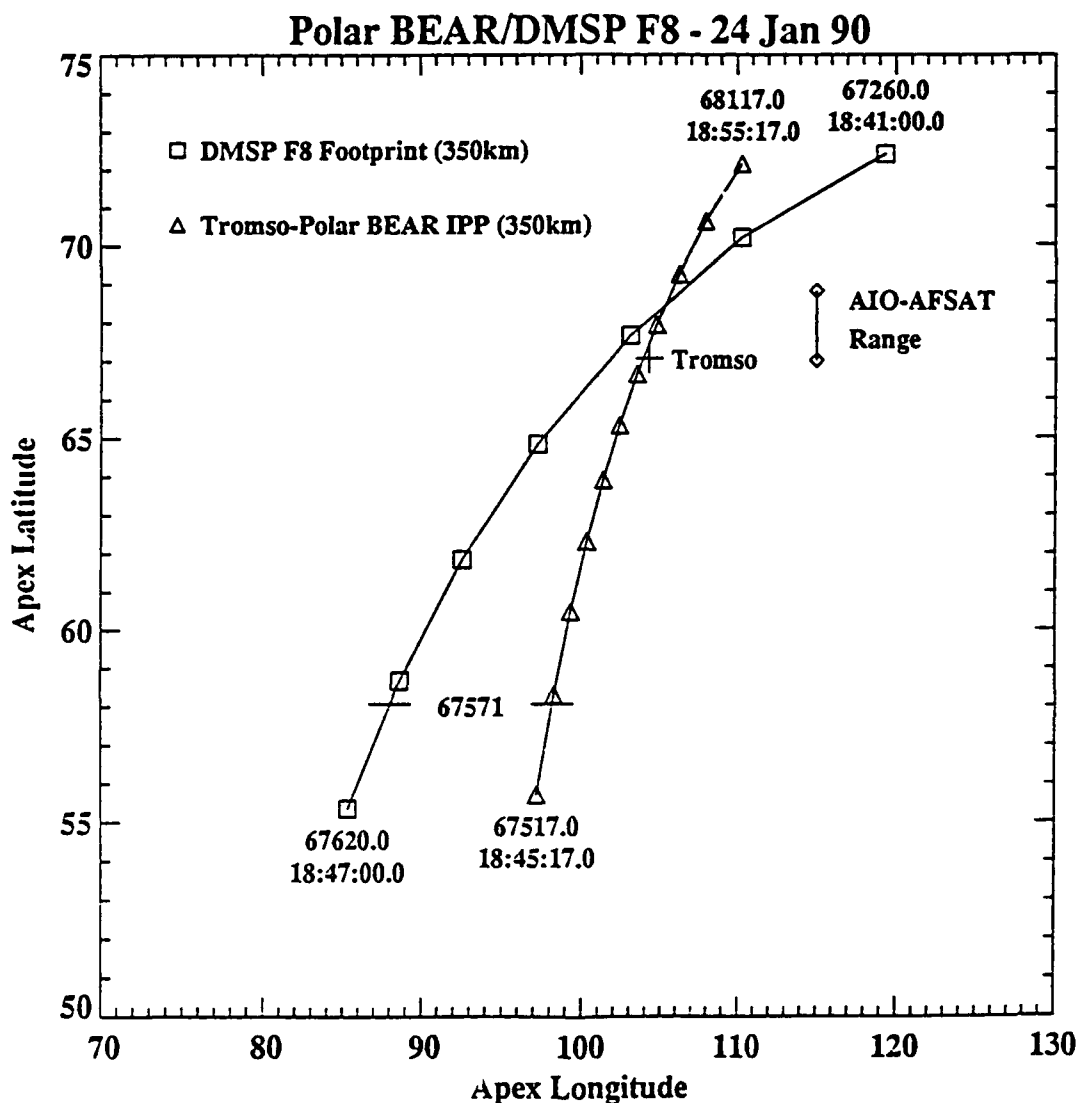


Figure 38a. Locations of the DMSP F8 satellite traced down to 350 km altitude and the 350 km IPP for the Tromso-Polar BEAR (PB) link for the 24 January 1990 data set. The location marked by a cross-bar on both traces indicates the point where the two experiments were collecting data on the same geomagnetic latitude. The symbols are plotted at center-points for data samples used to generate various irregularity/scintillation parameters. The location of Tromso is indicated, as is the latitude range covered by the AIO-AFSATCOM data set.

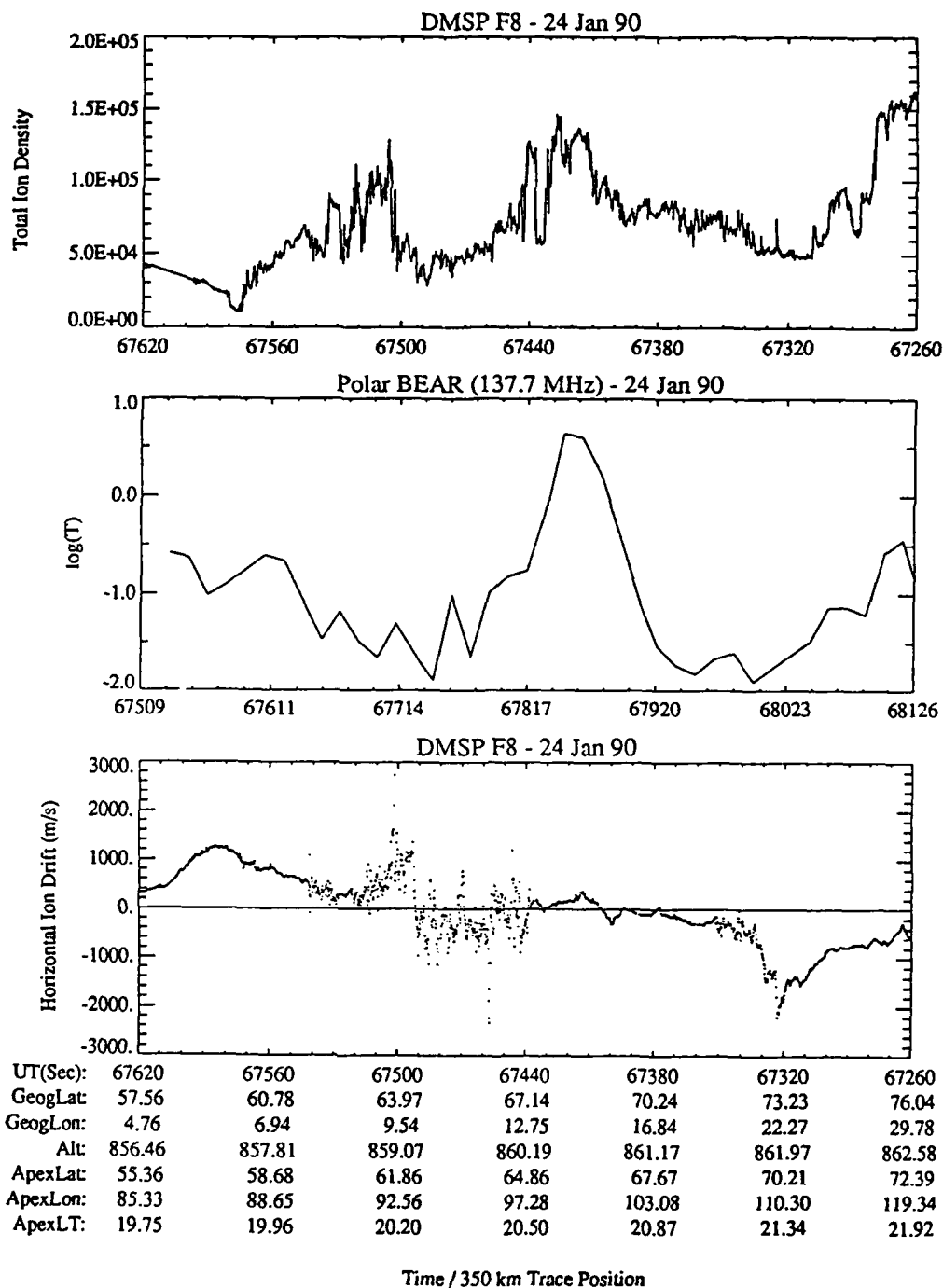


Figure 38b. Data from the DMSP SSIES/SM and SSIES/DM sensors and the Tromso-PB VHF link for the intervals shown in Figure 38a. The top plot is the SSIES/SM total ion density data and the bottom plot is the SSIES/DM horizontal cross-track ion drift velocity. Both are plotted in time-reverse order. The middle plot is the T parameter derived from the Tromso-PB VHF phase spectra.

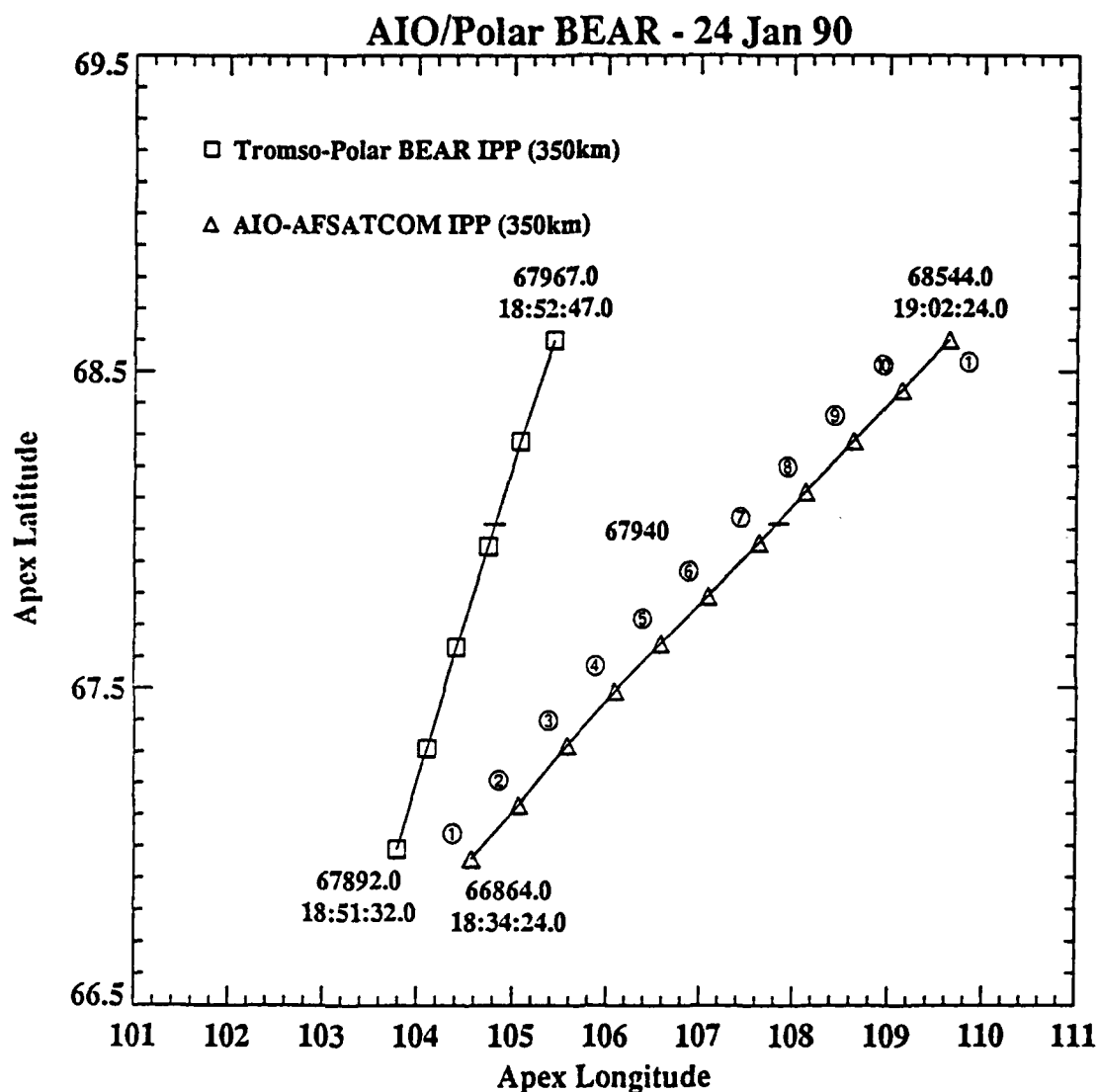


Figure 39a. Locations of the 350 km IPP for the AIO-AFSATCOM link and the 350 km IPP for the Tromso-PB link for the 24 January 1990 data set. The location marked by a cross-bar on both traces indicates the point where the two experiments were collecting data on the same geomagnetic latitude. The symbols are plotted at center-points for data samples used to generate various irregularity/scintillation parameters. The circled numbers on the AIO-AFSATCOM trace are used to identify individual data samples.

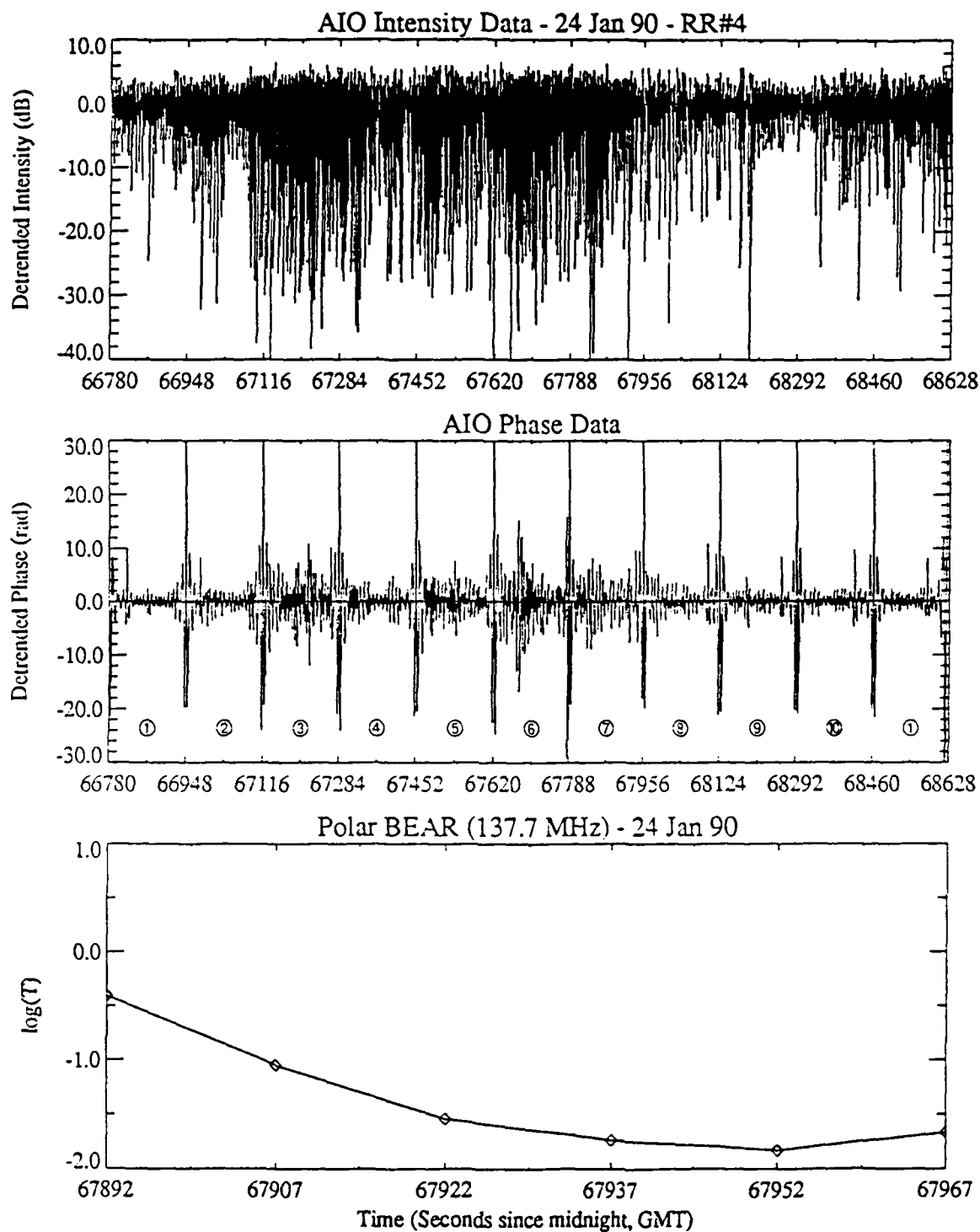


Figure 39b. Data from the AIO-AFSATCOM link and the Tromso-PB VHF link for the intervals shown in Figure 39a. The top plot is the detrended intensity and the middle plot is the detrended phase from the AIO-AFSATCOM link (both detrended using a low-pass filter with a 0.1 Hz cutoff), and the bottom plot is the T parameter derived from the Tromso-PB VHF phase spectra.

Figure 38a shows the location of the DMSP footprint and the Tromso-PB IPP. Labeling of this plot is similar to that in Figure 37a, with the addition of the location of Tromso (by a cross) and an indication of the latitude span of the AIO-AFSATCOM link IPP for this experiment. [Note the relatively narrow range covered by the AIO-AFSATCOM data set (over a relatively long period of time) compared to the range covered by DMSP and Polar BEAR data sets.] The data from these sets is shown in Figure 38b. The top plot shows the DMSP SSIES/SM density data (again, in time-reverse order), the middle plot is the T parameter derived from the Polar BEAR VHF phase data, and the lower plot is the cross-track ion drift velocity from the DMSP SSIES Drift Meter (DM) instrument (also in time-reverse order). The T parameter was derived from resampled phase spectra taken from the summary tape constructed for this Polar BEAR pass at the Tromso HiLat/Polar BEAR station. The method used to do this is identical to that used in building the HiLat/Polar BEAR database (i.e., a linear least-squares fit to $[\log(\text{frequency}), \log(T)]$ from 0.6104 Hz to an upper frequency established by an algorithm which locates the noise floor in the spectrum).

Figure 39a shows the location of the Tromso-PB IPP and the AIO-AFSATCOM IPP. Labeling of this plot is identical to that in Figure 37b. The top two plots in Figure 39b are the same as in Figure 37b, covering a wider time/latitude range, and the lower plot in this figure is the T parameter from the Tromso-PB data set. Note again the relatively high levels of scintillation in the AIO-AFSATCOM data and the relatively low levels in the Tromso-PB data (note that the upward trend in T toward the left of the plot is primarily due to geometrical enhancement).

The DMSP SSIES/SM data were converted to estimates of $C_k L$ using procedures established earlier. Since no EISCAT data were available for this data set, the topside profile model was used to calculate the scale factor to convert C_k to $C_k L$. Although no EISCAT data were available for this set, average values for various profile adjustment-parameters derived from fitting the profile to EISCAT data from other data sets were used in constructing the profiles used in this analysis. The primary effects of these adjustments were to increase the semi-thickness of the F2 region just above the F2 peak and to increase the scale height between the F2 region and the satellite. These $C_k L$ estimates were used to generate estimates of the T parameter for the two satellite beacon links using the single-regime power-law phase-screen theory from the WBMOD code. The *in-situ* slope parameter, q , was converted to estimates of the phase-slope parameter, p , using the pure-scatter assumption that $p=q+1$.

As mentioned earlier, the T and p parameters for the Tromso-PB data set were derived using the standard HiLat/Polar BEAR processing methods on resampled phase spectra obtained from a standard-format summary tape. The T/p data for the AIO-AFSATCOM data were derived from linear least-squares fits to phase spectra derived from 4096-point (81.92 second) sets of detrended (0.1 Hz cutoff) phase data centered on the time between AFSATCOM retunes. The fits were made over a frequency range of 0.5 to 10 Hz. The sets of T and p values were converted to $C_k L$ estimates using the same propagation theory used to convert the DMSP $C_k L$ estimates to estimates of T.

A major problem encountered, and not entirely surmounted, in converting between C_kL and T was the lack of complete information about the drift velocity of the irregularities with respect to the propagation paths. The only drift-velocity data available was the cross-track ion drift-velocity from the DMSP SSIES DM sensor. The along-track component was not available as this was to be provided by the SSIES Retarding Potential Analyzer (RPA) instrument, which died during the first few months of operation. Lacking any other information, the horizontal cross-track drift data were converted to a total horizontal-drift by assuming that the drift velocity in this particular local-time/latitude sector would be along lines of constant geomagnetic latitude (i.e., purely-zonal flow in the geomagnetic-coordinate frame). While this introduces potentially large uncertainties in the resulting derived parameters, it is unlikely that they can account for discrepancies between data sets shown later.

The comparison between the DMSP data and the Tromso-PB data is summarized in Figure 40. The top plot is C_kL derived from the DMSP SSIES/SM data and the bottom plot is the five-second average cross-track drift velocity from the SSIES/DM data, both plotted in time-reverse order. The middle plot shows the T data from the Tromso-PB set (solid curve) and T calculated from the DMSP SSIES C_kL and drift data (dashed curve). For the sake of comparison, these same plots are shown in Figure 41 using C_kL and *in-situ* drift from the WBMOD model. By and large, the T estimates generated from the *in-situ* plasma observations are fairly good, given that there is either a large spatial (at the left end of the plot) or temporal (at the right end) distance between the *in-situ* and the beacon measurements. The large peak in the T curves near the center of the plots is due to geometrical enhancement of phase scintillation as the link passes through the "line" in the sky tangential to geomagnetic L-shells (i.e., enhancement by "wing-like" irregularities). While the presence and overall magnitude of this peak is fairly well matched by both the DMSP-derived and the WBMOD T values, the shape of the peak as shown in the beacon observations is much better fit by the DMSP-derived values. This is a function of both an improved specification of C_kL and specification of a more realistic *in-situ* drift velocity (compare the bottom plots in Figures 40 and 41).

A second comparison of these sets is shown in Figure 42. The top plot shows C_kL derived from the Tromso-Polar BEAR VHF phase data (thin solid line), derived from the SSIES/SM data (thin dotted line), and generated by the WBMOD model (thick solid line). The bottom plot shows the phase spectral slope (p) obtained from these same sources. The C_kL plot reinforces the observations of the previous paragraph, and also illustrates how well, on average, the WBMOD model can do given just the date, time, K_p , and sunspot number.

The results shown in the p plot support an observation made in the last status report, that the *in-situ* slope at DMSP altitude is not representative of the slope throughout the irregularity layer as reflected in the slope of the phase spectrum. This could be due to two factors, either a breakdown in the assumption of pure scatter (i.e., $p \neq q+1$), or an indication that the characteristic slope of the spectrum is not constant throughout the irregularity layer. This latter conjecture is based on theoretical work on the effects of magnetosphere-ionosphere coupling on the growth of irregularities in the high-latitude ionosphere [Keskinen and Huba, 1990; Keskinen, 1990].

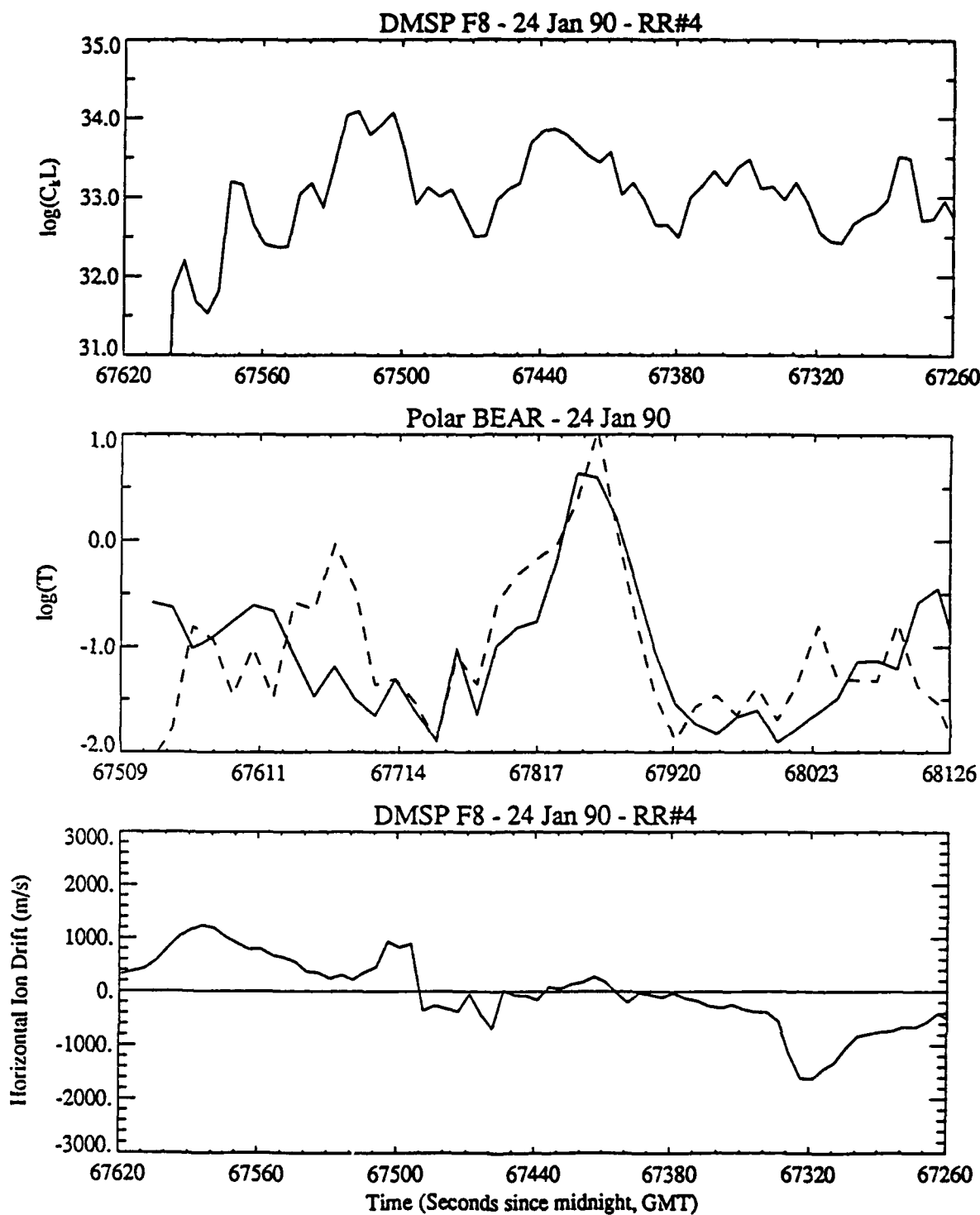


Figure 40. The top plot is $C_p L$ derived from the SSIES/SM data and the bottom plot is of five-minute averages of the SSIES/DM horizontal cross-track ion drift velocity. The middle plot shows the Tromso-PB VHF T values (solid curve) plotted with T values generated for the Tromso-PB geometry using the $C_p L$ values shown in the top plot (dashed curve).

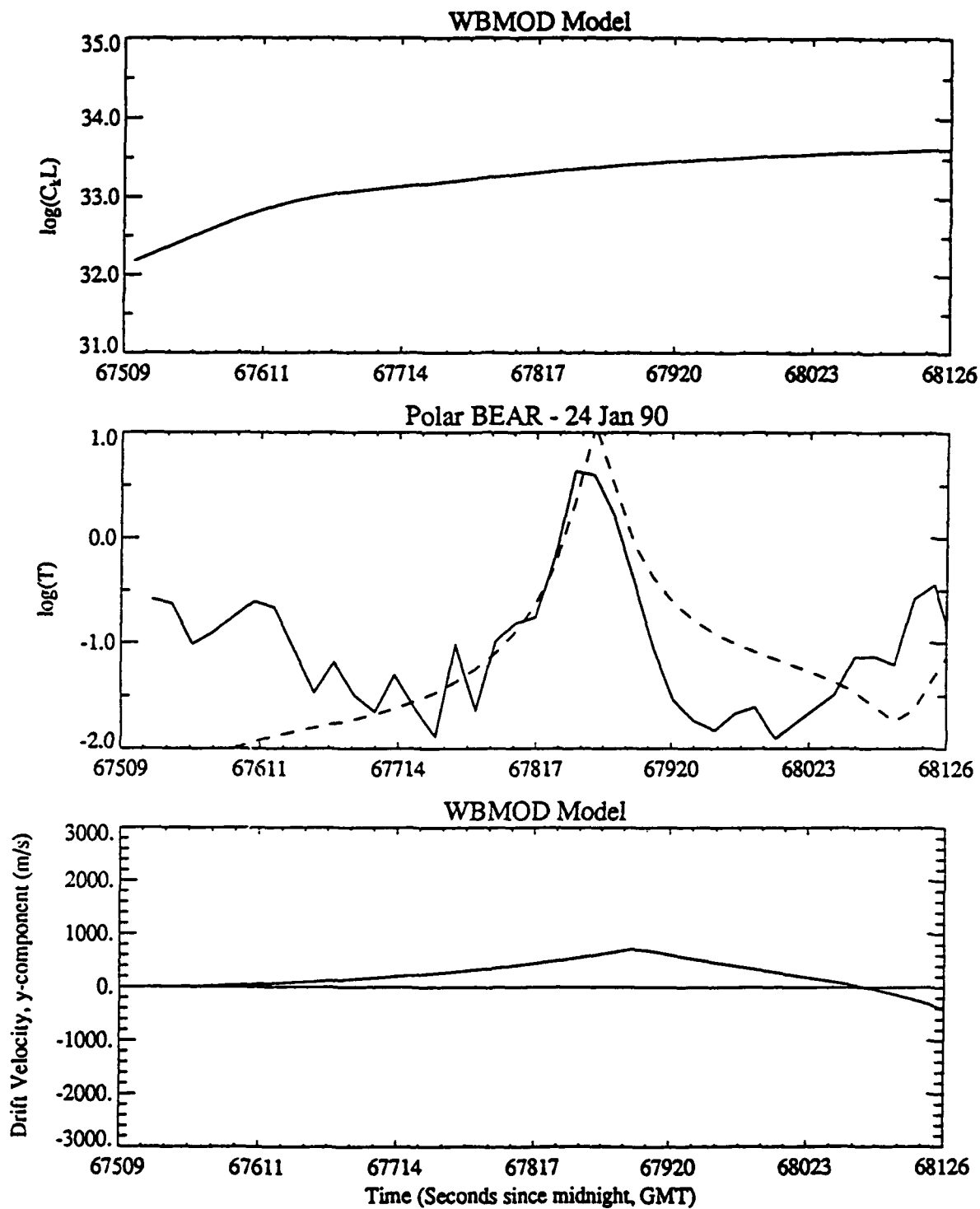


Figure 41. This figure is identical to Figure 40, except that the $C_t L$ values and the drift velocity have been generated from the standard WBMOD model. The dashed curve in the middle plot was also generated from the standard WBMOD.

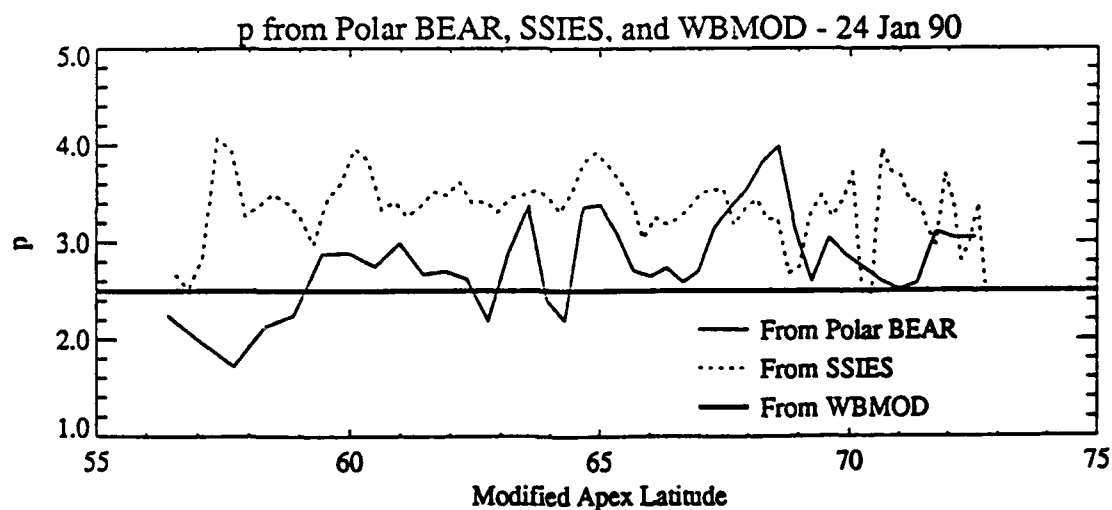
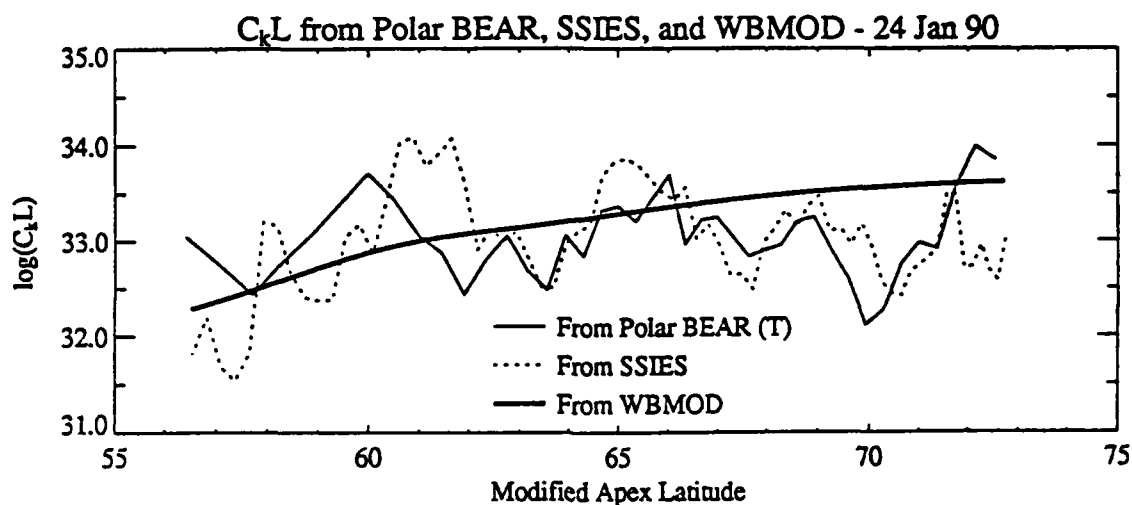


Figure 42. The top plot shows comparisons of the variation of $C_k L$ as a function of geomagnetic latitude from the DMSP SSIES data (dotted line), the Tromso-PB VHF T data (thin solid line), and from the standard WBMOD model (thick solid line). The bottom plot shows comparisons of the variation of the phase spectral slope parameter, p , as a function of geomagnetic latitude from the DMSP SSIES data (dotted line), the Tromso-PB VHF phase data (thin solid line), and from WBMOD (thick solid line).

The essential question is how well the spectrum at the center of the irregularity layer (nominally near the F2 peak at 350 km altitude) maps along field lines to DMSP altitudes (nominally near 850 km). This, according to the theory, will be strongly affected by whether the evolution of the irregularities is controlled by collisional (i.e., ionospheric) or inertial (magnetospheric) conditions [Keskinen, private communication]. At the present time, it appears that either condition is possible in different high-latitude regimes and will be a function of the distribution of plasma along the field-line in question.

Looking at the p plot in Figure 42, it is almost possible to convince yourself that both the DMSP and Tromso-PB values are fluctuating between two nominal values, one near 3.4 and the other near 2.7. The DMSP values are mostly at the higher value, although there are a few at the lower value near 70° apex latitude, and the Tromso-PB values are mostly near the lower value. This might be interpreted as the beacon data being most strongly influenced by irregularities controlled by the collisional regime, while the SSIES/SM sensor at 850 km altitude is most often sampling plasma controlled by the inertial regime. This is a highly tentative, preliminary conjecture, but one which might be worth following up at a later time. The "bottom line" to this digression about the p values is that the values of p derived from the *in-situ* data should not be used to update WBMOD until the relationship between the slope of the *in-situ* density spectrum at DMSP altitudes and the slope at F2-region altitudes is better understood.

This problem of mapping the irregularity spectrum along field lines may also affect the $C_k L$ observations, but possibly not as severely given that this parameter is a measure at kilometer scale-sizes. These scale sizes *might* map along field lines since the effect of the inertial-vs.-collisional question appears to become less important at larger scales, with the transition occurring around kilometer scales [Keskinen, private communication]. Comparing the relative behavior of $C_k L$ from DMSP and Tromso-PB and p from DMSP and Tromso-PB in Figure 42, there is no clear signal in the differences between the two $C_k L$ estimates similar to that seen between the two p estimates. This is also an area worthy of future study.

Figure 43 shows a comparison of T values from the DMSP SSIES data to the Tromso-PB data (top plot), and the DMSP SSIES data AIO-AFSATCOM data (bottom plot). [Note: SSIES-derived T values were not calculated for the entire AIO-AFSATCOM data set as the geometry is for only the first part of the set is currently available.] The SSIES-derived values have been calculated for the geometry valid for the receiver-satellite link at the time the data point is plotted. The most obvious observation which can be made from these two plots is the good agreement between the DMSP and Tromso-PB data and the almost complete disagreement between the DMSP and AIO-AFSATCOM data (and, indirectly, between the Tromso-PB and AIO-AFSATCOM data). The AIO-AFSATCOM T values are as much as three orders of magnitude higher than the DMSP-derived values.

This comparison is extended in the plots in Figure 44. The top plot shows the variation of $C_k L$ with latitude as derived from the DMSP and Tromso-PB VHF-phase data sets, from three of the AIO-AFSATCOM data sets (σ_ϕ , S_4 , and T), and from WBMOD. The bottom plot shows the variation of p from the DMSP, Tromso-PB (VHF phase), AIO-AFSATCOM (VHF phase),

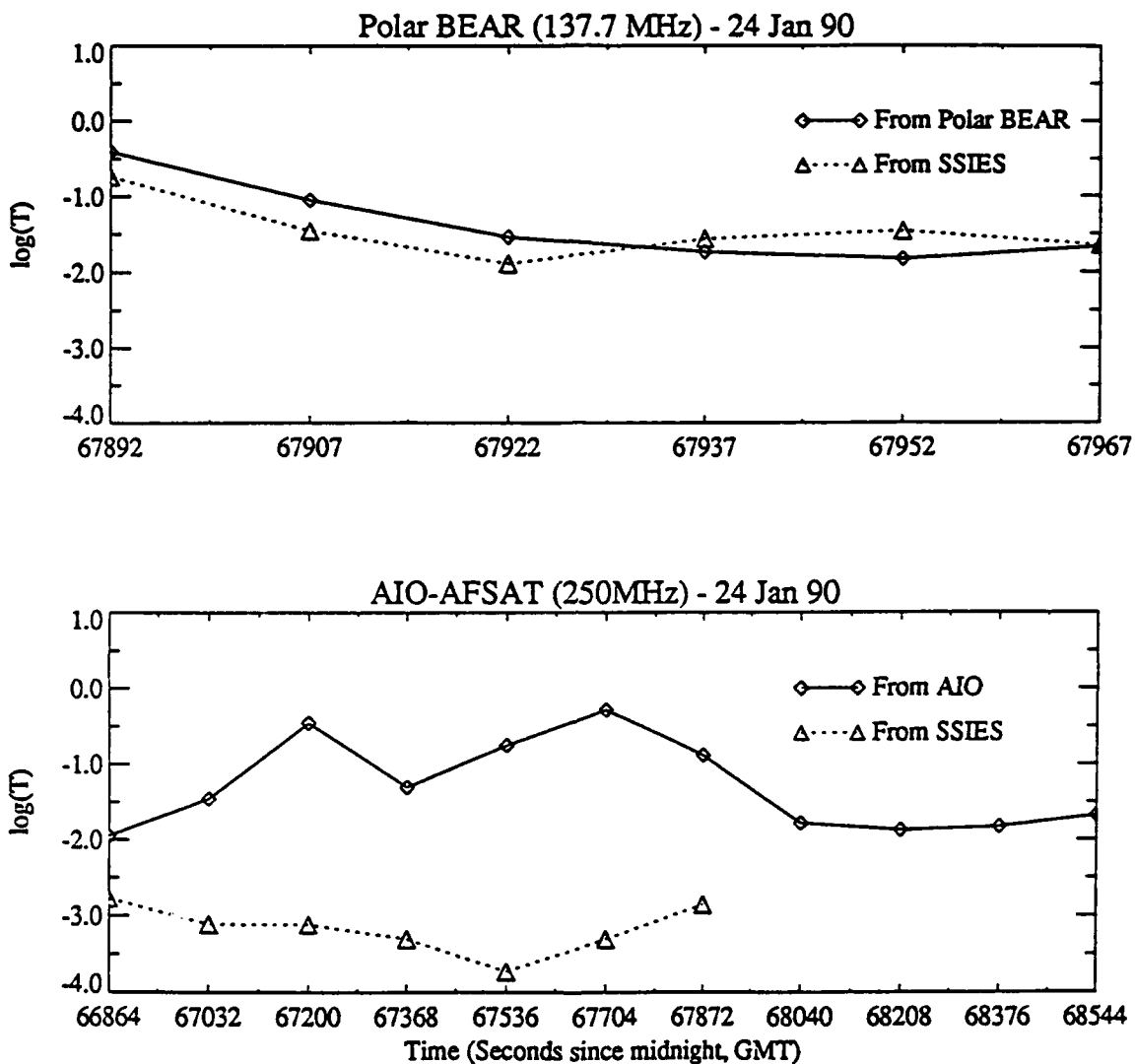


Figure 43. The top plot shows a comparison of T calculate from the SSIES/SM data (dotted line) and from the Tromso-PB VHF data (solid line) over the latitude range coincident with the AIO-AFSATCOM trace (i.e., the same coverage as shown in Figure 39a). The bottom plot shows the same comparison of the SSIES/SM T (dashed line) with that calculated from the AIO-AFSATCOM phase data (solid line).

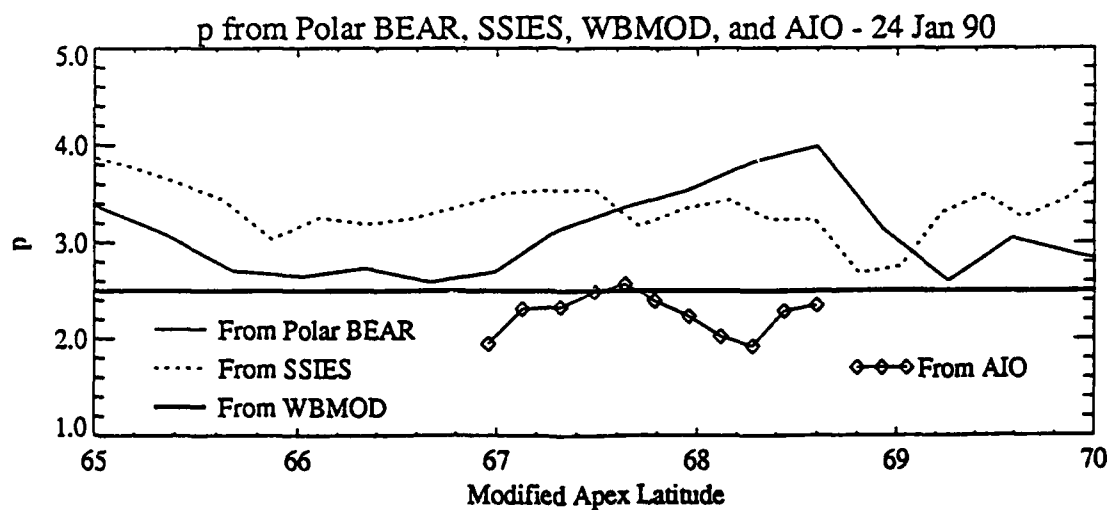
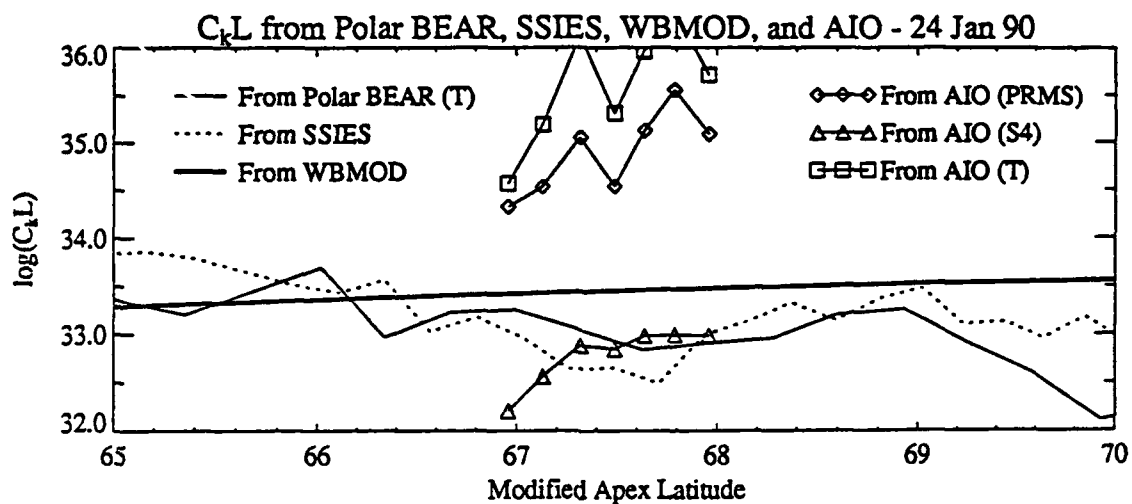


Figure 44. The top plot shows the variation of $C_k L$ from all data sources as a function of geomagnetic latitude, and the bottom plot shows the variation of p as a function of geomagnetic latitude.

and WBMOD sources. In the C_kL plot, the DMSP and Tromso-PB data again show fairly good agreement, as does the C_kL derived from the AIO-AFSATCOM S_4 data (excepting the drop to low values at the low-latitude end). The C_kL values generated from the AIO-AFSATCOM phase data (σ_ϕ and T), however, are two to three orders of magnitude above those from the other sources. This disagreement between the Tromso-PB and AIO-AFSATCOM phase data extends to the phase spectral-slope, where the AIO-AFSATCOM values are almost all below the WBMOD value of 2.5 (which has been found to be too low in other studies) while the Tromso-PB values at the same latitudes almost all exceed 3.0. The phase spectra from both data sets are included in Appendix B.

It appears that only the intensity data from the AIO-AFSATCOM link is useful for the purpose of validating the C_kL values generated from DMSP SSIES/SM data. This is unfortunate for two reasons: first, S_4 saturates as the level of scintillation increases beyond a certain point making calculation of an unambiguous C_kL from that data difficult (if not impossible); second, we had hoped that comparisons could be made between the *in-situ* and phase spectra to investigate the issue discussed earlier about mapping the irregularity spectrum from the F2 region to DMSP altitudes.

5. Drift-Velocity Effects

The comparison plots of S_4 and σ_ϕ for each of the five days are repeated in Figures 45 and 46, respectively (note that these are the results presented in Section 2). In none of the cases analyzed are the results as good as found in the analysis of data from the January 1988 campaign [Secan and Reinleitner, 1989], and the present results are not consistent from data set to data set, or even within a single data set. For example, the DMSP-derived S_4 values are higher than the AIO-AFSATCOM values for most of the 17, 23, and 25 January sets, lower for most of the 24 January set, and both above and below in the 28 January set. The phase results are equally mixed. In addition, while the DMSP-based results are often better than those provided by the WBMOD model (run using only SSN and K_p), there are cases when both the level and the trend are reflected better by the WBMOD results.

One potentially-major problem with the σ_ϕ calculations from the DMSP data is the uncertainty in the drift velocity of the irregularities. As described in Appendix A, the only information available about this velocity is the horizontal cross-track drift component from the DMSP Drift Meter (DM). This was used to estimate the total drift velocity by assuming that the drift was wholly zonal (sunward) in the F8 satellite cases (near 1800 geomagnetic local time (GMLT)), and by simply setting the y-component of the drift to the cross-track value and the x-component to zero in the F9 satellite cases (near geomagnetic midnight). Neither of these procedures was entirely satisfying (particularly in the midnight-sector cases). This will only impact the σ_ϕ values calculated from the DMSP data, as the velocity is not a factor in the S_4 calculations. In order to assess the impact of errors in the drift velocity on the phase results, the DMSP-derived σ_ϕ values were calculated for seven different drift velocity inputs (components are

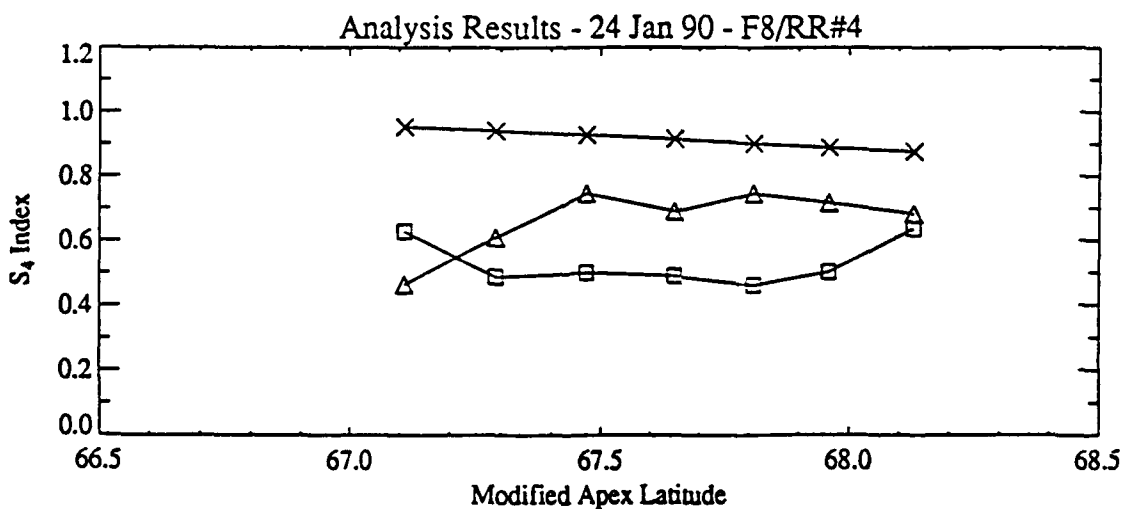
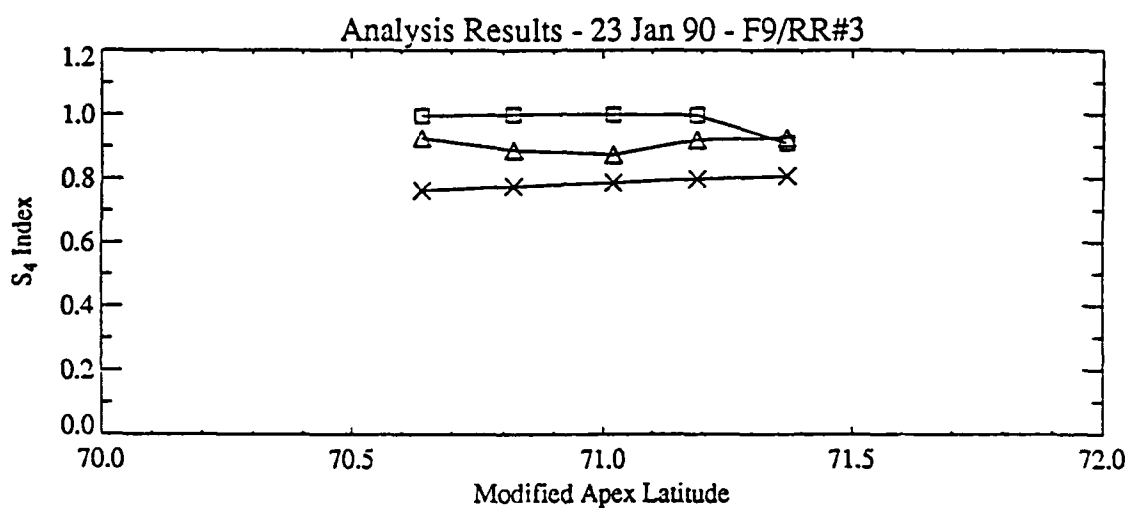
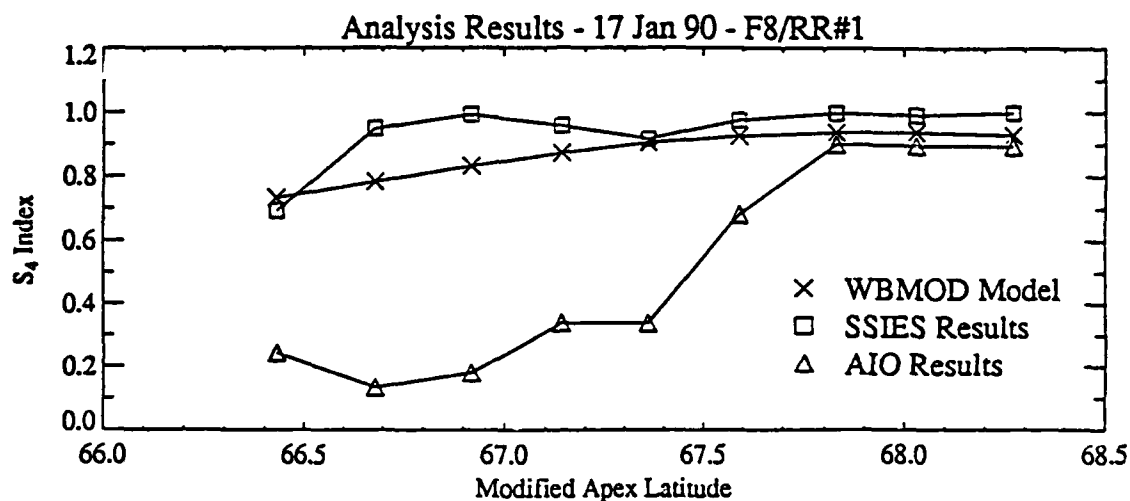


Figure 45. Comparison of S_4 values from the WBMOD model, the AIO-AFSATCOM data, and the DMSP/SSIES data for all five days included in the analysis.

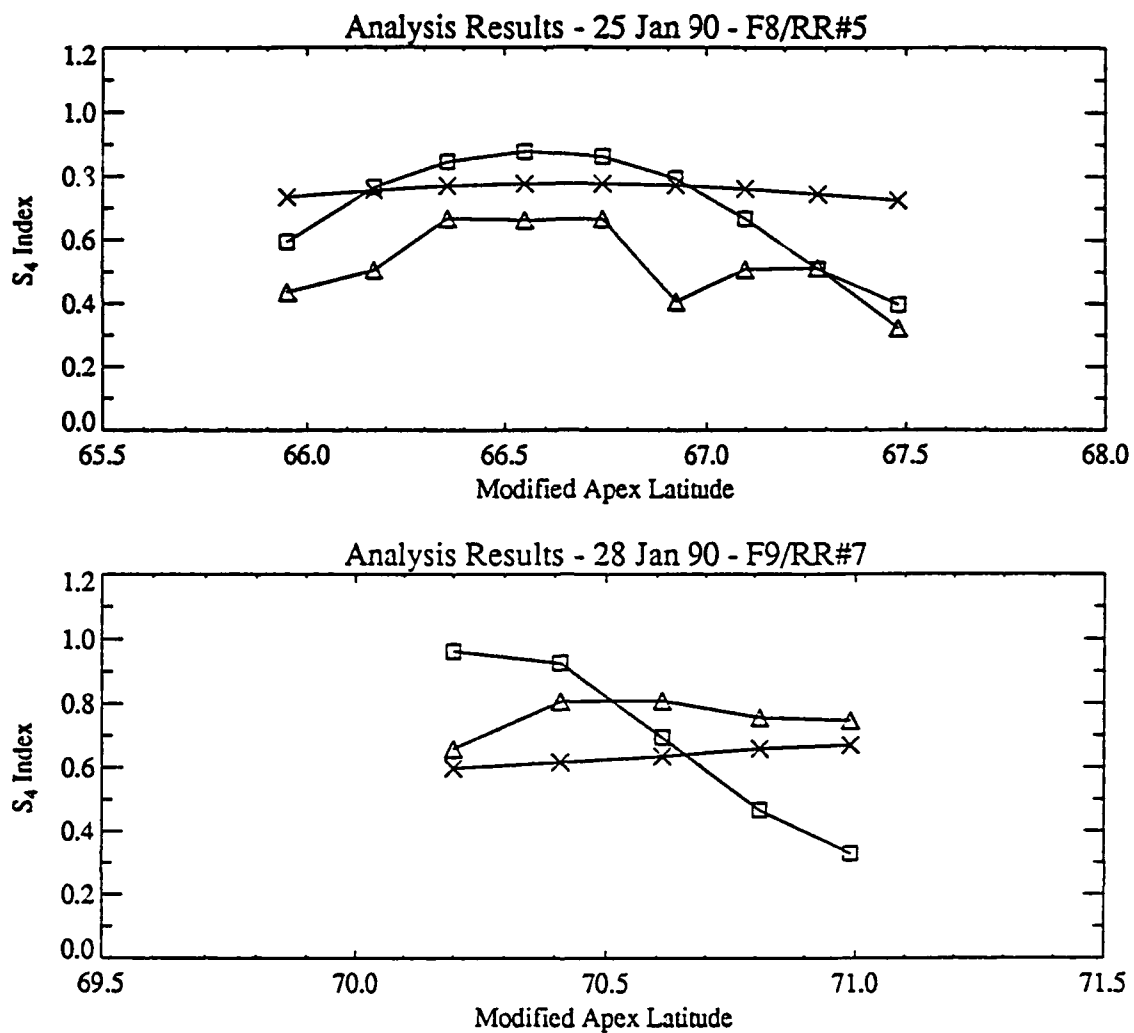


Figure 45. (Continued)

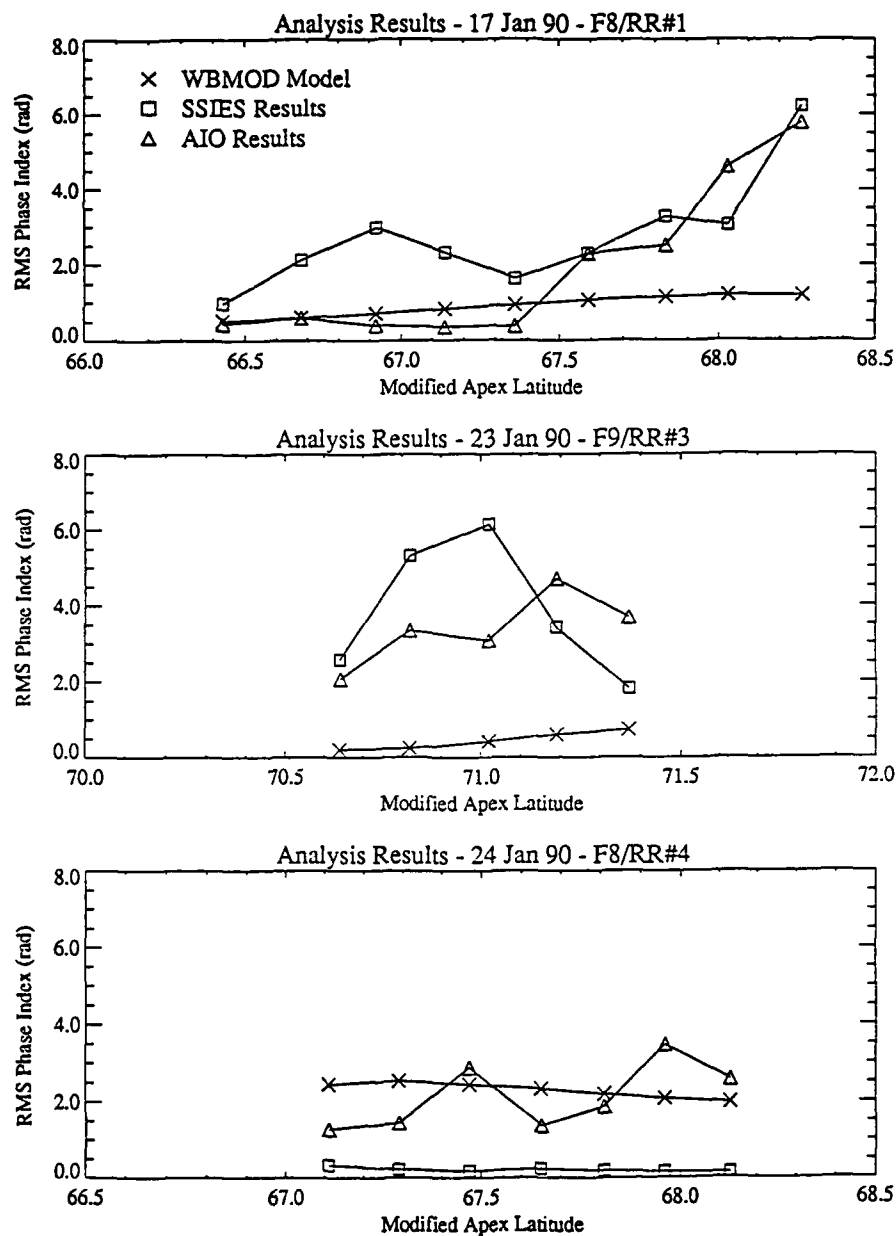


Figure 46. Comparison of σ_p values from the WBMOD model, the AIO-AFSATCOM data, and the DMSP/SSIES data for all five days included in the analysis.

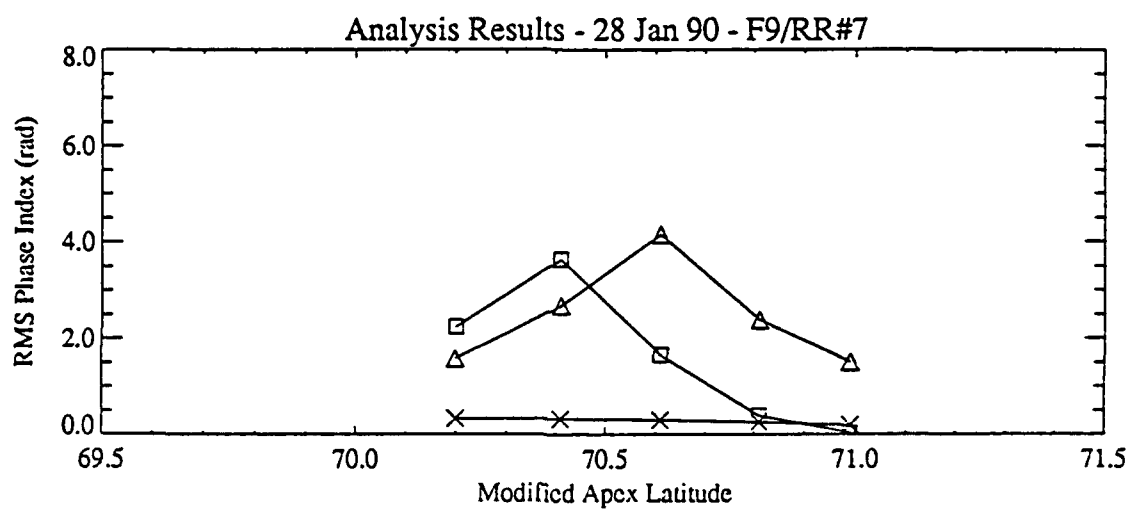
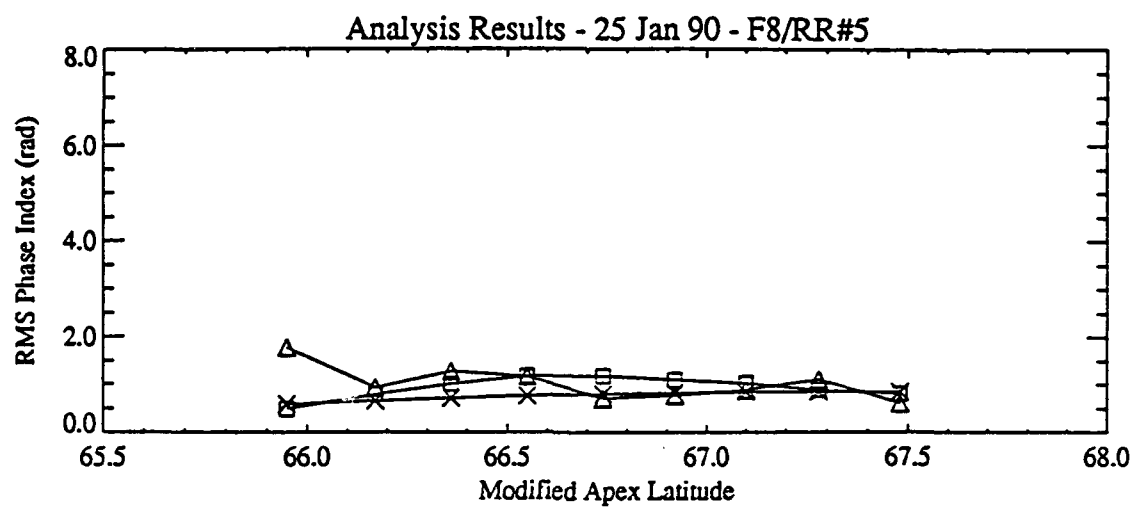


Figure 46. (Continued)

defined in a local cartesian system aligned with the geomagnetic field such that +x is north in the geomagnetic meridian, +z is in the local nadir direction, and +y is east):

Case 1a:

x-component: 0.0
y-component: As described in Appendix A
z-component: 0.0

Case 1b:

x-component: 0.0
y-component: As described in Appendix A, reduced by 50%
z-component: 0.0

Case 1c:

x-component: 0.0
y-component: As described in Appendix A, increased by 50%
z-component: 0.0

Case 2a:

x-component: +250 m/s
y-component: As described in Appendix A
z-component: 0.0

Case 2b:

x-component: -250 m/s
y-component: As described in Appendix A
z-component: 0.0

Case 2c:

x-component: +500 m/s
y-component: As described in Appendix A
z-component: 0.0

Case 2d:

x-component: -500 m/s
y-component: As described in Appendix A
z-component: 0.0

The results of these calculations are shown in Figure 47. [Note that the changes in the x-component of the drift has no effect on the two midnight-sector cases (23 and 28 January) due to the geometry of these cases. In both cases, the IPP is due north (geomagnetic) from the AIO loca-

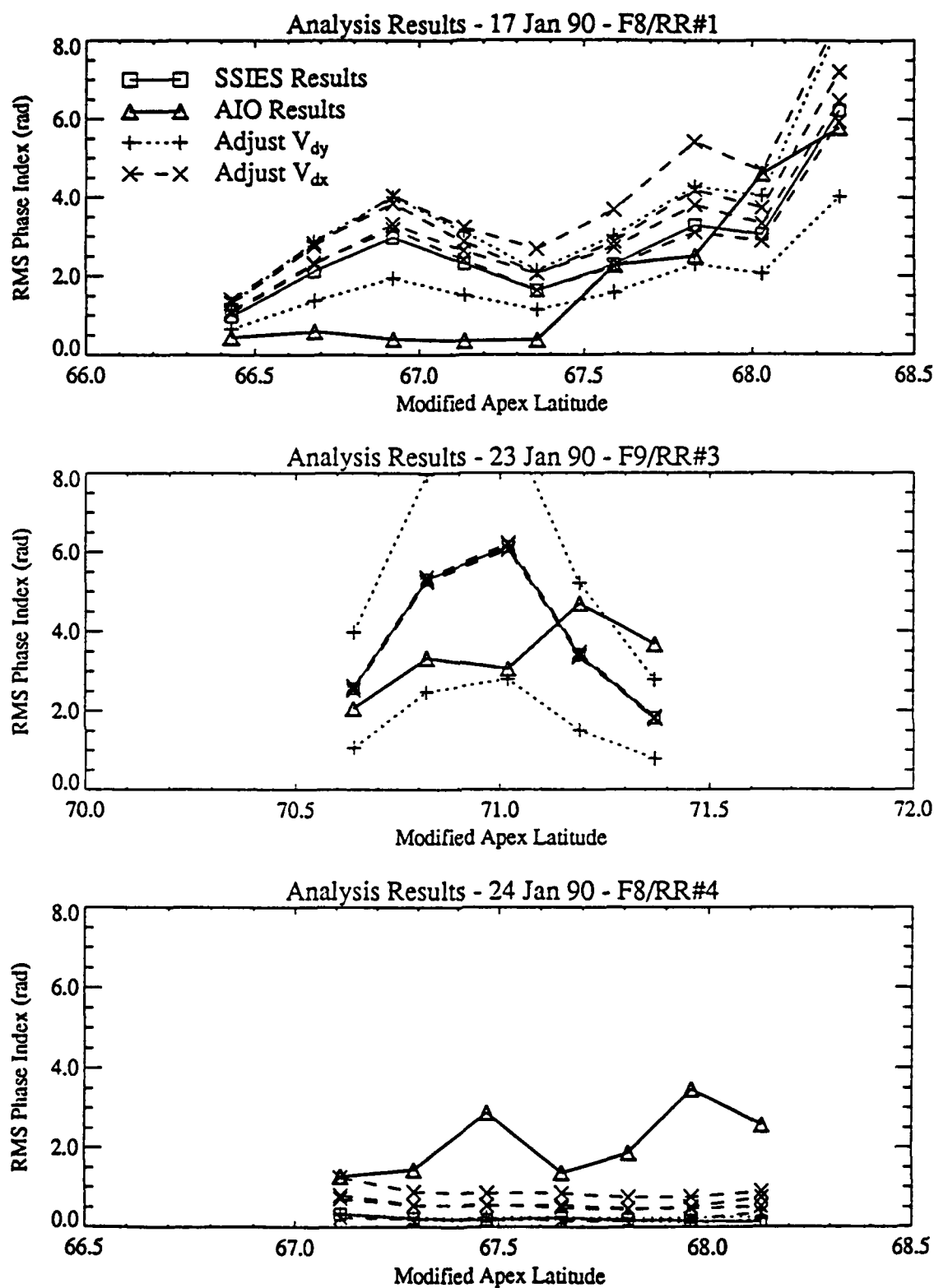


Figure 47. Comparison of σ_ϕ values from the WBMOD model, the AIO-AFSATCOM data, and the DMSP/SSIES data for all five days included in the analysis using different modifications to the drift velocities used in the calculation.

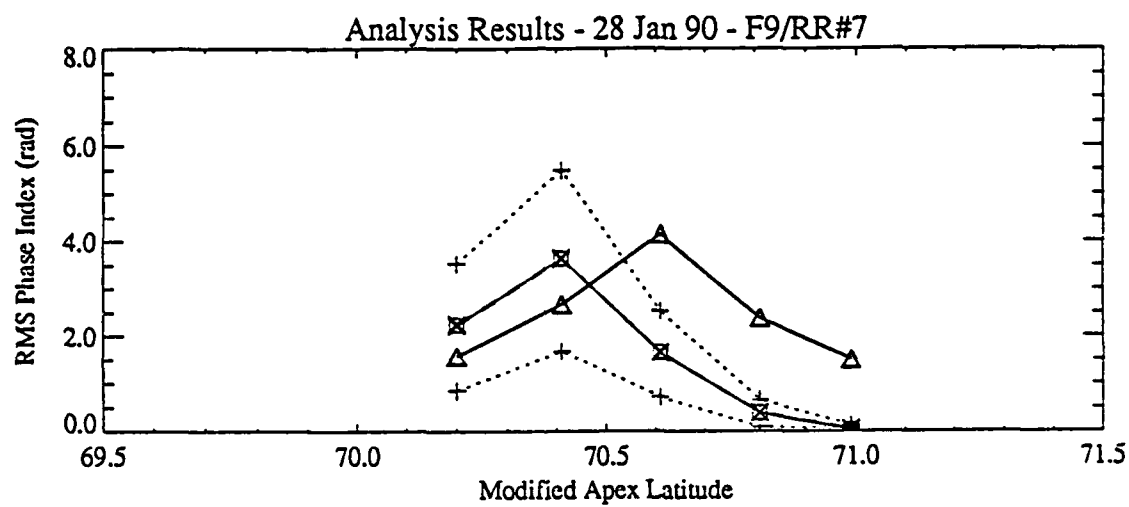
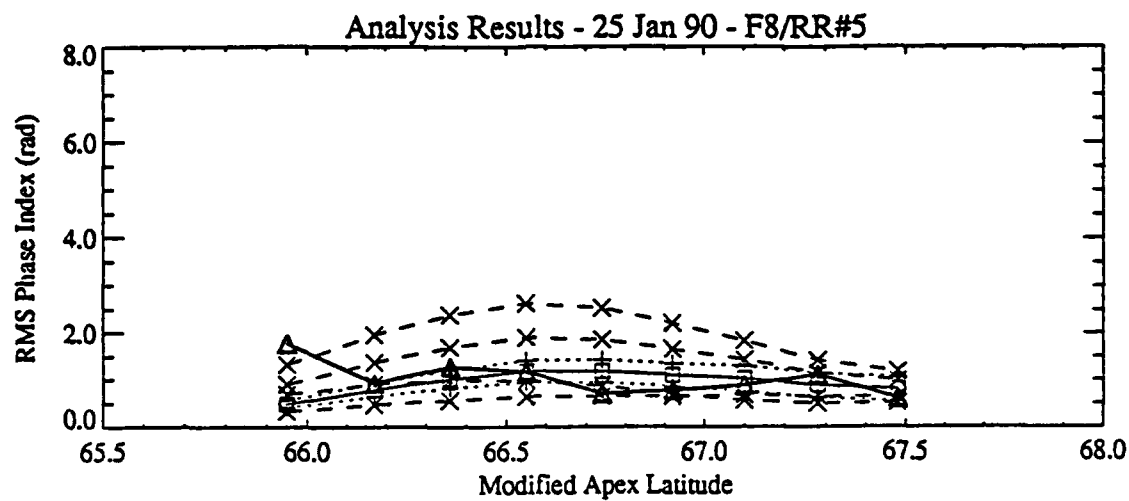


Figure 47. (Continued)

tion. Thus, all motion along the x-axis (in the geomagnetic meridian) is along the elongated axis of the irregularities. This reduces the contribution of motion in that direction by roughly a factor of 20 with respect to contributions from motion along the y-axis.]

In many of the cases, the σ_ϕ values observed on the AIO-AFSATCOM link fall within the range of σ_ϕ values calculated from the SSIES data using various models for the *in-situ* drift. The primary exceptions to this are at the southern end of the 17 January data set, almost all of the 24 January data set, and at the northern end of the 28 January set. The 17 and 24 January data sets have been discussed in some detail in Sections 3 and 4, and there are concerns about the quality of the data at the northern end of the 28 January data set, so we will not discuss any of those sets further. The results from the remaining cases indicate that the results obtained from the SSIES data are comparable to the results obtained from the beacon measurements within the uncertainties in the *in-situ* drift velocities.

Note: This section focused on the effects of uncertainties in the *in-situ* drift velocities on the calculation of the SSIES-derived $C_k L$ values, not on the issue of which SSIES-derived values to compare with which AIO-AFSATCOM values due to the bulk drift of the structured plasma. This issue was addressed in the discussion of the data from 17 January in Section 3.1.]

6. Discussion

While the results obtained in the study reported in this document are not as clear (nor as positive) as those obtained in the previous study of this problem [Secan *et al.*, 1990], a number of things have been learned:

1. It is essential to have either a near-coincident observation of, or a good model for, the density at the peak of the F2 layer in order to calculate the effective layer thickness used to scale the *in-situ* C_k measurement to an estimate of the height-integrated $C_k L$ parameter.

2. It is also important to have measurements of both components of the horizontal *in-situ* drift velocity near-coincident with the density measurements used in calculating C_k . These values are important for calculating C_k from the T and p parameters derived from the ΔN power density spectrum (PDS). They are essential when attempting to compare the *in-situ* measurements to remote measurements made at different locations and times to permit correct ordering of the comparisons.

3. While the constant- $\Delta N/N$ model appears to work well a good portion of the time, there is some evidence that it is not a universally applicable model. The data from the southern section of the 17 January set may be an example of conditions where the scaling approaches that predicted by a constant- ΔN model. At this time, it is not at all clear how one might differentiate between cases where one or the other model should be used based strictly on data available from DMSP, or even using other data. If these data are to be used operationally, this is an issue which needs to be addressed.

Two other assumptions used in calculating the scaling factor are also still open to question. The first is that the irregularities observed at the DMSP altitude are the result of structuring occurring near the F2 region (i.e., in the bulk of the irregularity layer). The second is that this structure then maps along the field line to DMSP altitude in a way which preserves the shape of the ΔN power density spectrum (PDS). It is almost impossible to address the validity of these two assumptions with the data available. We had hoped to be able to compare the *in-situ* ΔN PDS with the PDS of the AIO-AFSATCOM phase, which would allow use to look at differences between the spectrum at 840 km altitude with the height-integrated spectrum. Problems with the AIO-AFSATCOM phase data (high levels of low-frequency phase noise as described in *Secan and Reinleitner* [1989]) made this comparison impossible. Additional comparisons with near-coincident Polar BEAR or HiLat passes at either Tromso or other high-latitude sites (Ft. Churchill, Poker Flat, or Pt. Barrow) similar to the study presented in Section 4 could be one way to investigate this further. A second method would be to conduct a joint rocket-DMSP experiment in which a rocket with an *in-situ* density probe was flown along a trajectory through the F2 region along the base of the field lines sampled by a coincident DMSP pass. The ΔN spectra measured in the F2 region by the rocket could then be compared with the spectrum measured at the DMSP altitude. In any case, these issues need to be resolved.

7. Conclusion

While this study has not come to the conclusion that the $C_k L$ values derived from DMSP SSIES observations are valid at all times, it has demonstrated that the methods used produce estimates of scintillation comparable with that observed on a near-coincident transionospheric path, and has established what information is critical to the process of scaling the *in-situ* C_k measurements to $C_k L$. It has also found that there are times when at least one of the assumptions used in this scaling process appears to break down, at which time the level of scintillation predicted by the *in-situ* measurement typically overestimates the level observed by a beacon measurement.

The next step towards operational use of these data would be to deal with the issues raised in Section 6. In particular, ways need to be developed to determine from the *in-situ* measurements alone when the assumptions used in scaling are invalid.

REFERENCES

- Keskinen, M. J., Scaling laws for the spectrum of interchange instabilities in the high-latitude ionosphere, *J. Geophys. Res.*, 95, 19,137-19,141, 1990.
- Keskinen, M. J. and J. D. Huba, Nonlinear evolution of high-latitude ionospheric interchange instabilities with scale-size dependent magnetospheric coupling, *J. Geophys. Res.*, 95, 15,157-15,166, 1990.

- Secan, J. A., *An Assessment of the Application of In Situ Ion-Density Data From DMSP to Modeling of Transionospheric Scintillation, Scientific Report No. 1, AFGL-TR-87-0269*, Air Force Geophysics Laboratory, Hanscom AFB, MA, 1987, ADA188919.
- Secan, J. A., *An Investigation of Methods for Updating Ionospheric Scintillation Models Using Topside In-Situ Plasma Density Measurements, Scientific Report No. 1, PL-TR-91-2171*, Phillips Laboratory, Hanscom AFB, MA, 1991, ADA243378.
- Secan, J. A. and R. M. Bussey, *DMSP SSIES Flight Data Processor, System Documentation, Volume I: Functional Description, NWRA-CR-87-R011*, Northwest Research Associates, Inc., Bellevue, WA, 1987.
- Secan, J. A. and R. M. Bussey, *An Assessment of the Application of In Situ Ion-Density Data From DMSP to Modeling of Transionospheric Scintillation, Scientific Report No. 2, AFGL-TR-88-0280*, Air Force Geophysics Laboratory, Hanscom AFB, MA, 1988, ADA202415.
- Secan, J. A. and L. A. Reinleitner, *An Assessment of the Application of In Situ Ion-Density Data From DMSP to Modeling of Transionospheric Scintillation, Scientific Report No. 3, AFGL-TR-89-0264*, Air Force Geophysics Laboratory, Hanscom AFB, MA, 1989, ADA222695.
- Secan, J. A., L. A. Reinleitner, and R. M. Bussey, *An Assessment of the Application of In Situ Ion-Density Data From DMSP to Modeling of Transionospheric Scintillation, Final Report, GL-TR-90-0093*, Geophysics Laboratory, Hanscom AFB, MA, 1990, ADA224392.

Appendix A. Data Analysis Procedures (AIO and DMSP)

A.1 AIO-AFSATCOM data.

The intensity and phase data from the 250 MHz link between the AIO and AFSATCOM satellite were provided by Dr. R. Livingston (SRII) on magnetic tapes in DEC binary format. A translation program was developed to read these tapes and convert the data to SUN (UNIX) binary format. The accuracy of the translation was verified using listings of the data provided by Dr. Livingston and by comparing plots of the data to plots generated earlier at SRII. The data provided were generated directly from the I and Q data collected on the AIO, and had not been further processed at SRII to remove effects of the frequency shift which occurs on the signal every 168 seconds.

Both types of data were detrended by removing a low-frequency trend constructed using a two-pass, six-pole Butterworth filter with a 6dB cutoff frequency of 0.1 Hz (10 seconds). The intensity data were detrended by dividing each intensity observation by the output of the filter corresponding to that observation, thus normalizing the data to generate a mean value of 1.0 for data samples longer than 10 seconds. The phase data were detrended by subtracting the filter values, normalizing to a zero mean.

Figures A-1 and A-2 show the detrended intensity and phase data, respectively, from a portion of the AIO-AFSATCOM data for 17 January 1990. The periodic spike-features seen in the detrended phase data are located at the times when the AFSATCOM frequency was changed. The rather restrictive cutoff frequency of 0.1 Hz used in the detrending process was selected in part to limit the range of the effects of the phase discontinuities and in part to remove low-frequency noise found in the phase data in analyzing the data from the January 1988 campaign [Secan and Reinleitner, 1989].

In order to avoid contamination from the frequency shift, the scintillation indices, S_4 and σ_ϕ , were calculated from 120-second data samples centered on times halfway between frequency shifts. This provided a 24-second "buffer" between the ends of the data samples used and the nearest frequency-shift time. In all cases where the effects of the frequency shift could be clearly distinguished, this isolated the "ringing" seen in Figure A-02 at the frequency-shift points from the data used in calculating σ_ϕ .

A.2 DMSP/SSIES Data.

The DMSP/SSIES raw-telemetry data were provided on magnetic tape in Air Weather Service (AWS) PREPFILE format by Dr. Fred Rich (PL/GPSG). The data from the Scintillation Meter (SM) and Drift Meter (DM) instruments were processed to generate files of the total ion density (N_i) from the SM sensor and total ion density, horizontal cross-track ion drift velocity (U_h) and vertical cross-track ion drift velocity (U_v) from the DM sensor. This processing is done using modified versions of software used by AWS to process the data, with some hand-analysis

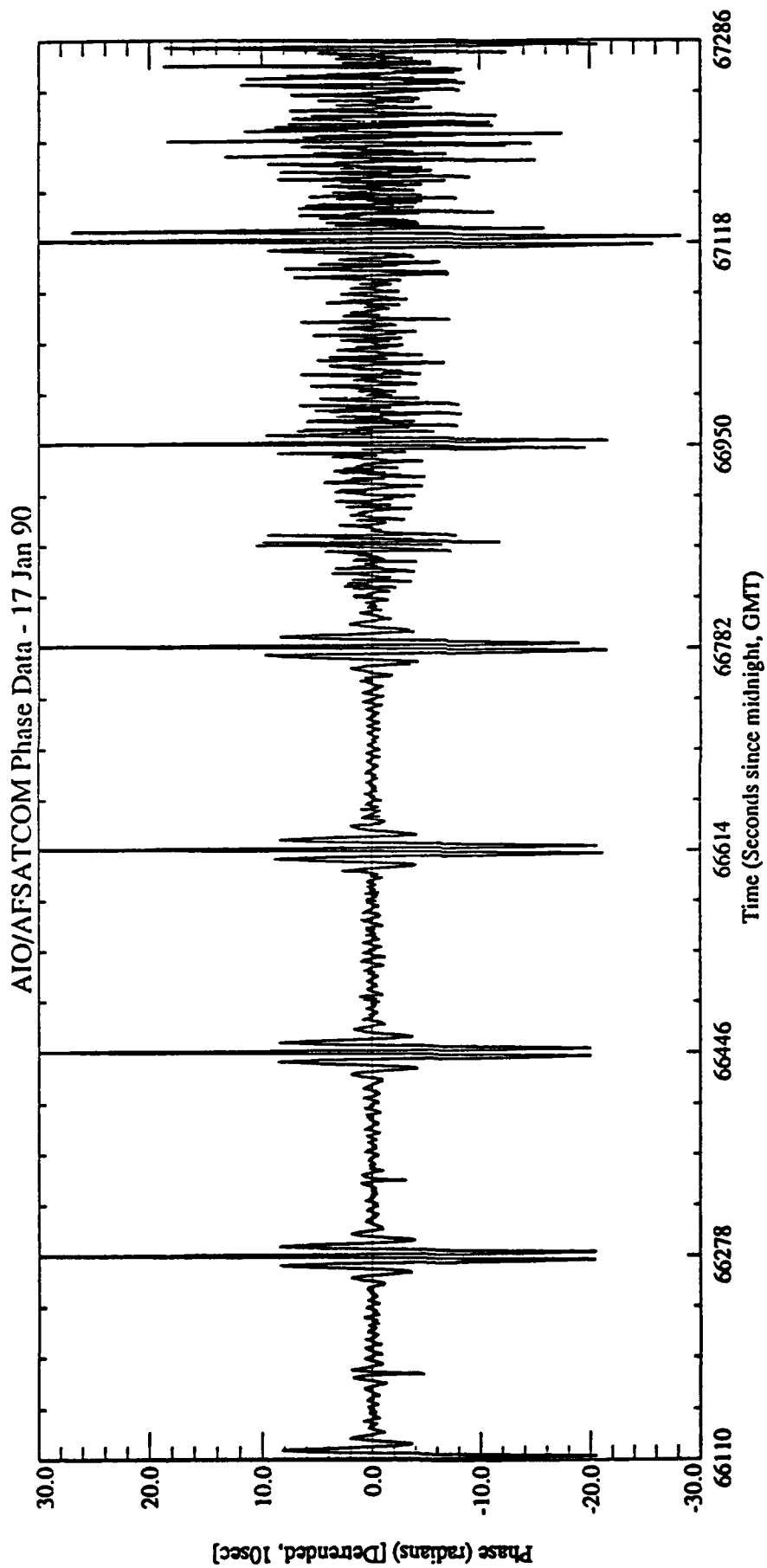


Figure A-1. Sample detrended AIO/AFSATCOM intensity record.

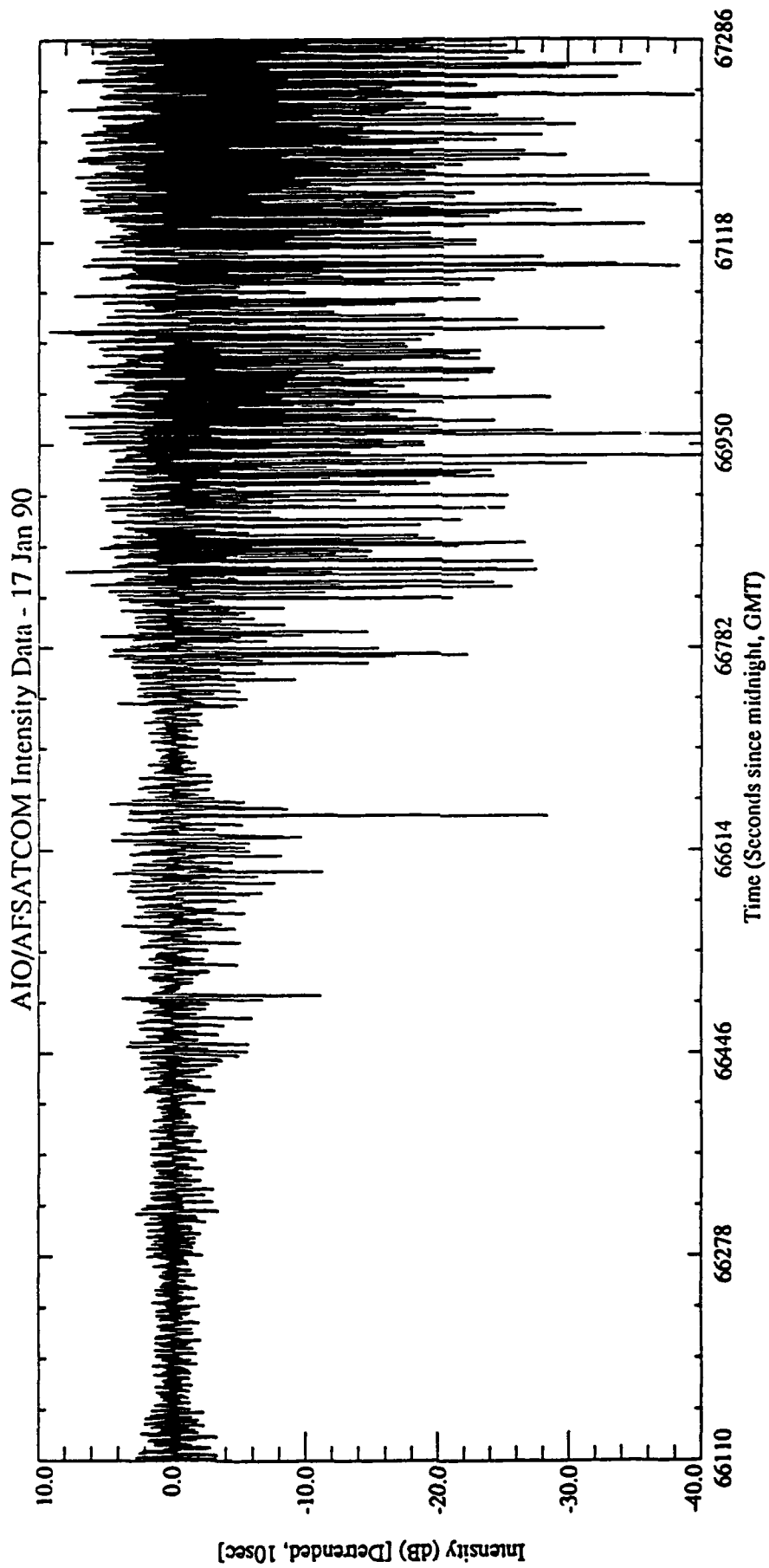


Figure A-2. Sample detrended AIO/AFSATCOM phase record.

[1987].) The procedures used to calculate estimates of S_4 and σ_ϕ for the AIO-AFSATCOM geometry are essentially the same as those described in detail in *Secan* [1988]. They will be summarized here with indications of changes which have been made since that publication.

The first step is to calculate estimates of the *in situ* spectral strength parameter, C_k , from the density and drift-velocity data. The SM N_i data are detrended using the same filter employed in detrending the AIO-AFSATCOM phase data with a 0.046875 Hz (21.333... second) cutoff frequency, and the DM U_h data are smoothed by creating five-second centered-averages. An estimate of C_k is calculated every five seconds using the following procedure:

1. Select a 256-point (10.666... seconds) data sample from the detrended (ΔN_i) density data centered on the analysis time.
2. Generate a power-density spectrum (PDS) from the sample using an FFT. The data are windowed using a 30% cosine taper prior to the FFT and are smoothed using a centered five-point smoothing function (binomial weights) after the FFT.
3. Generate estimates of the slope (q) and spectral strength (T_1) parameters from a linear least-squares fit to $\log(\text{frequency})$ and $\log(\text{PDS})$ over the frequency range 0.3 to 5.0 Hz. The q parameter is the negative of the slope of the fit, and the T_1 parameter is the zero-intercept of the fit.
4. Calculate an estimate of C_k from q , T_1 , the satellite velocity (v_s), and U_h using Equation [1] from *Secan* [1987].

In order to calculate estimates of the scintillation indices, an estimate of the line-of-sight integrated irregularity strength, $C_k L$, must be made from the C_k estimates. This is done by assuming that the $\Delta N/N$ and the irregularity spectrum observed at the satellite altitude are constant along the field line down to the F2 region peak. This permits calculation of an effective layer-thickness parameter, L_{eff} , defined by Equation [4-01] in *Secan and Bussey* [1988], which is solely a function of the ionospheric plasma-density profile from just below the F2 peak to the satellite altitude. This profile is generated using a two-component (O+ and H+) model of the ionosphere which is fit to the observed N_i at the satellite and adjusted to the F2 peak densities observed by the EISCAT radar (when available). The estimate for $C_k L$ is then the product of C_k and L_{eff} .

The estimates of S_4 and σ_ϕ for a particular AIO-AFSATCOM case are generated using a modified version of the WBMOD scintillation program (version 10H1). The propagation geometry is determined from input values for the location of the AIO aircraft, the AFSATCOM satellite, and the velocity of the IPP in the plane of the phase screen. Values for five of the eight irregularity model parameters are taken from models internal to WBMOD: the axial ratios (a and b), the phase-screen altitude (h_p), the angle between sheet-like irregularities and geomagnetic L-shells (δ), and the outer-scale size (α_o). The slope of the *in situ* irregularity spectrum (q)

is input to the program, and has been set to a value of 1.8 based on analysis of the HiLat and Polar BEAR databases. Values for $C_k L$ and the *in situ* drift velocity (\underline{v}_d) are extracted from data files by interpolating (cubic interpolation) to the geomagnetic latitude of the 350 km IPP for the AIO-to-AFSATCOM link. The values in the $C_k L$ file are simply the output of the $C_k L$ processing described above. The values in the \underline{v}_d file are derived from the SSIES/DM U_h data according to the following rules:

1. For data from satellite F8 (evening sector), the x- and z-components of the drift (v_{dx} and v_{dz}) are set to zero and the y-component (v_{dy}) is set to $-U_h \csc \gamma$, where γ is the angle between the DMSP satellite velocity vector and the geomagnetic meridian. This is based on the assumption that the predominant drift in this sector is zonal.

2. For data from satellite F9 (midnight sector), there is no satisfying assumption that one can make (such as purely-zonal or purely-meridional flow) to expand the single-component measurement of U_h to v_{dx} and v_{dy} . For these cases, v_{dy} is set equal to $-U_h$ and v_{dx} and v_{dz} are set to zero.

(Note: The effects of these assumptions about the *in situ* drift velocities are discussed in Section 5.)

A similar methods was used to calculate estimates of T for the comparison of DMSP/SSIES observations to those from the Polar BEAR satellite. A second modified version of WBMOD was developed in which the propagation geometry is determined from input values for the location of the ground station (Tromso) and the Polar BEAR satellite at the start and end points of the pass. The velocity of the IPP in the plane of the phase screen is calculated from a circular orbit fit to the input end points of the pass (a standard WBMOD option). The irregularity model parameters (a , b , δ , h_p , α_o , q , $C_k L$, and \underline{v}_d) are all specified or input in the same fashion as described above.

Appendix B. Phase Spectrum Plots — Polar BEAR and AIO-AFSATCOM

This appendix contains plots of phase spectra from the Tromsø Polar BEAR (PB) VHF signal and from the AIO-AFSATCOM VHF signal for times shown in Figure 43. The Tromsø-PB plots show the resampled spectra from the standard HiLat/Polar BEAR summary tapes plotted with the linear fit used to derive T and p . The AIO-AFSATCOM plots show full spectra generated from the 4096-point data sets plotted with the linear fits along with the detrended phase data used to generate each spectrum.

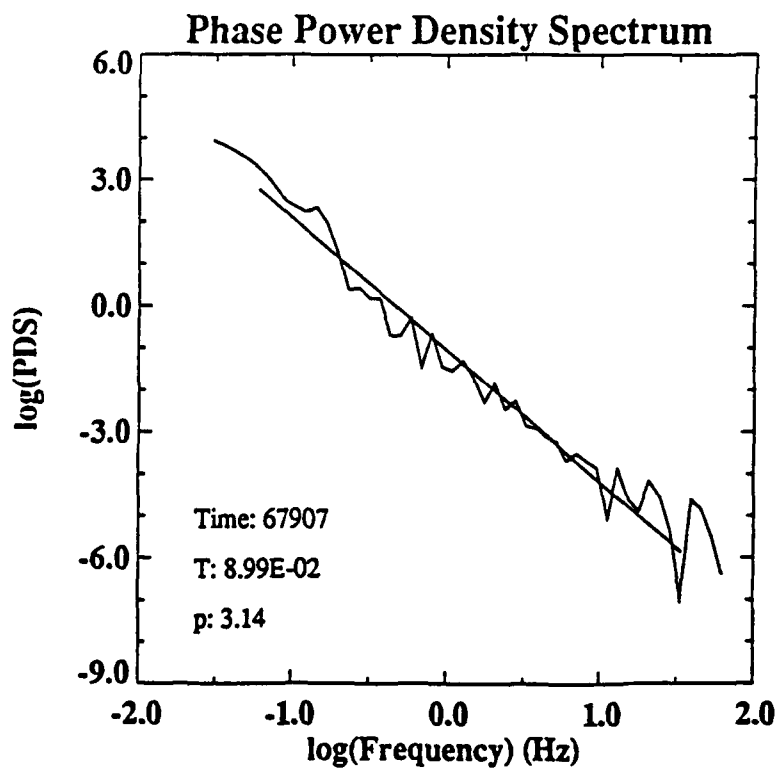
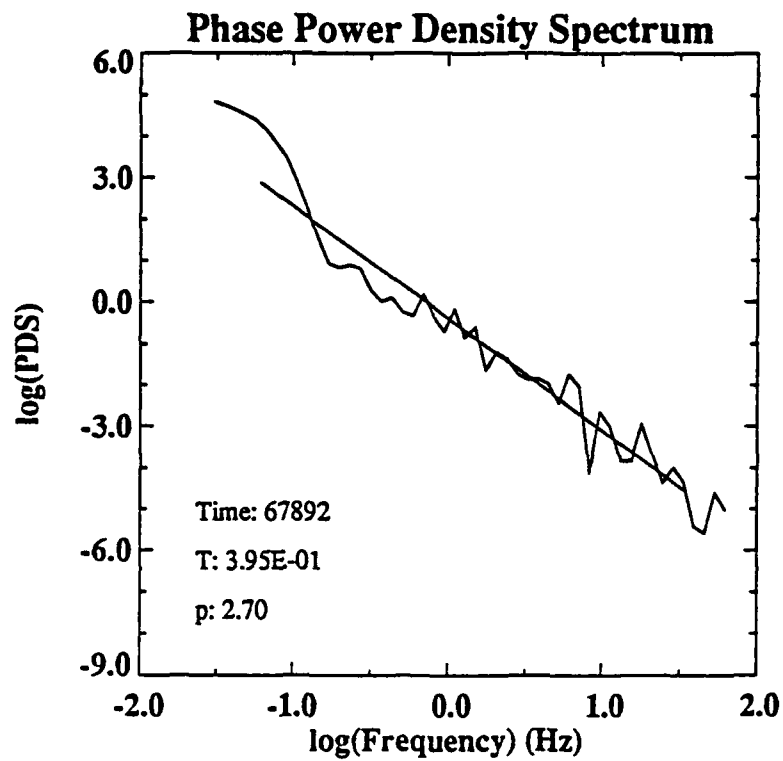


Figure B-1. Resampled VHF phase spectra from the Tromso-Polar BEAR data set overplotted with the linear fits used to calculate T and p.

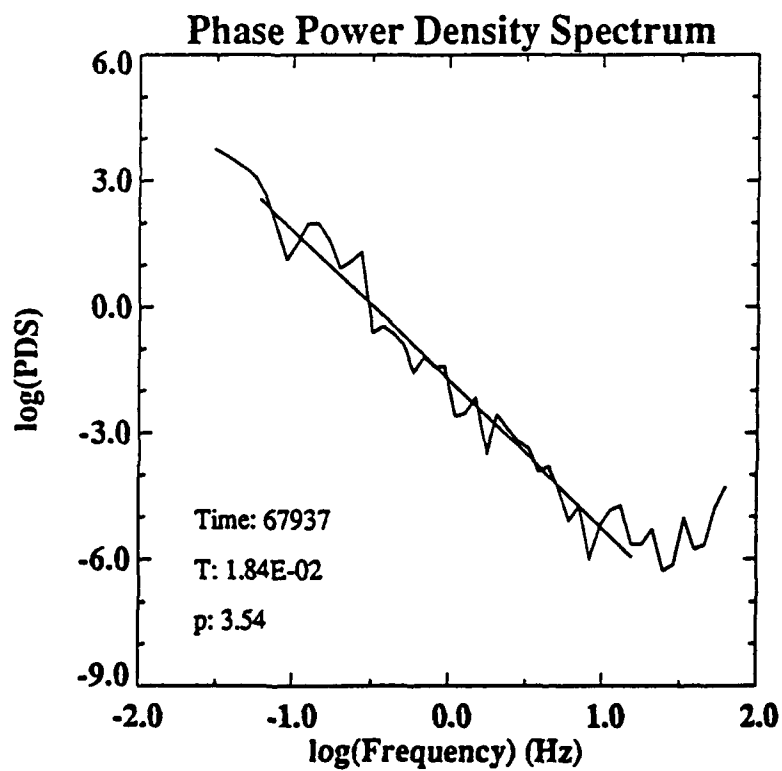
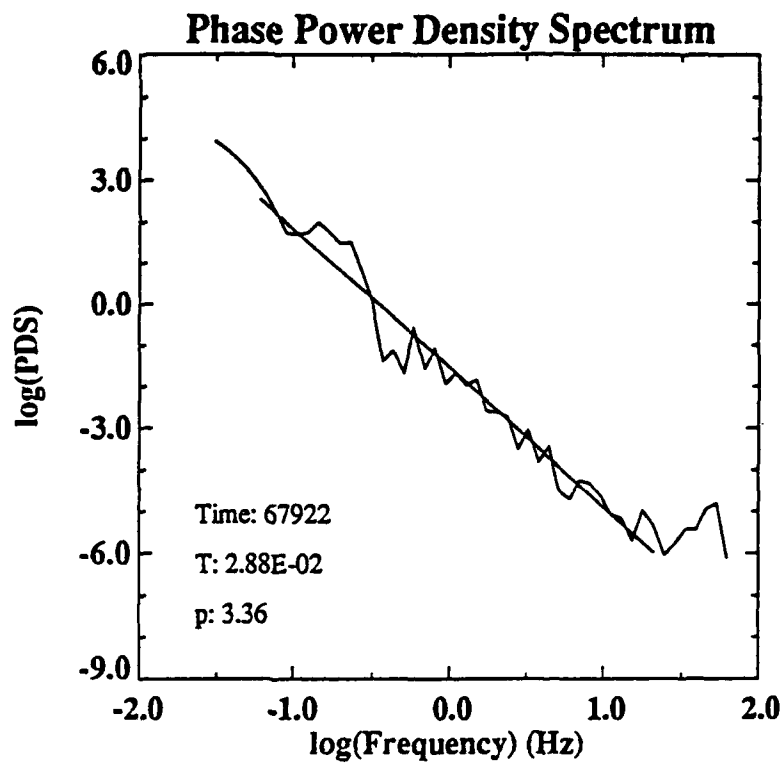


Figure B-1. (Continued).

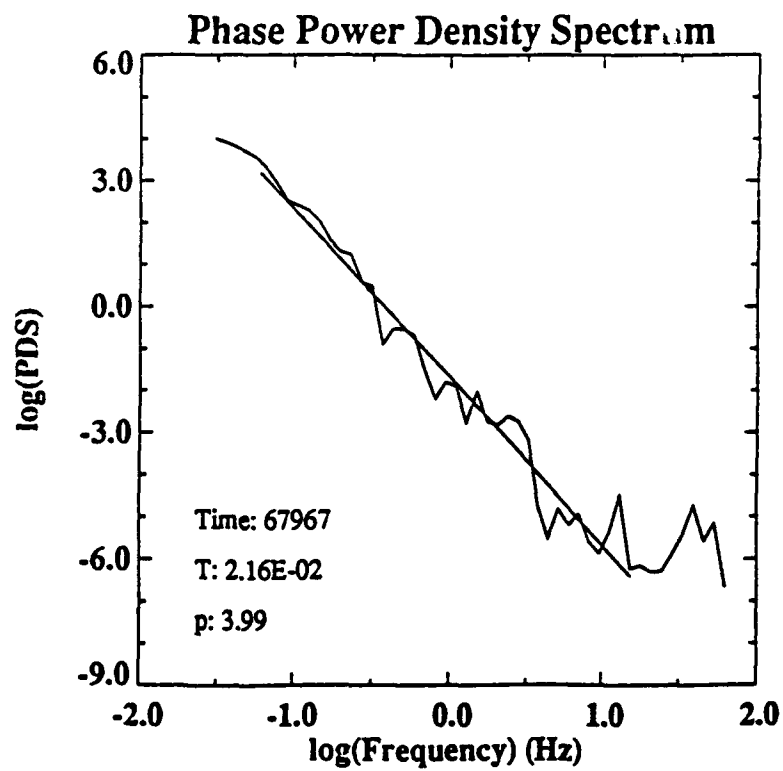
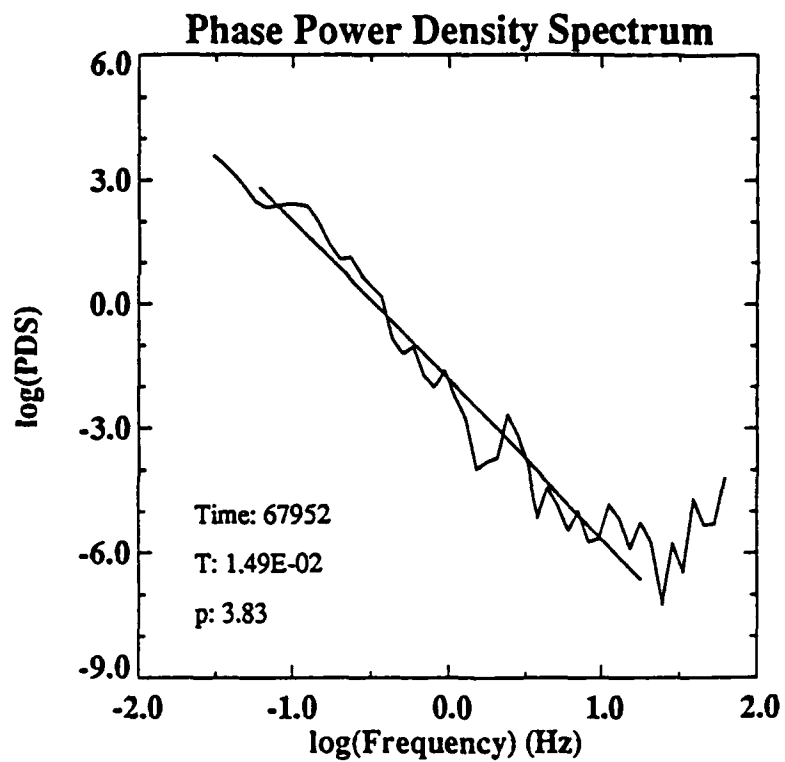


Figure B-1. (Continued).

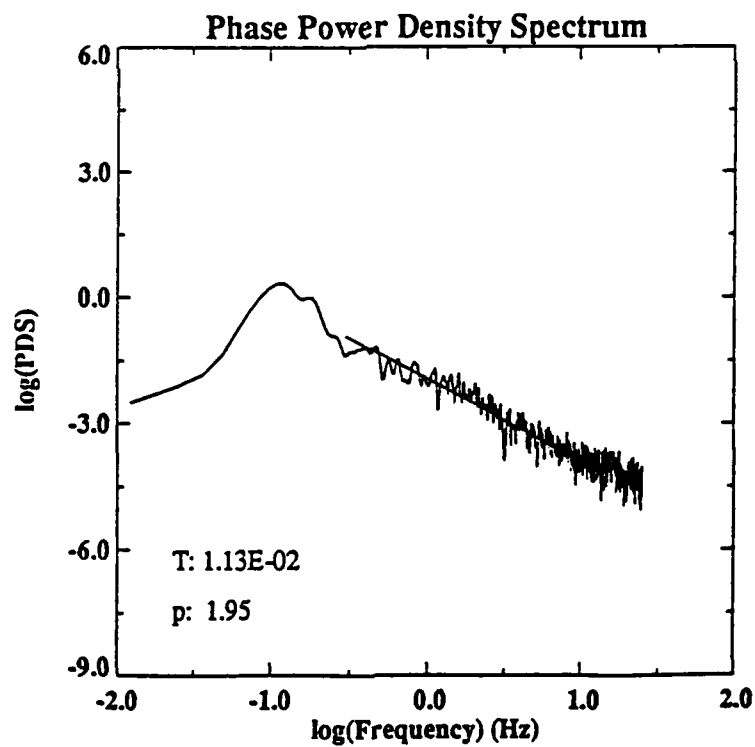
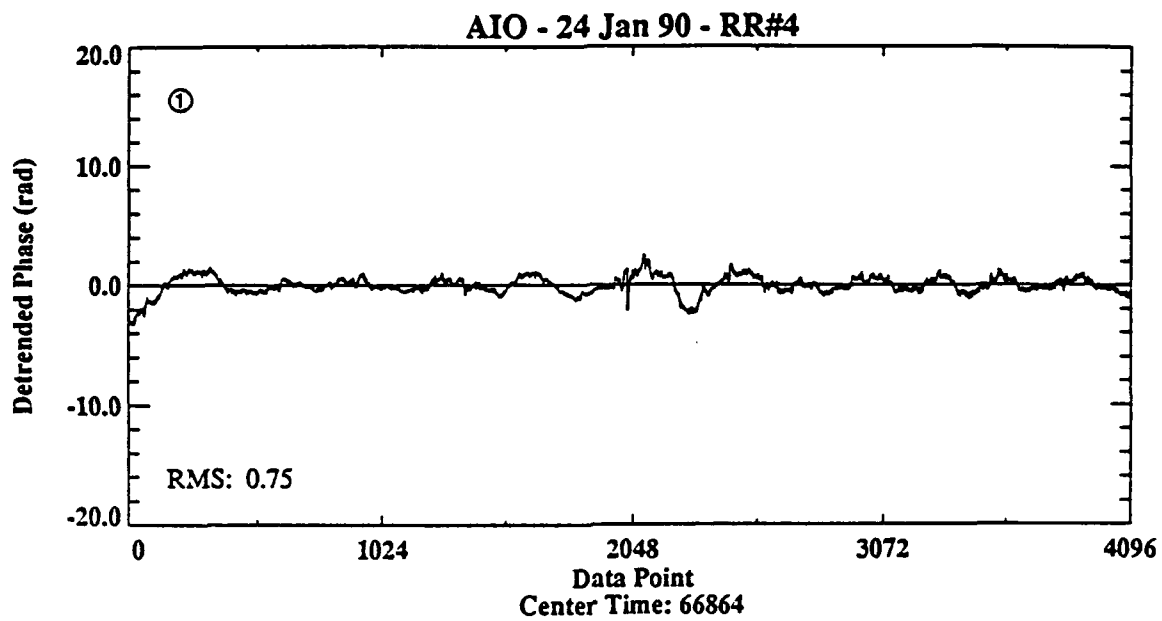


Figure B-2. Detrended VHF phase data records from the AIO-AFSATCOM data set and the spectra generated from them. The linear fits used to calculate T and p are plotted over the phase spectra.

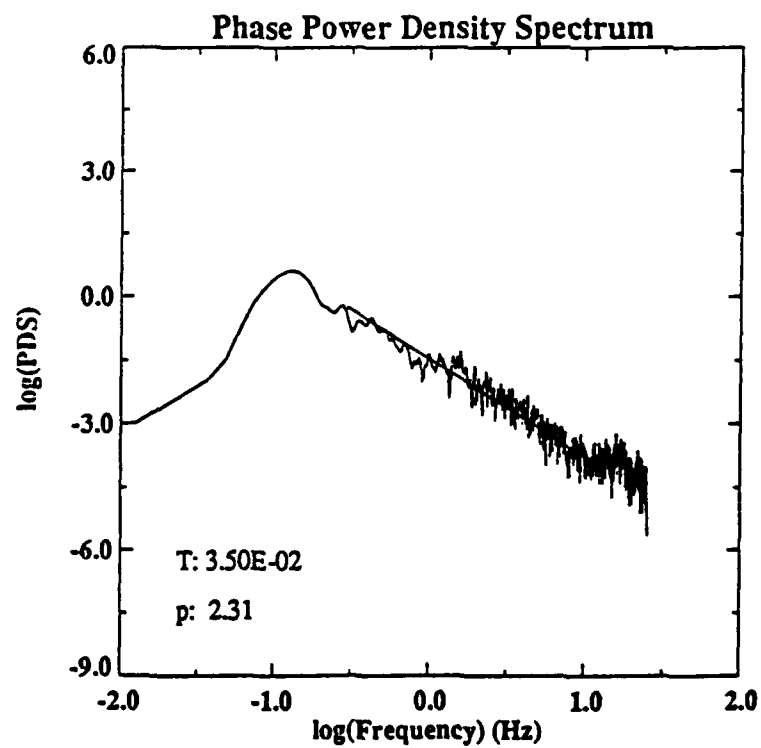
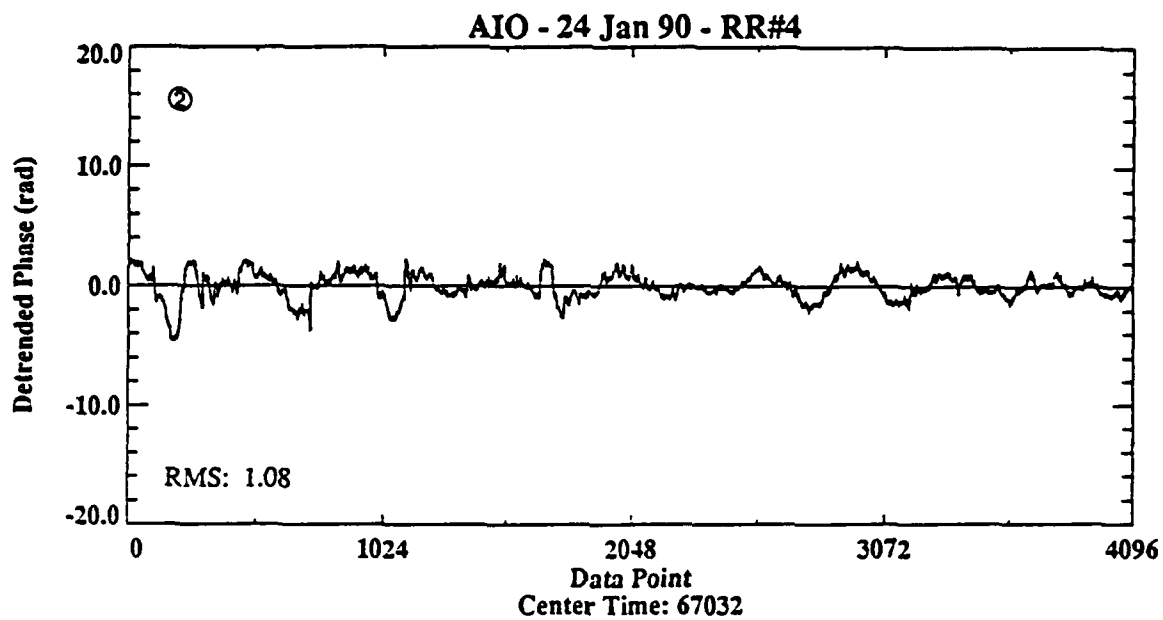


Figure B-2. (Continued).

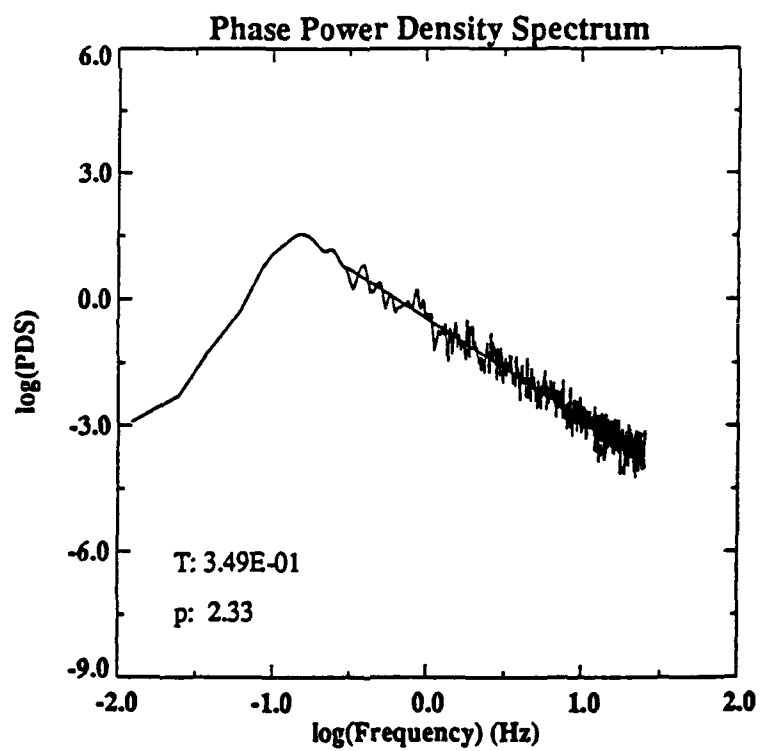
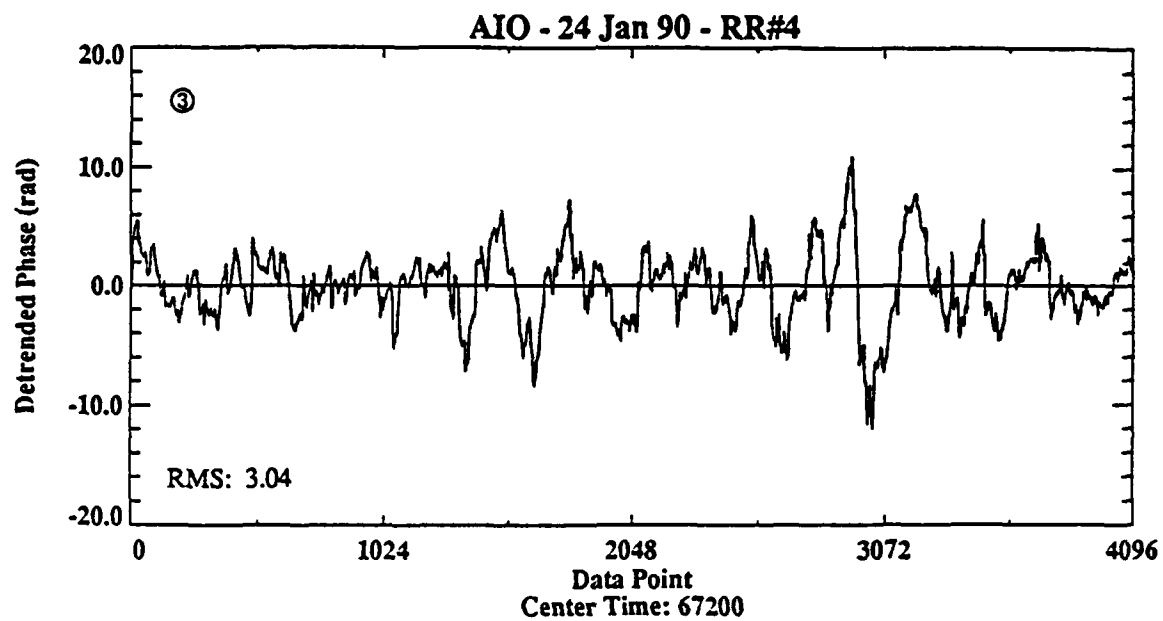


Figure B-2. (Continued).

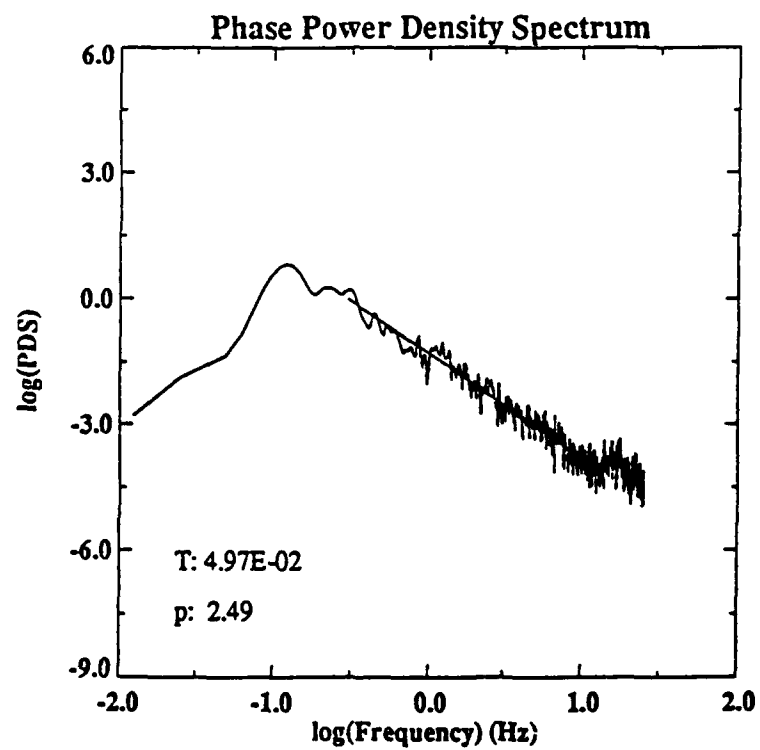
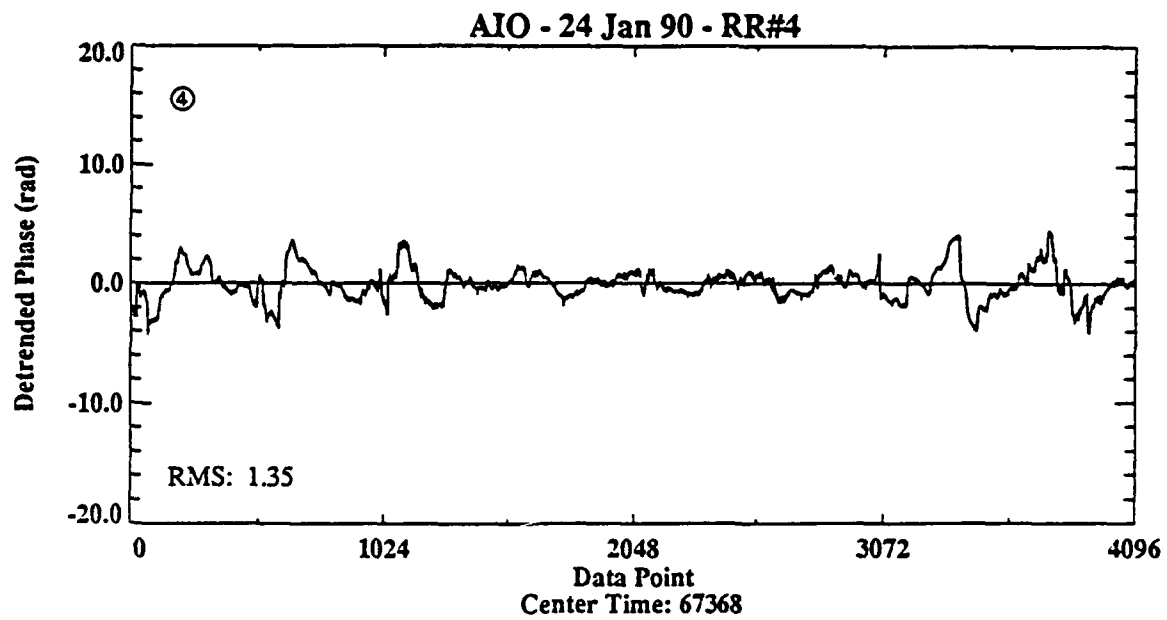


Figure B-2. (Continued).

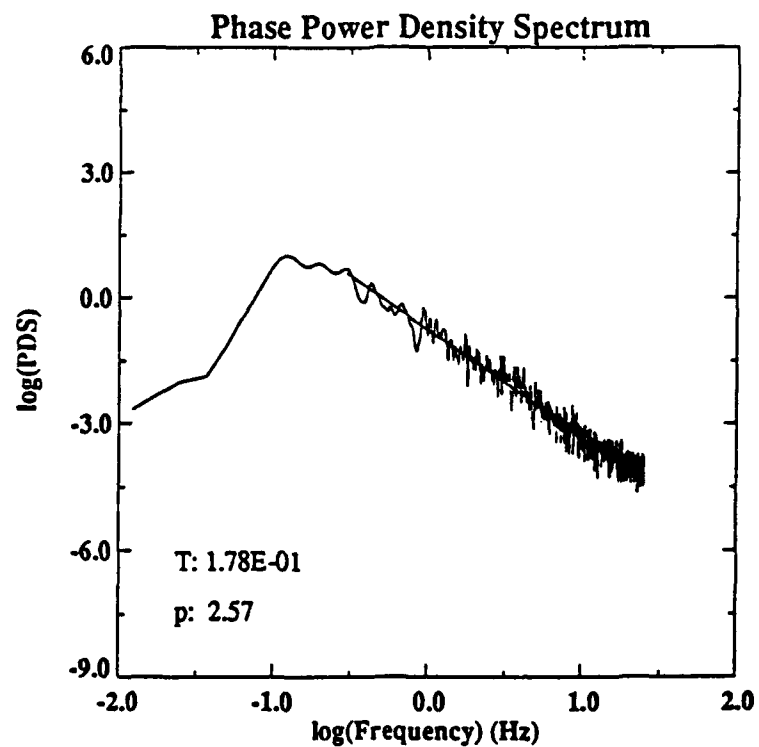
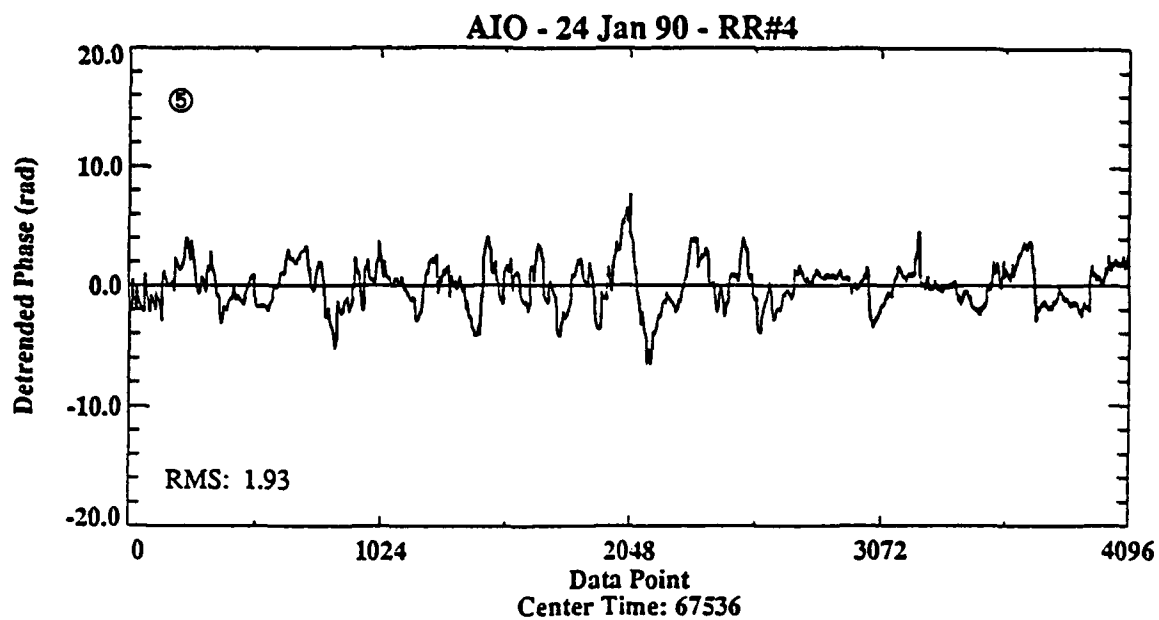


Figure B-2. (Continued).

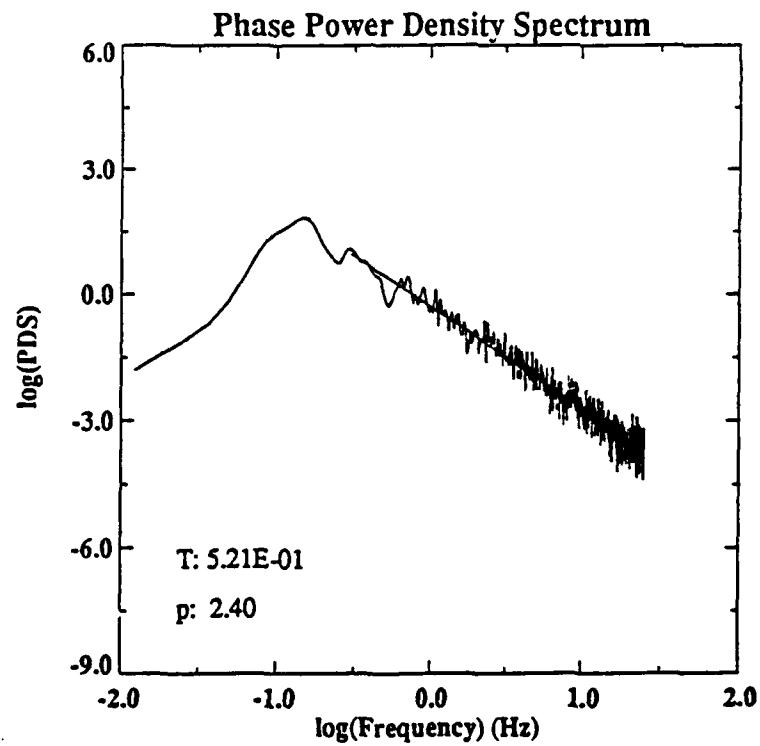
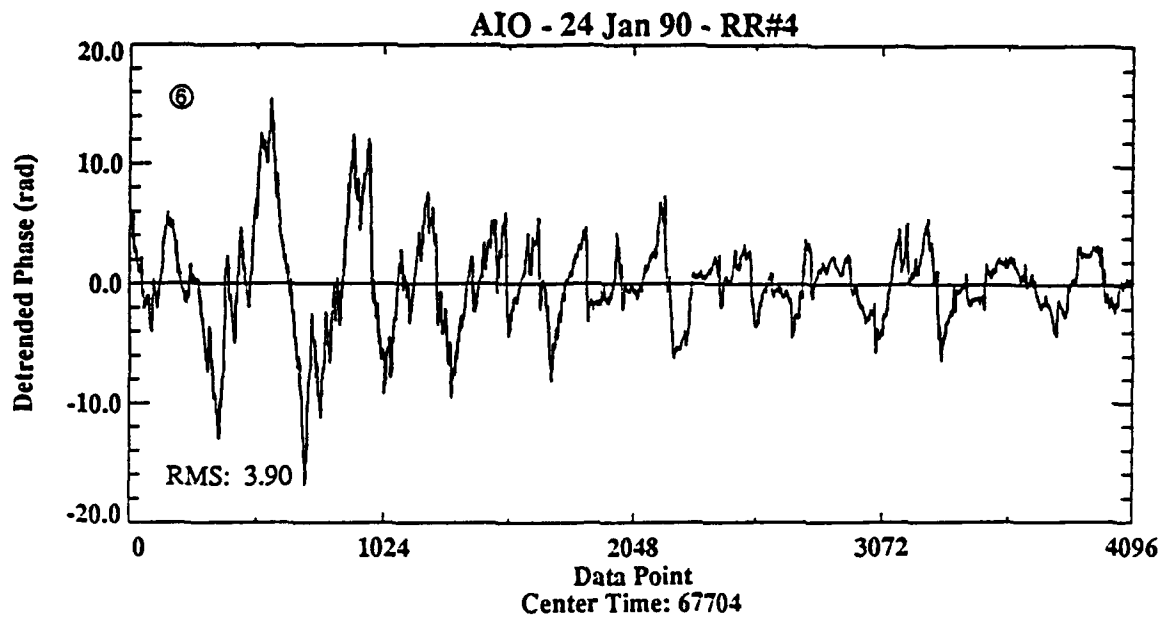


Figure B-2. (Continued).

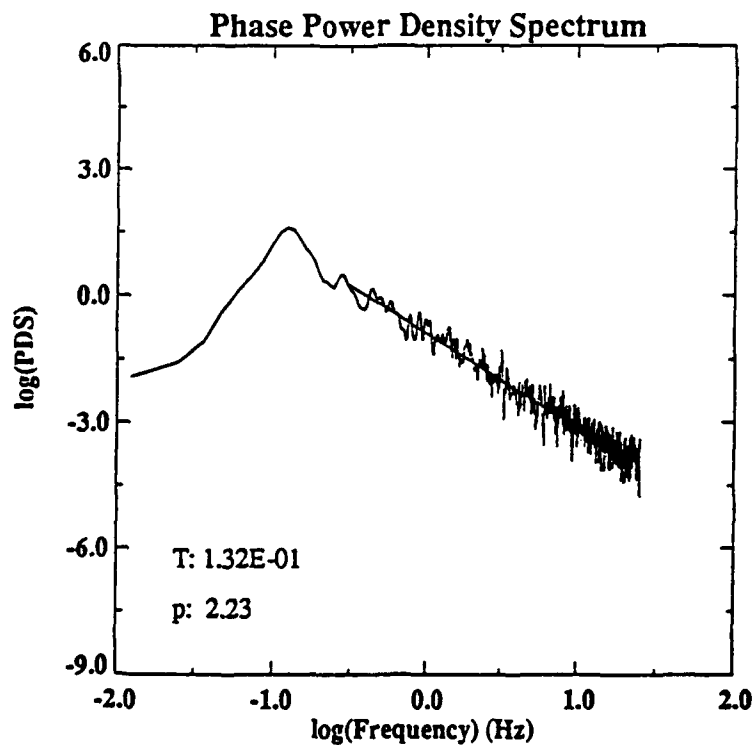
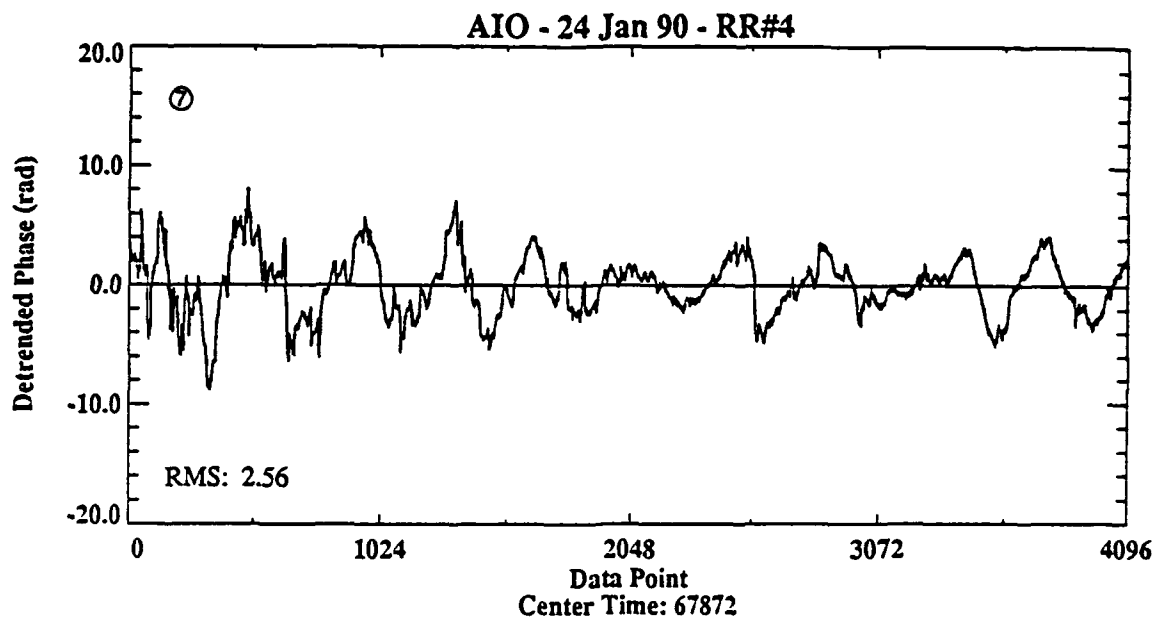


Figure B-2. (Continued).

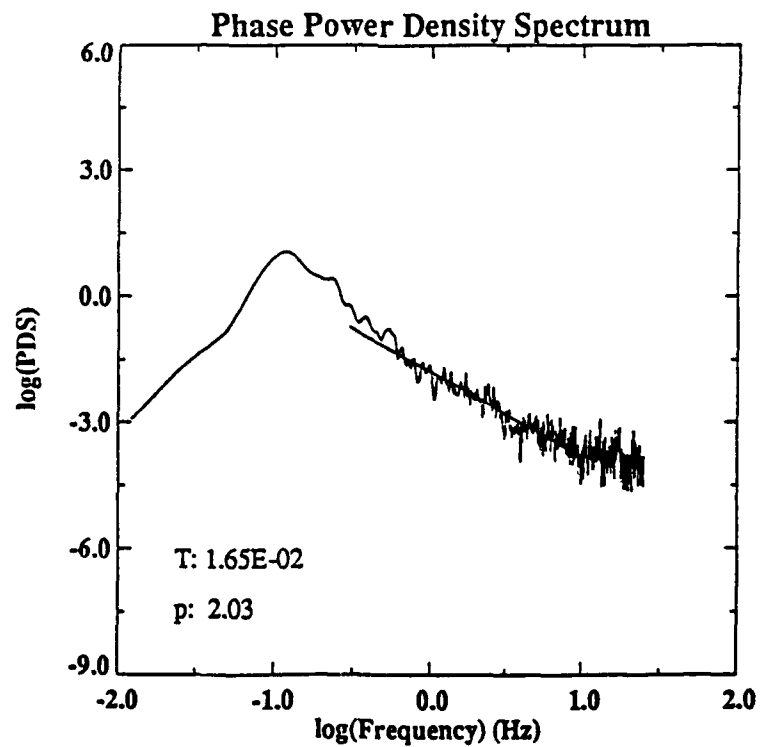
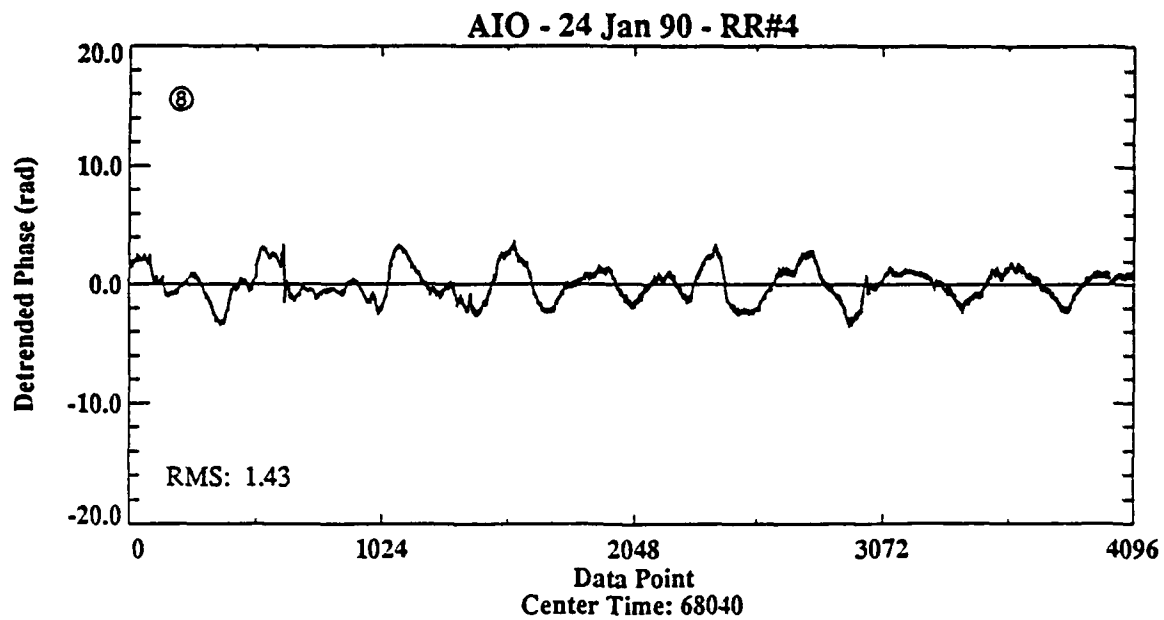


Figure B-2. (Continued).

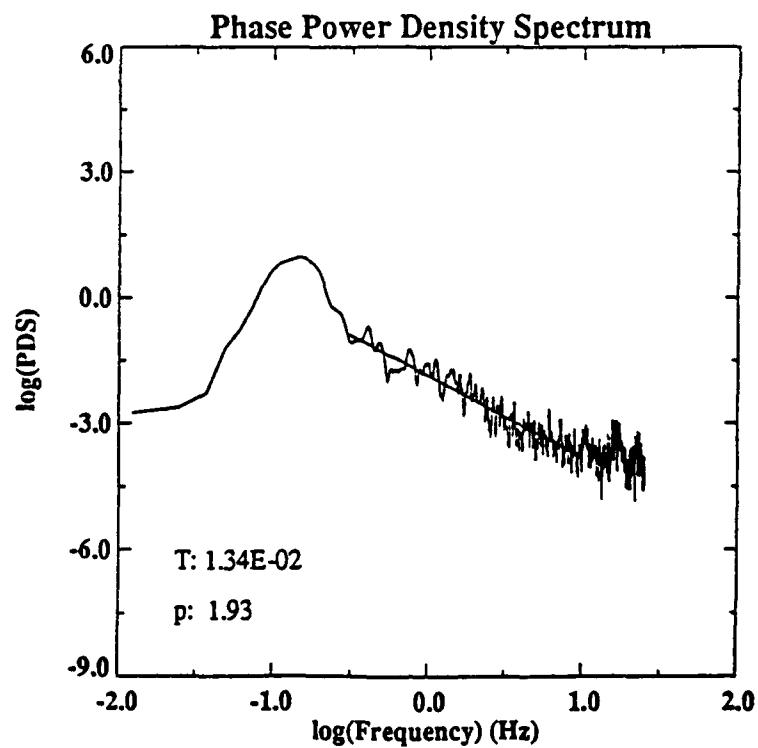
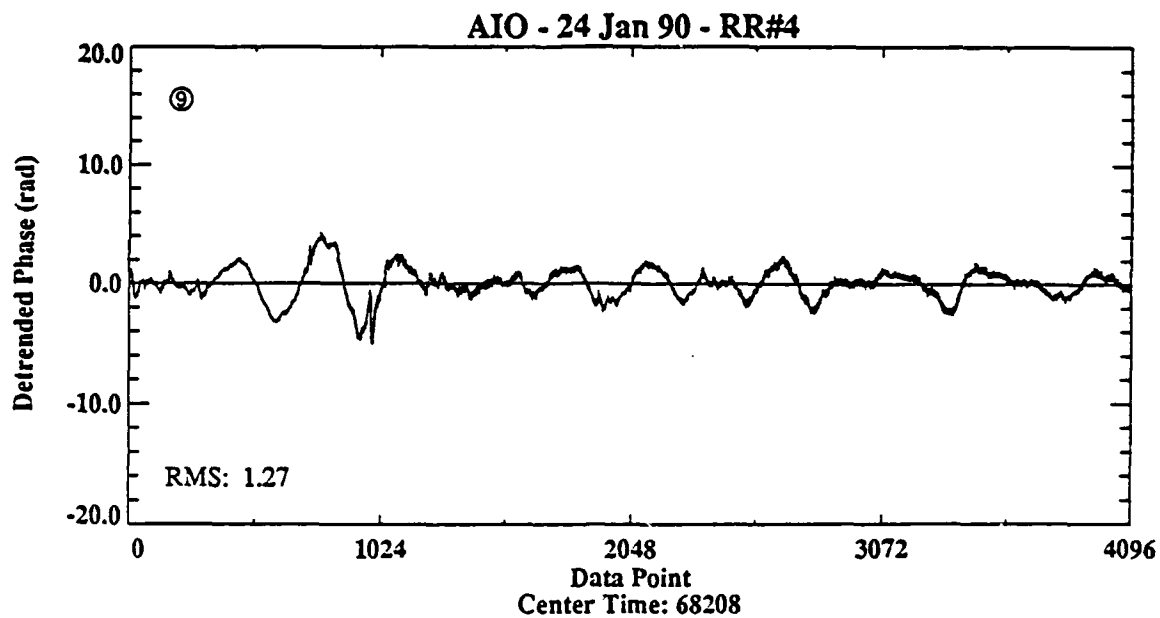


Figure B-2. (Continued).

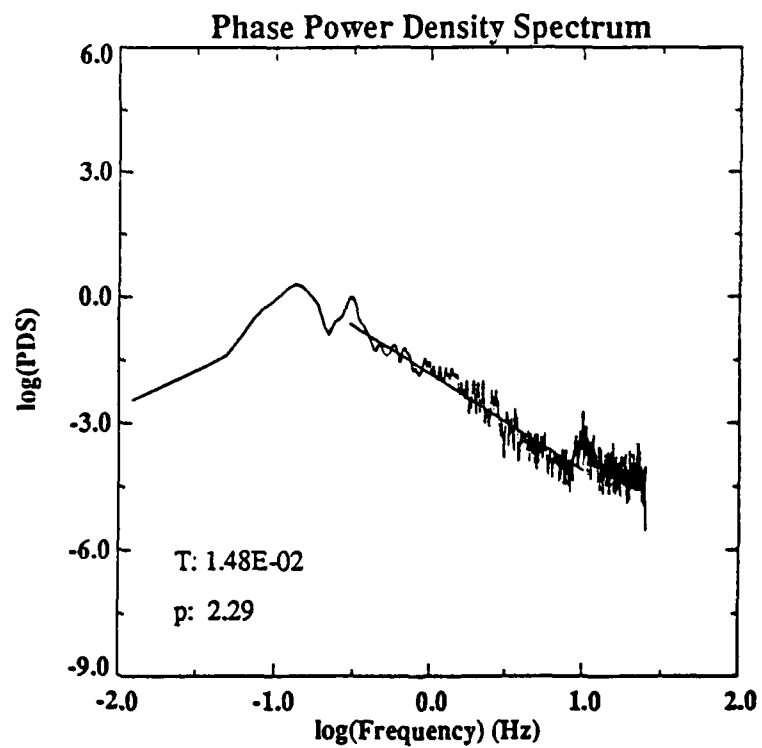
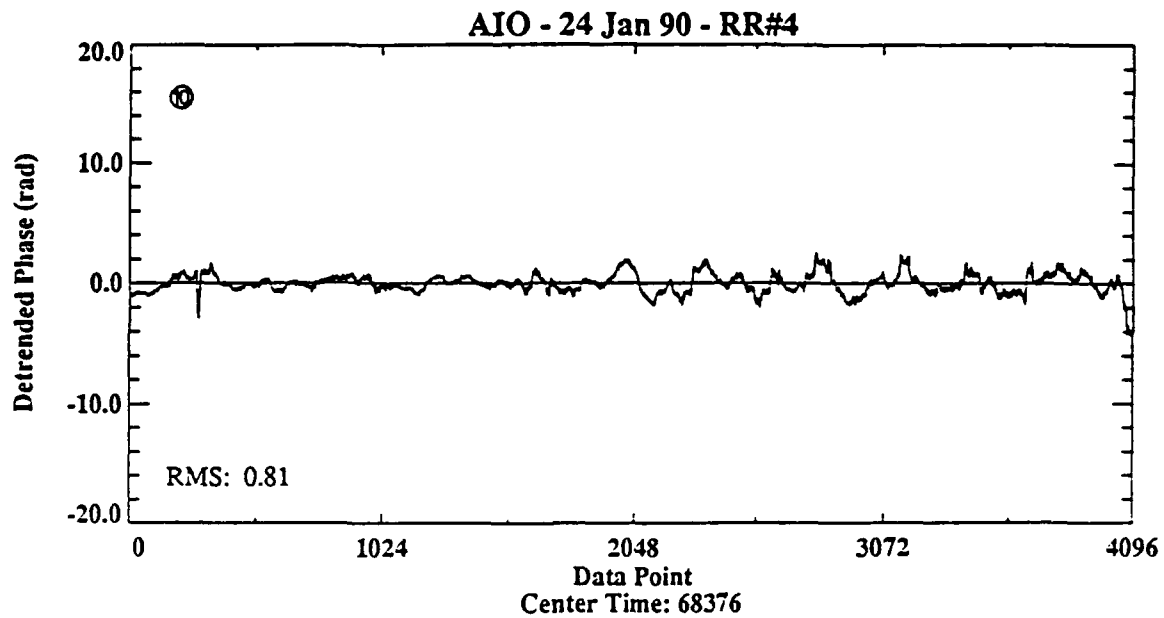


Figure B-2. (Continued).

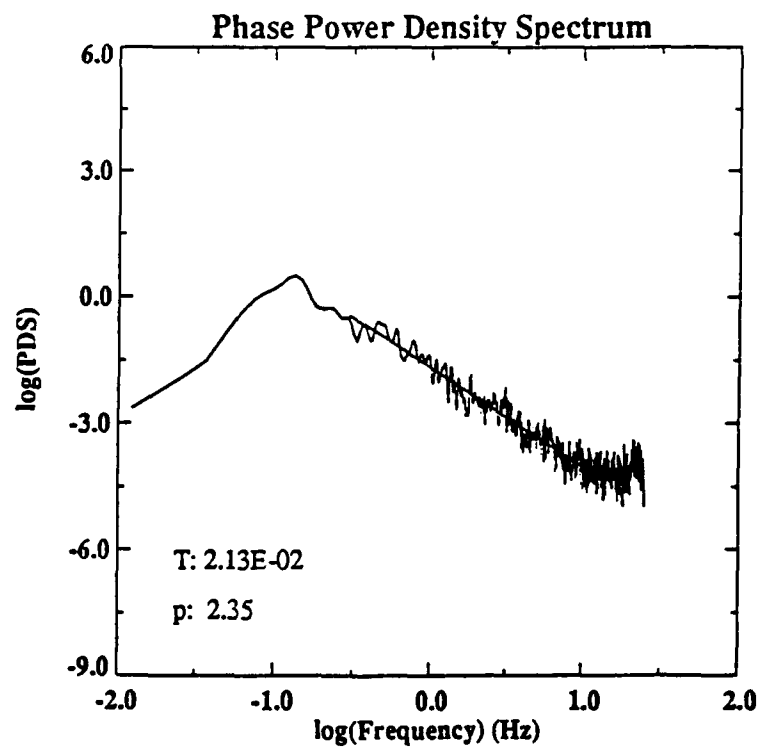
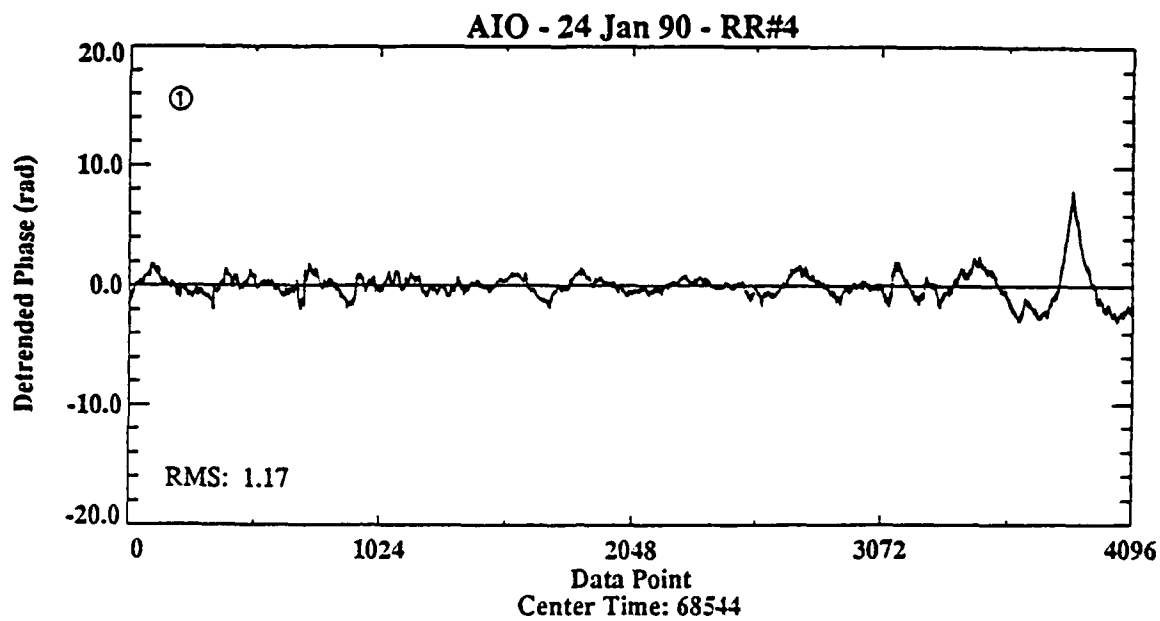


Figure B-2. (Continued).